The Institute of Paper Chemistry

Appleton, Wisconsin

Doctor's Dissertation

The Synthesis and Crystal Structure Determination of *trans*-2-Methylene-5-(2-isopropylol)-cyclohexanol, a New Terpenoid Diol

William E. Scott

January, 1969

THE SYNTHESIS AND CRYSTAL STRUCTURE DETERMINATION OF TRANS-2-METHYLENE-5-(2-ISOPROPYLOL)-CYCLOHEXANOL, A NEW TERPENOID DIOL

A thesis submitted by

William E. Scott

B.S. 1962, Miami University
M.S. 1964, Miami University
M.S. 1966, Lawrence University

in partial fulfillment of the requirements
of The Institute of Paper Chemistry
for the degree of Doctor of Philosophy
from Lawrence University
Appleton, Wisconsin

January, 1969

TABLE OF CONTENTS

SUMMARY

In the course of identifying the products from the oxidation of β-pinene with lead tetraacetate, a white, crystalline substance was isolated from the transesterified product mixture. The compound was believed to be trans-sobrerol, in line with the results of previous workers. Comparison of the infrared and NMR spectra of the two compounds revealed that they were not identical, however. The infrared spectrum of the new material contained a strong band at 906 $cm.^{-1}$, suggesting the presence of an exocyclic double bond. A literature survey failed to reveal the existence of such a compound, and it was decided that its structure should be determined. Single crystal, x-ray crystallographic methods were chosen for the study because they provide a wealth of detailed structural information with only a small investment of material.

Prior to the x-ray work, the synthesis experiments were repeated in order to confirm the original findings.

The new compound ($C_{10}H_{18}O_2$) crystallized from water in space group $P2_12_12_1$ with four molecules per unit cell and one molecule per asymmetric unit. The x-ray experiments were carried out at a temperature of about -193°C. A liquid nitrogen gas-flow cryostat was used to maintain this low temperature. The following unit cell dimensions were obtained with the back-reflection Weissenberg technique: a = 6.952(2) A., b = 17.526(9) A., c = 8.016(1) A., where the number in parentheses refers to the estimated standard deviation in the last decimal place. Three-dimensional intensity data were collected around the a and c axes by the multiple-film, equi-inclination Weissenberg technique. Intensities were estimated by visual comparison with a standard intensity scale. The usual Lorentz and polarization corrections were applied to the data, and all reflections were put on a common scale. A total of 999 observed reflections were obtained.

The structure was solved through the application of the symbolic addition method for noncentrosymmetric crystals. All twelve nonhydrogen atoms were found in the initial E-maps. Fourier and least squares refinement reduced the R value to 0.112, at which time the eighteen hydrogen atoms were located in a difference Fourier synthesis. Further least squares refinement, including constant hydrogen parameters, lowered the R to 0.083 for the observed data.

The structure was found to be trans-2-methylene-5-(2-isopropylol)-cyclohexanol (or trans-MIC, for discussion purposes). The hydroxyl on C1 was axial, and the isopropylol group on C5 was equatorial. The methylenecyclohexane ring took on the ordinary chair conformation.

The average length of bonds C1-C6, C6-C5, C5-C4, and C4-C3 is 1.533 A., which is within 1 σ of the value reported for cyclohexane. The average ring angle of 110.9° (range 108.8°-112.1°) agrees with the value for cyclohexane, also. The C2-C10 double bond length is 1.314 A., slightly shorter than the 1.334 A. reported for ethylene.

The dihedral angle between the planes determined by C1,C2,C3, and C1,C3,C4,C6 is 45.5°, while the angle between the latter plane and plane C4,C5,C6 is 52.6°. Both of these angles are less than the 60° associated with the so-called ideal cyclohexane ring. Thus, the ring in trans-MIC takes on a somewhat flattened appearance.

The molecules are held together in the crystal by a network of hydrogen bonds in which each hydroxyl participates in linkages with two other molecules.

A comparison of the three-dimensional phases obtained from the symbolic addition procedure with those associated with the final structure revealed an average error of 22° in the former. The average error for all phases was only 16°.

INTRODUCTION

Wood often contains appreciable amounts of volatile oils, which are responsible for the characteristic odors associated with fresh wood. Depending on the species, the volatile constituents consist of terpenes and related substances, paraffin compounds, and aromatic compounds. These substances, for the most part, have boiling points over 100°C., but they are characterized by an appreciable vapor pressure at room temperature and by the fact that they distill with steam.

The carbon skeleton of the acyclic and cyclic hydrocarbon oils and their derivatives contain a repeated isopentane skeleton and may be regarded as derivatives of isoprene, C_5H_8. The monoterpenes contain two isoprene units; the sesquiterpenes, three; the diterpenes, four; and the triterpenes have six such units.

The so-called "isoprene rule" deduced from these observations has proved valuable for the elucidation of terpene structures, both simple and complex. It should be regarded only as a working hypothesis for the elucidation of structure, because exceptions to the rule are known (1).

Terpenes often occur as mixtures of related materials which are difficult to separate. Some of the compounds isomerize readily and others undergo disproportionation reactions. They are usually optically active. Much of the published research on terpenes was carried out before the development of modern methods of separation and purification. Consequently, there are often differences in the physical constants that have been reported. Simonsen has written five books which review the early work in terpene chemistry (1-4).

α-Pinene is probably the most important monoterpene (see Fig. 1). It occurs widely distributed in nature and is one of the major components of sulfate turpentine. The designation pinene was given to the hydrocarbon fraction, b.p. 155-165°, of oil

of turpentine (5). This name was selected to indicate its association with the various species of Pinus, in which it is so largely found. In view of the ease with which α-pinene could be obtained, its reactions have been investigated from a very early date. [See Reference (2) for a discussion of the chemistry of α-pinene.]

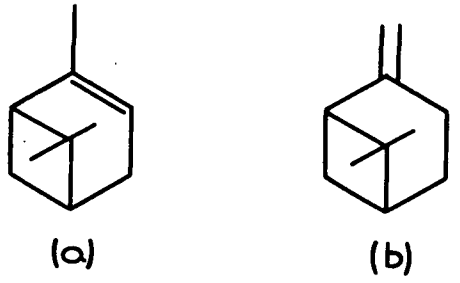

Figure 1. α-Pinene (a) and β-Pinene (b)

β-Pinene occurs in nature in the majority of the oils in which α-pinene is found. The percentage present is variable and usually considerably lower than that of α-pinene.

β-Pinene resembles α-pinene closely in its general reactions. Early investigators were hampered by the difficulty of obtaining an effective separation of β-pinene and α-pinene. A further difficulty involved the tendency of β-pinene to isomerize to α-pinene under a variety of reaction conditions. Modern distillation techniques have solved the problem of obtaining highly pure β-pinene. In addition, procedures have been developed for the production of β-pinene through the isomerization of α-pinene (6, 7).

The hydrocarbon terpenes have found use as solvents, starting materials for the production of camphor, toxaphene, and other chemicals. The largest use for turpentine is reported to be the production of synthetic pine oil (8). Pine oil is composed of secondary and tertiary cyclic terpene alcohols. This material finds use as disinfectants, wetting agents, solvents, and household and industrial cleaners.

The development of methods to produce quantities of relatively pure β-pinene has resulted in increased utilization of terpene resins in various kinds of adhesives.

Several workers have synthesized various oxygenated terpene compounds through the oxidation of α-pinene (9-12). Matsubara (13) reported the results of oxidizing β-pinene with red lead in acetic acid. He obtained the following products (Table I). Figure 2 illustrates the structures for the various compounds.

TABLE I

PRODUCTS OF REACTION BETWEEN β-PINENE AND RED LEAD IN GLACIAL ACETIC ACID (13)

	Yield, %	Structure[a]
Dipentene	0.7	A
α-Pinene	4.2	B
β-Terpinyl acetate	2.7	C
Perilla acetate	3.5	D
Myrtenyl acetate	8.5	E
1-p-Menthene-8,9-diacetate	1.6	F
β-Pinene glycol diacetate	1.3	G
Sobrerol diacetate	2.9	H
8-p-Menthene-1,7-diacetate	4.0	I

[a]Letter corresponding to structure in Fig. 2.

Gruenewald and Johnson (14) extended the studies to include the oxidation of β-pinene with lead tetraacetate in acetic acid and benzene solvents. They obtained a substantial yield of trans-pinocarvyl acetate (Fig. 3) in both solvents, along with myrtenyl acetate. The solvent had a marked effect on the relative yields of the two monoacetates, however. Table II indicates the results. Gas chromatographic

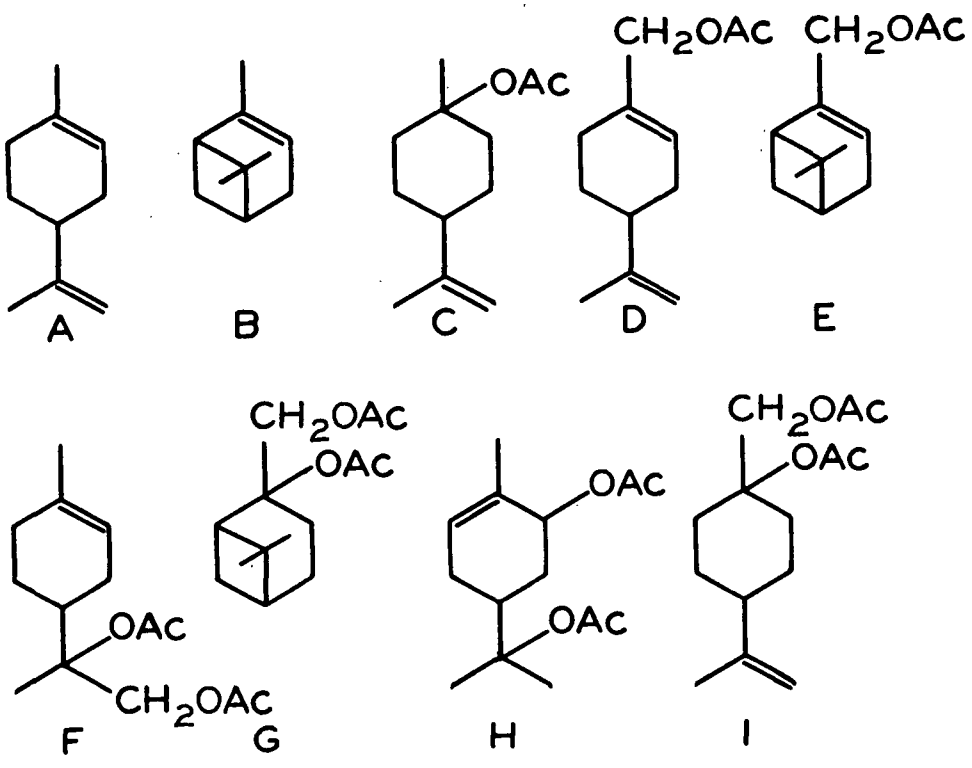

Figure 2. Oxidation Products (13)

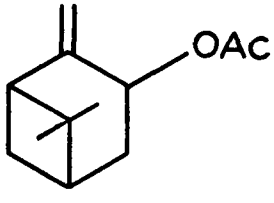

Figure 3. trans-Pinocarvyl Acetate

analysis indicated that the acetic acid product mixture was much more complex than the benzene product mixture, with a greater percentage of higher boiling constituents.

TABLE II

EFFECT OF SOLVENT ON MONOACETATE YIELDS

Solvent	trans-Pinocarvyl Acetate, %	Myrtenyl Acetate, %
Glacial acetic acid	10.0	12.0
Benzene	46.0	10.5

A similar study was reported by Sato (15). He obtained myrtenyl acetate (18%), trans-pinocarvyl acetate (4%), perilla acetate (10%), β-pinene glycol diacetate (13%), sobrerol diacetate (3%), and 1-p-menthene-7,8-diacetate (3%) (Fig. 4) in acetic acid medium. Sobrerol diacetate (14%) and trans-pinocarvyl acetate (53%) were obtained by running the oxidation in benzene.

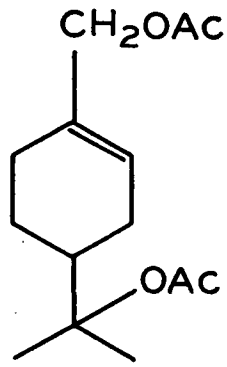

Figure 4. 1-p-Menthene-7,8-diacetate

This worker became interested in the oxidation of β-pinene with lead tetraacetate because no mechanism had been proposed which satisfactorily accounted for the behavior of the reaction. It was hoped that the effects of solvent and temperature on products and product ratios could be explained through further studies.

An initial reaction between lead tetraacetate and β-pinene in acetic acid was carried out for the purposes of developing a gas chromatographic product analysis procedure (16). Myrtenyl acetate (10%), trans-pinocarvyl acetate (5%), and perilla acetate (5%) were isolated and identified. In addition, a white crystalline material was isolated from the transesterified product mixture. Table III contains some of the properties of the substance.

TABLE III

PROPERTIES OF CRYSTALLINE MATERIAL

Property	Value
Melting point	130.0-130.5°C.
$[\alpha]_D^{20}$	-9.5° (1.452 g./100 ml. $CHCl_3$)
Elemental Analysis (averages of two determinations)	
Calculated as $C_{10}H_{18}O_2$	C=70.6% H=10.6% O=18.8%
Found	C=70.8% H=10.6% O=18.6%
Density	1.123 g./cm.^{3} (see p. 42)
Mixed melting point with trans-sobrerol[a]	110° = -130°C.

[a] trans-Sobrerol provided by Dr. Kyle Ward (10).

The result of the mixed melting point indicated that the crystalline material was not trans-sobrerol. Confirmation of this fact was made by comparing the infrared spectra of the two compounds (Fig. 5). The two infrared spectra were similar in the 1100 cm.$^{-1}$ to 5000 cm.$^{-1}$ region. They differed markedly from 600 cm.$^{-1}$ to 1000 cm.$^{-1}$, however. The presence of a band at 906 cm.$^{-1}$ in spectrum (b) suggested the presence of an exocyclic carbon-carbon double bond. A structure was proposed which was compatible with the infrared data and also was related to β-pinene (Fig. 6). The

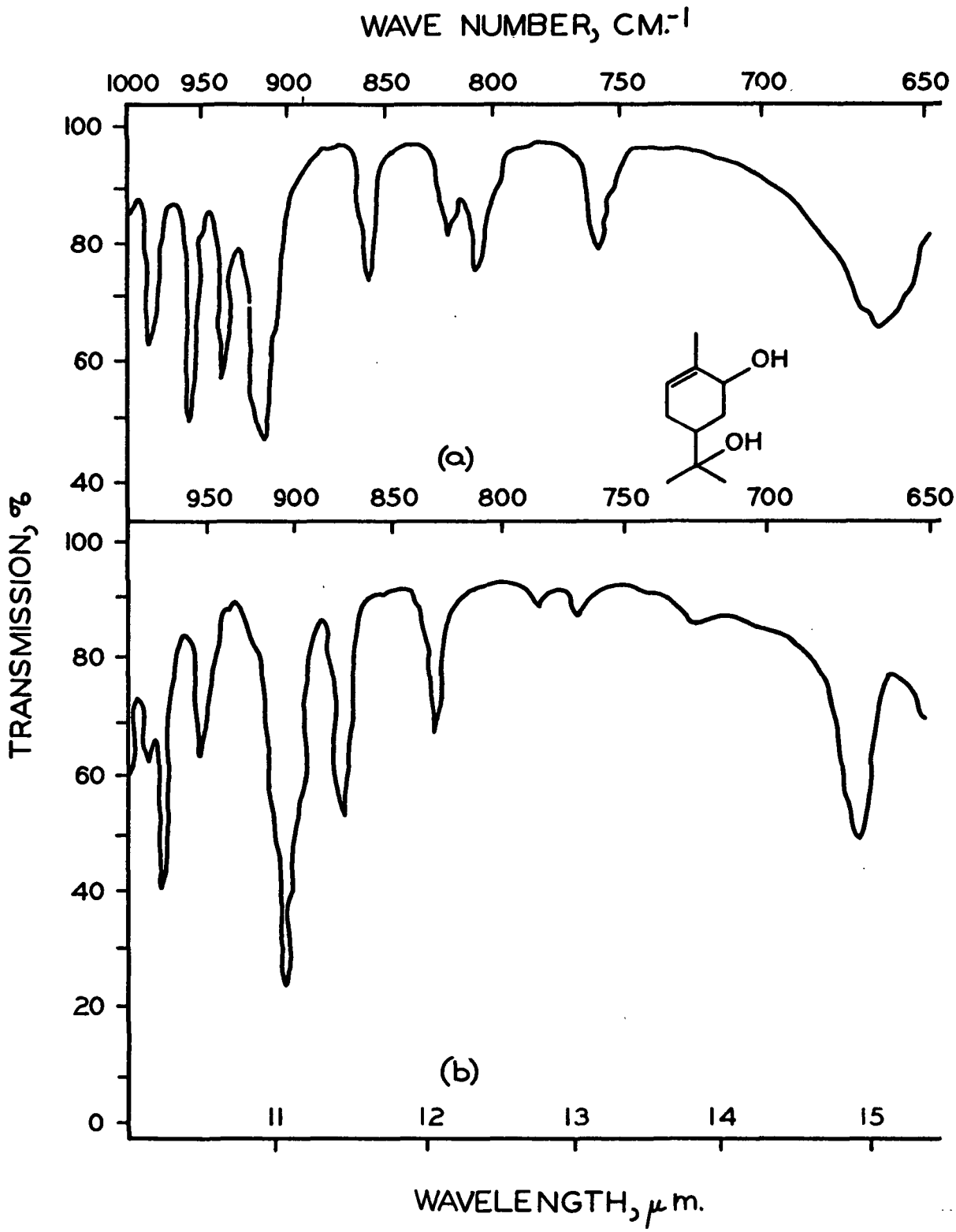

Figure 5. Infrared Spectra of <u>trans</u>-Sobrerol (a) and the Crystaline Compound, $C_{10}H_{18}O_2$ (b)

nuclear magnetic resonance spectrum was in agreement with the proposed structure. No reference to any such structure or similar structures was found in the literature, however. In fact, the occurrence of the methylenecyclohexane grouping seemed to be uncommon, the isomeric methylcyclohexene grouping being produced most often.

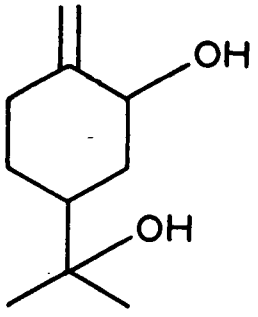

Figure 6. Proposed Structure for $C_{10}H_{18}O_2$

It was obvious that certain structural features of the compound should be established before any further oxidation studies were attempted. Among the features of interest were the general arrangement of the atoms, the types and locations of bonds, the stereochemical relationships of ring substituents (if a ring was present), and conformational details of the molecule. It was probable that chemical investigations would provide information regarding the first two points. The stereochemical details could not be readily obtained, however. The classic approach to elucidation of cis-trans relationships in a ring system has been the comparison of reaction rates in a number of compounds whose structures differed only in the configurational features under study. Such a line of attack would not apply to a single compound.

Of the various physical techniques available for structure analysis, x-ray diffraction appeared to be the most promising. X-ray methods provide a wealth of detailed information concerning the stereochemistry of a molecule and its surroundings, using only a very small amount of material.

A survey of the literature revealed that the monocyclic and bicyclic terpenes have been virtually ignored by crystallographers. References to the structure analyses of bromoisofenchone (17), anti-7-norbornenyl-p-bromobenzoate (18), and alpha-X-camphor (X = Cl, Br, CN) (19) were found. No structure analysis of a compound having the pinane bicyclic configuration (Fig. 7) has been reported. This is difficult to understand in view of the tremendous volume of chemical research that has been carried out in the area. Information from a detailed structure analysis would enable the chemist to speak more confidently regarding the effects of the bicyclic stereochemistry on chemical reactivities and mechanisms.

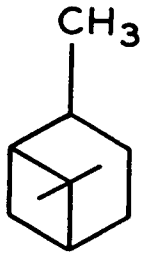

Figure 7. Pinane Bicyclic Configuration

It was decided that the structure determination of a bicyclic terpene would be attempted, if the solution of the first compound went smoothly. cis-Pinocarvyl-p-nitrobenzoate (Fig. 8) was selected for the study because it was closely related to β-pinene, and crystals were available.

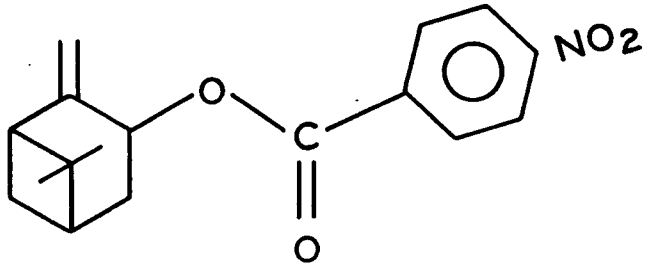

Figure 8. cis-Pinocarvyl-p-nitrobenzoate

STATEMENT OF THE PROBLEM

In summary, the goals of this thesis were as follows:

The original synthesis work was to be confirmed by repeating the oxidation experiments. It was hoped that the results of the chemistry experiments would enable this worker to decide whether or not Matsubara (13) and Sato (15) had mistakenly identified the new compound as sobrerol.

The complete crystal and molecular structure of the crystalline compound, produced by the above synthesis, was to be determined by single crystal x-ray crystallography.

In the event that the above goals were successfully accomplished, the structure analysis of a bicyclic terpenoid was to be attempted. cis-Pinocarvyl-p-nitrobenzoate was chosen for the study. The results of this work are discussed in Appendix VI. While not completely successful, it is the opinion of the author that the analyses carried out thus far will contribute substantially to the eventual solution of the structure.

X-RAY CRYSTALLOGRAPHY

An x-ray crystallographer is a person who uses the methods and tools of x-ray diffraction ... "to study the arrangement of atoms in matter, its causes, its nature and its consequences ..." (20). It would be virtually impossible to treat all of the various areas, both practical and theoretical, which are included in the general science of x-ray crystallography. Fortunately, several excellent texts have been written on the subject by workers in the field (21-24). Special attention should be paid to the recent book by Stout and Jensen (24). The authors have oriented their writing toward the chemist who, with little prior knowledge, decides to become acquainted with the techniques and practices of x-ray crystallography. Owing to the interests of the authors, many of the chapters and examples show a bias toward problems more likely to be encountered in the analysis of organic structures.

The purpose of this discussion is to consider a few concepts and assumptions which are central to the science of crystallography, and, therefore, to this thesis. For a more detailed treatment of the various concepts, the reader is encouraged to consult the references listed throughout this discussion.

SOME FUNDAMENTAL CONCEPTS IN X-RAY CRYSTALLOGRAPHY

DIFFRACTION OF X-RAYS

Figure 9 illustrates a simplified three-atom structure. The structure can be resolved into three sets of stacks for every $\underline{hk\ell}$ direction. Each stack in the collection scatters the incident x-ray beam in phase according to Bragg's Law,

$$n\lambda = 2d \sin \theta \qquad (1)$$

where

$\underline{n}$ = order of the reflection in question;

λ = wavelength of incident radiation;

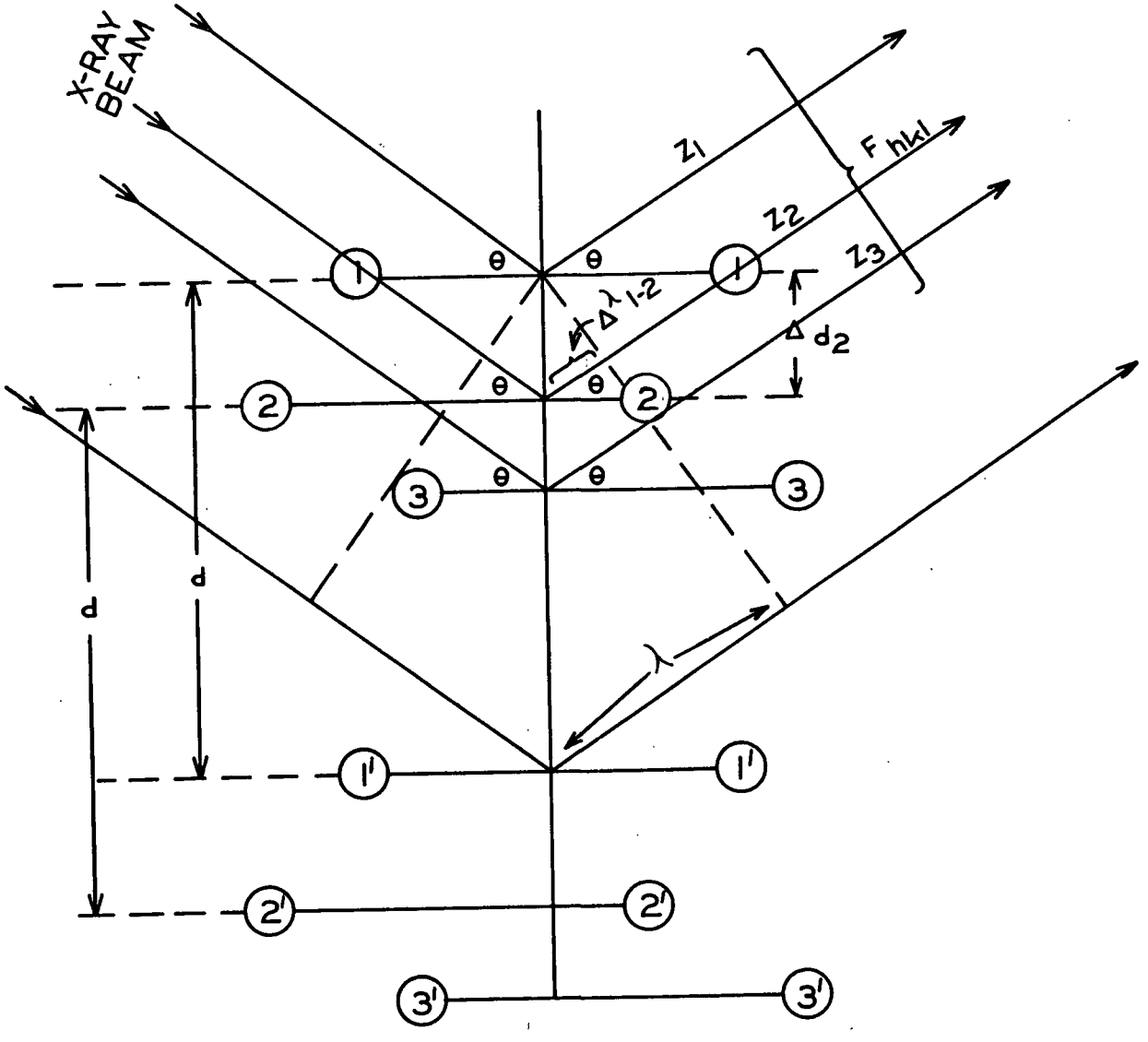

Figure 9. Three Atom Structure and Incident X-ray Beam (23)

d = period of the lattice;

θ = angle between incident x-ray beam and reflecting plane.

The waves scattered by the separate lattice stacks differ in phase. Figure 9 shows a pair of planes of each of three stacks. A pair of neighboring planes of a stack, e.g., 1 and 1' of Fig. 9, separated by spacing d, reflect x-rays with a path difference of λ and a phase difference of 2π if θ is chosen so as to satisfy Equation (1). A pair of planes 1 and 2 of separation Δd_2 reflect x-rays with a path difference $\Delta\lambda_{12}$ and a phase difference $\Delta\phi_{12} = (\Delta d_{12}/d)\cdot 2\pi$.

The total wave diffracted from the unit cell in direction $hk\ell$, $F_{hk\ell}$, is proportional to the sum of the wavelets diffracted from each individual atom in the unit cell. For Fig. 9,

$$F_{hk\ell} = Z_1 + Z_2 + Z_3. \tag{2}$$

The symbols in Equation (2) all represent quantities which vary sinusoidally with time, and they can be regarded as occurring in the complex plane as shown in Fig. 10, where Z_j is the amplitude of the wave and ϕ_j is its phase relative to the wave scattered by fictitious electrons at the origin of the unit cell. Each Z_j in Equation (2) can be expressed as $f_j e^{i\phi_j}$ in terms of complex notation. The individual f_j is called the atomic scattering factor for atom j. The total energy then becomes

$$F_{hk\ell} = f_1 e^{i\phi_1} + f_2 e^{i\phi_2} + f_3 e^{i\phi_3}, \tag{3}$$

or, in general,

$$F_{hk\ell} = \sum_j f_j \exp(i\phi_j)^* \tag{4}$$

---

*$\exp(i\phi_j)$ means $e^{i\phi_j}$.

The $\underline{F}_{\underline{hk\ell}}$ varies sinusoidally, also, and may, therefore, be expressed in terms of an amplitude, $|\underline{F}_{\underline{hk\ell}}|$, and a phase, $\phi_{\underline{hk\ell}}$. The quantity, $|\underline{F}_{\underline{hk\ell}}|$, is usually referred to as the structure factor amplitude.

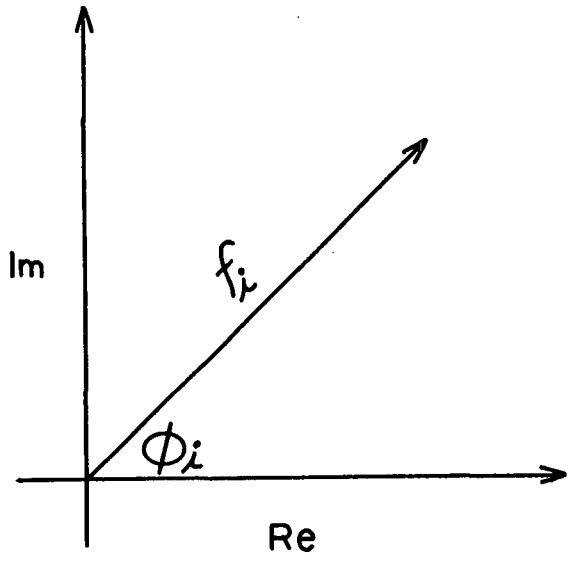

Figure 10. Complex Plane

The structure factor amplitude is related to the experimentally observed intensities in the following manner (23).

$$|F_{hk\ell}|^2 = \frac{KAI_{hk\ell}}{Lp} \qquad (5)$$

$\underline{I}_{\underline{hk\ell}}$ is the experimentally determined intensity. $\underline{L}$ is the Lorentz factor, $\underline{p}$ is the polarization factor, $\underline{A}$ is the absorption correction, and $\underline{K}$ is a scale factor.

The Lorentz factor ($\underline{L}$) arises because the time during which a reflection occurs varies as a function of θ in the diffraction process. The exact function depends on the experimental conditions and apparatus.

The polarization term ($\underline{p}$) arises because there is a variation in reflection efficiency with angle. The incident x-ray beam is usually unpolarized. The portion of the beam whose electric vectors are perpendicular to the plane of incidence is

reflected to an extent which is determined only by the electron-density in the plane. The reflection of the component whose electric vectors lie in the plane of incidence depends on the electron density and $\cos^2\theta$, and decreases to 0 at $2\theta = 90°$. The initial energy is equally divided between the two components and no more than half the intensity is lost to this effect.

The Lorentz and polarization corrections can be made exactly. The absorption correction (A) depends upon the dimensions of the crystal and the type and number of atoms in the unit cell. It is possible to make a calculated correction for this effect if the exact dimensions of the crystal are known exactly, although the computations are time-consuming and inexact. The best approach is to select a small crystal whose dimensions are as uniform as possible.

The scale factor, K, is primarily a function of crystal size, exposure time, temperature, and film development methods. Its exact value is of importance only if the structure factor amplitudes are to be put on an absolute basis (see page 62). If the scaling is omitted, relative structure factor amplitudes, $|F_{rel,hkl}|$, are obtained. For later purposes, we define the observed structure factor amplitude, $|F_{o,hkl}|$, as

$$|F_{o,hkl}| = K|F_{rel,hkl}|. \qquad (6)$$

CALCULATED STRUCTURE FACTOR AMPLITUDES

The scattering power of a given atom for a given reflection at absolute zero is known as its atomic scattering factor, f_o, and is expressed in terms of the scattering power of an equivalent number of electrons located at the position of the atomic nucleus. If one assumes spherical atoms, this scattering power is a function only of the atom type and $(\sin\theta)/\lambda$. It is independent of the position of the atom in the unit cell. At $(\sin\theta)/\lambda = 0$ the value of f_o is always equal

to the total number of electrons in the atom. As $(\sin\theta)/\lambda$ increases, f_o decreases because x-rays scattered from different parts of the electron cloud become increasingly out of phase. The variation of the scattering power with $(\sin\theta)/\lambda$ is a direct result of the finite size of the electron cloud.

As previously discussed, the structure factor, $F_{hk\ell}$, is the resultant of j waves scattered in the direction of the reflection $hk\ell$ by the j atoms in the unit cell. [See Equations (2)-(4).] Each of these waves had an amplitude, f_j, the scattering factor for the atom, and a phase, ϕ_j, with respect to the wave scattered by hypothetical electrons at the cell origin. The phase, ϕ_j, is a function of the position of the atom in the unit cell and the direction of reflection.

$$\phi_j = 2\pi(hx_j + ky_j + \ell z_j) \tag{7}$$

The integers h, k, and ℓ indicate the direction of the reflection. x_j, y_j, and z_j are the fractional coordinates of the atom and are defined by

$$x_j = u_j/a \tag{8}$$

$$y_j = v_j/b \tag{9}$$

$$z_j = w_j/c \tag{10}$$

where

u_j, v_j, w_j = absolute coordinates along the a, b, and c axes (A.);

a,b,c = lengths (A.) of unit cell axes.

The expression for the structure factor given by Equation (4) can be rewritten in the form

$$F_{hk\ell} = \sum_j f_{o,j} \exp(2\pi i(hx_j + ky_j + \ell z_j)). \tag{11}$$

For purposes of computation, the trigonometric equivalent of $e^{i\phi_j}$ is substituted

into (11), giving

$$F_{hk\ell} = \sum_j f_{o,j} \cos 2\pi(hx_j + ky_j + \ell z_j) + i \sum_j f_{o,j} \sin 2\pi(hx_j + ky_j + \ell z_j). \quad (12)$$

If we let

$$A(hk\ell) = \sum_j f_{o,j} \cos 2\pi(hx_j + ky_j + \ell z_j), \quad (13)$$

and

$$B(hk\ell) = \sum_j f_{o,j} \sin 2\pi(kx_j + ky_j + \ell z_j), \quad (14)$$

the structure factor amplitude and phase can be calculated by the following relationships:

$$|F_{hk\ell}| = (A^2(hk\ell) + B^2(hk\ell))^{1/2} \quad (15)$$

$$\phi_{hk\ell} = \tan^{-1}(B(hk\ell)/A(hk\ell)). \quad (16)$$

Since $f_{o,j}$ refers to the scattering power of an atom at absolute zero, a temperature correction must be applied to each atomic scattering factor. The nature of this correction factor will be discussed in some detail in a later section. For the present purposes, we will only acknowledge the necessity of a temperature correction.

The conclusions to be drawn from this discussion are as follows: Given the respective unit cell coordinates for the members of an arbitrary collection of atoms, it is possible to calculate the phases and amplitudes of the structure factors associated with that set of atoms. Notice that only <u>one</u> set of structure factors can be obtained from any given collection of atoms.

The question of importance in structure determination is the converse of the one we've been discussing, namely, if a set of structure factor amplitudes (the

diffraction data) is given, can we compute the structure? Consideration of this question leads to the most important problem in x-ray crystallography — the so-called phase problem.

THE PHASE PROBLEM IN X-RAY CRYSTALLOGRAPHY

Equation (11) may be more generally written as an integral,

$$F_{hk\ell} = \int \rho(\vec{r})\exp(2\pi i(hx + ky + \ell z))dr, \qquad (17)$$

where

$\rho(\vec{r})$ = the electron density distribution function;

$\vec{r}$ = vector from origin to point (x,y,z) in unit cell.

By means of the Fourier inversion theorem $\rho(\vec{r})$ may be expressed in terms of $F_{hk\ell}$, giving

$$\rho(\vec{r}) = \rho(x,y,z) = \frac{1}{V}\sum_{h=0}^{\infty}\sum_{k=0}^{\infty}\sum_{\ell=0}^{\infty} F_{hk\ell}\exp(-2\pi i(hx+ky+\ell z)), \qquad (18)$$

the maxima of which represent the positions of the atoms (25). The symbol V represents the volume of the unit cell. See Buerger (23), Chapter 13, for another approach to the derivation of Equation (18).

It would appear, from Equation (18), that if the structure factor amplitudes and phases are known, the electron-density distribution of the unit cell can be calculated. Thus, if the Fourier series given by (18) could be computed from diffraction data, the structure would immediately be known. Only the structure factor amplitudes are given by the diffraction data. The necessity for supplying the missing information is the source of the phase problem.

The solution of the phase problem by the symbolic addition method, as applied to the present problem, is discussed in the next section.

One question which should be examined, in view of the previous discussion, is whether there is necessarily a unique relationship between structure factor amplitudes and electron density, i.e., whether a given set of intensity data corresponds to one and only one chemical structure. It would appear from Equation (18) that any arbitrary set of phases, $\phi_{\underline{hk\ell}}$, would give rise to an acceptable electron-density distribution, and the answer to the question would be "no." What has been overlooked in this argument is that the electron-density distribution is severely restricted. Since we are concerned with real objects, we expect the $\rho(\underline{xyz})$ to be everywhere real, positive, and continuous. We also expect the electron density to be more or less concentrated in spherical regions which we call atoms. We also require that the atoms be located so as to form structures with reasonable interatomic distances and angles and that the molecules not approach one another too closely. Taken together, these restrictions become so severe that the solutions appear to be unique for practical purposes.

The importance of the above conclusion is evident. If it were possible to obtain more than one solution which satisfied the above requirements for a given set of diffraction data, then the usefulness of x-ray crystallography for structure determination would be diminished greatly.

SOLUTION OF THE PHASE PROBLEM BY THE SYMBOLIC ADDITION METHOD

INTRODUCTION (23, 25)

Little progress had been made toward a general solution to the phase problem prior to 1950. The relative inactivity in this area was due to the general belief among crystallographers that a solution to the phase problem did not exist, even in principle.

The first breakthrough occurred in 1947 when Harker and Kasper discovered that some explicit relationships existed between amplitudes and phases (26). Their discovery initiated a new era in the science of crystal-structure analysis.

The symbolic addition method is one of several schemes proposed during the last twenty years for the solution of the phase problem. It has proved to be the most powerful approach available for the solution of light-atom, centrosymmetric crystals. In 1963, a generalization of the method to include noncentrosymmetric structure problems was introduced.

DEVELOPMENT OF SYMBOLIC ADDITION METHOD

Karle has written an excellent review of the many different attempts to find a general solution to the phase problem (25). In this paper, he describes the derivation of the early phase-determining formulas which led eventually to the symbolic addition method. His approach was based on the thought that the probability that the sign of a given structure factor was positive was one-half, until other intensities were known. Once a set of intensities was known, this probability deviated from one-half. This approach yielded phase-determining relations involving structure factor amplitudes alone, structure factors alone, or a mixture of the two. The manner in which the theory was developed, by integrating the atomic coordinates over all positions in the unit cell, implied that the probability answered the following question:

> Given the set of magnitudes and signs involved in a particular phase-determining relation, and given all possible atomic configurations having that set of magnitudes and signs, what is the fraction of the configurations which have a positive sign for the particular structure factor in question?

For the larger structure factors, it was likely that the relative number of possible configurations leading to a particular sign far exceeded the number leading to the opposite sign. In such a case, this was indicated by the probability theory, and a sign could be accepted with considerable assurance. A detailed account of the initial use of the joint probability distribution was published in ACA Monograph No. 3 (64).

The phase determination procedure outlined in ACA Monograph No. 3 involved defining a basic set of signs through the use of probability formulas which utilized the observed $|\underline{F}_{hk\ell}|$'s. This basic set was then used in conjunction with additional probability formulas to continue the phase generation. One of the major objections to this procedure was that the generation of the basic set of signs involved difficult and/or extensive, time-consuming calculations. In order to alleviate this difficulty, the phase determination procedure was revised, and the so-called symbolic addition method came into being.

In the revised procedure, the phase generation was initiated and carried out in terms of a small, properly chosen set of specified signs and unknown symbols. The advantage of employing symbols at the start was that it permitted the use of simpler formulas with the largest structure factor amplitudes immediately, without the requirement for establishing their signs initially.

NORMALIZED STRUCTURE FACTORS

In order to simplify the expressions for the probability distribution of the structure factor amplitudes, Karle and Hauptman defined the normalized structure factor $\underline{E}_{\underline{h}}$ (27)[1]. The normalized structure factor amplitude was defined by

$$|\underline{E}_{\underline{h}}|^2 = |\underline{F}_{\underline{h}}|^2/\varepsilon \sum_{j=1}^{N} f_j^2 \qquad (19)$$

where

$|\underline{F}_{\underline{h}}|$ = structure factor magnitude on an absolute scale;

$\sum_{j=1}^{N} f_j^2$ = sum of squares of atomic scattering factors for all $\underline{N}$ atoms in the unit cell;

ε = an integer which is generally 1 but may assume other values, as discussed below.

[1] $\underline{E}_{\underline{h}}$ is the same as $\underline{E}_{hk\ell}$, $\underline{h}$ will be substituted for $hk\ell$ in the discussion whenever it is convenient.

The effect of including ε is to reduce the significance of reflections which belong to a class having, for reasons of space group symmetry, abnormally large $|\underline{F_h}|$.

The distribution of $|\underline{E_h}|$ is, in principle, and often in practice, independent of the size and content of the unit cell. It does depend on the presence or absence of a center of symmetry and provides a statistical test for centric or acentric distribution of intensities. The distributions are subject to being disturbed by particular atomic distributions in the unit cell and should be treated with caution. (For examples, see pages 62, 143.)

NONCENTROSYMMETRIC SYMBOLIC ADDITION

Two addition formulas have found the greatest applicability for phase determination in acentric crystals: namely, the sigma-2 formula and the tangent formula. An addition formula involves relationships between certain phases, $\phi_{\underline{h}}$[2], $\phi_{\underline{k}}$[2], and $\phi_{\underline{h-k}}$[2] where the values of $\phi_{\underline{h}}$ is related to the values of pairs of phases, $\phi_{\underline{k}}$, $\phi_{\underline{h-k}}$, the sum of whose indices is $\underline{h}$.

Derivation of the Tangent Formula (28)

Karle and Hauptman derived a relation for $\underline{E_h}$ by probability methods,

$$E_{\underline{h}} \approx \sigma_2^{3/2}\ \sigma_3^{-1}\ \left\langle E_{\underline{k}} E_{\underline{h-k}} \right\rangle_{\underline{k}} \quad , \tag{20}$$

where

$$\sigma_{\underline{m}} = \sum_{\underline{j}=1}^{\underline{N}} \underline{Z_j^m};$$

$\underline{Z_j}$ = atomic number of the $\underline{j}$th atom in the unit cell;

$\underline{N}$ = total number of atoms in the unit cell.

---

[2] If $\underline{h} = \underline{h_1}, \underline{k_1}, \underline{\ell_1}$, $\underline{k} = \underline{h_2}, \underline{k_2}, \underline{\ell_2}$, then $\underline{h-k} = (\underline{h_1}-\underline{h_2})$, $(\underline{k_1}-\underline{k_2})$, $(\underline{\ell_1}-\underline{\ell_2})$; or, $\underline{h} = \underline{k} + \underline{h-k}$.

If we write $\underline{E}_{\underline{h}} = |\underline{E}_{\underline{h}}| \cos \phi_{\underline{h}} + i|\underline{E}_{\underline{h}}| \sin \phi_{\underline{h}}$, then (20) becomes

$$|E_{\underline{h}}| \cos \phi_{\underline{h}} \approx \sigma_2^{3/2}\sigma_3^{-1} \left\langle |E_{\underline{k}}||E_{\underline{h-k}}| \cos (\phi_{\underline{k}} + \phi_{\underline{h-k}}) \right\rangle_{\underline{k}} \qquad (21)$$

$$|E_{\underline{h}}| \sin \phi_{\underline{h}} \approx \sigma_2^{3/2}\sigma_3^{-1} \left\langle |E_{\underline{k}}||E_{\underline{h-k}}| \sin (\phi_{\underline{k}} + \phi_{\underline{h-k}}) \right\rangle_{\underline{k}} \qquad (22)$$

With a sufficient number of terms in the averages and $\underline{k}$ random, $|\underline{E}_{\underline{h}}| \cos \phi_{\underline{h}}$ and $|\underline{E}_{\underline{h}}| \sin \phi_{\underline{h}}$ are normally distributed about the means given by (21) and (22).

A particular virtue about (21) and (22) is that $\tan \phi_{\underline{h}}$ may be computed with good accuracy with only a restricted number of basic phases associated with the larger $|\underline{E}_{\underline{h}}|$'s.

$$\tan \phi_{\underline{h}} \approx \frac{\left\langle |E_{\underline{k}}||E_{\underline{h-k}}| \sin (\phi_{\underline{k}} + \phi_{\underline{h-k}}) \right\rangle_{\underline{k}}}{\left\langle |E_{\underline{k}}||E_{\underline{h-k}}| \cos (\phi_{\underline{k}} + \phi_{\underline{h-k}}) \right\rangle_{\underline{k}}} \qquad (23)$$

Equation (23) is called the tangent formula and will be referred to throughout this thesis. One important feature of the tangent formula is that it is valid for all $|\underline{E}_{\underline{h}}|$. There are no restrictions on the magnitude of the structure factors which can be used.

Derivation of the Sigma-2 Formula (28)

For the larger structure factor amplitudes, Equation (20) leads to an approximate formula which plays a significant role in the initial phase determination. Equation (20) can be rewritten,

$$1 \approx \sigma_2^{3/2}\, \sigma_3^{-1} \left\langle |E_{\underline{h}}^{-1}||E_{\underline{k}}||E_{\underline{h-k}}| \exp [i(-\phi_{\underline{h}} + \phi_{\underline{k}} + \phi_{\underline{h-k}})] \right\rangle_{\underline{k}}, \qquad (24)$$

by setting $\underline{E}_{\underline{h}} = |\underline{E}_{\underline{h}}| \exp (i\phi_{\underline{h}})$. Probability arguments show that for the largest $|\underline{E}_{\underline{h}}|$ values, $(\phi_{\underline{h}} - \phi_{\underline{k}} - \phi_{\underline{h-k}})$ is distributed about zero and, generally, assumes small values.

We then write

$$1 \approx C\ \sigma_2^{3/2}\sigma_3^{-1} \left\langle |E_{\bar{h}}^{-1}||E_{\bar{k}}||E_{\overline{h-k}}|[\cos(-\phi_{\bar{h}} + \phi_{\bar{k}} + \phi_{\overline{h-k}}) + i \sin(-\phi_{\bar{h}} + \phi_{\bar{k}} + \phi_{\overline{h-k}})] \right\rangle_{\bar{k}_r} \tag{25}$$

where $\bar{k}_r$ represents the restricted values of $hk\ell$ for which the corresponding $|E_{\bar{k}}|$ and $|E_{\overline{h-k}}|$ values are large. Restricting attention to the imaginary part of (25) gives

$$\left\langle |E_{\bar{k}}||E_{\overline{h-k}}| \sin(-\phi_{\bar{h}} + \phi_{\bar{k}} + \phi_{\overline{h-k}}) \right\rangle_{\bar{k}_r} \approx 0. \tag{26}$$

We take the first term of the Taylor expansion of the sine function since its argument is generally small and obtain

$$\left\langle |E_{\bar{k}}||E_{\overline{h-k}}| (-\phi_{\bar{h}} + \phi_{\bar{k}} + \phi_{\overline{h-k}}) \right\rangle_{\bar{k}_r}$$

$$= p^{-1} \sum_{\bar{k}_r} |E_{\bar{k}}||E_{\overline{h-k}}| (-\phi_{\bar{h}} + \phi_{\bar{k}} + \phi_{\overline{h-k}}) \approx 0 \tag{27}$$

where there are p terms included in $\bar{k}_r$. Equation (27) may be rewritten to give a new phase-determining formula,

$$\phi_{\bar{h}} \approx \frac{\sum_{\bar{k}_r} |E_{\bar{k}}||E_{\overline{h-k}}| (\phi_{\bar{k}} + \phi_{\overline{h-k}})}{\sum |E_{\bar{k}}||E_{\overline{h-k}}|} \tag{28}$$

in which the $\phi_{\bar{h}}$ are defined as linear functions of other phases, specifically the weighted averages of $(\phi_{\bar{k}} + \phi_{\overline{h-k}})$ associated with the largest $|E_{hk\ell}|$ values. If all the $|E_{hk\ell}|$ are of the same order of magnitude, we obtain

$$\phi_{\overline{h}} \approx \left\langle \phi_{\overline{k}} + \phi_{\overline{h-k}} \right\rangle_{\overline{k}_r} . \qquad (29)$$

Equation (29) is called the sigma-2 formula and is referred to throughout the thesis.

Probability Considerations (28)

The sigma-2 formula is only an approximation and cannot be used to determine phases without auxiliary information. This information is provided by the use of a probability criterion which determines the acceptability of a given phase indication from the sigma-2 formula.

For acentric crystals, the variance of a given phase indication is computed for a given set of $(\phi_{\underline{k}} + \phi_{\underline{h-k}})$ and κ, where

$$\kappa = 2\,\sigma_3\sigma_2^{-3/2}\,|E_{\overline{h}}||E_{\overline{k}}||E_{\overline{h-k}}| . \qquad (30)$$

The variance of $\phi_{\underline{h}}$ for a fixed set of $(\phi_{\underline{k}} + \phi_{\underline{h-k}})$ and κ is given by Equation (31).

$$V = \pi^2/3 + [I_o(\alpha)]^{-1} \sum_{n=1}^{\infty} \frac{I_{2n}(\alpha)}{n^2} + 4\,[I_o(\alpha)]^{-1} \sum_{n=0}^{\infty} \frac{I_{2n+1}(\alpha)}{(2n+1)^2} , \qquad (31)$$

where

$$\alpha = \left\{ \left[\sum_{\overline{k}_r} \kappa \sin (\phi_{\overline{k}} + \phi_{\overline{h-k}}) \right]^2 + \left[\sum_{\overline{k}_r} \kappa \cos (\phi_{\overline{k}} + \phi_{\overline{h-k}}) \right]^2 \right\}^{1/2} \qquad (32)$$

and

$$I_j(\alpha) = \text{a Bessel function}^3 .$$

In practice, the variance was evaluated with the aid of a plot of $\underline{V}$ versus α, as shown in Fig. 11. A phase indication was accepted if $\underline{V}$ was less than 0.5 square radians.

---

[3] The Bessel function of order $\underline{p}$ is defined by $\underline{I}_{\underline{p}}(\underline{x}) = \sum_{\underline{m}=0}^{\infty} \frac{(1/2\underline{x})^{\underline{p}+2\underline{m}}}{\underline{m}!\,\Gamma(\underline{p}+\underline{m}+1)}$ (71).

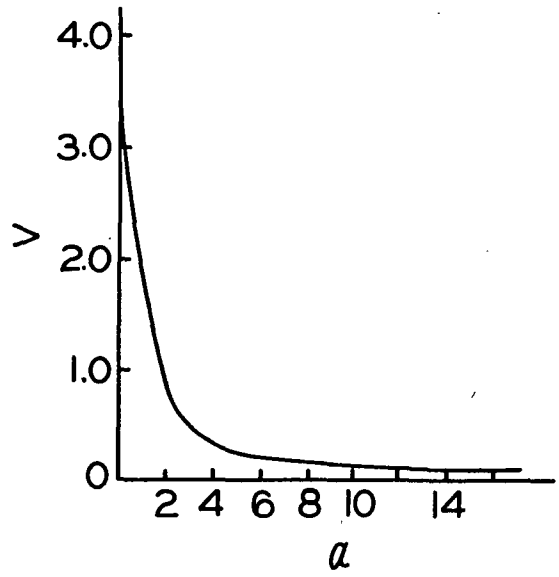

Figure 11. Curve Showing the Variance, V (in Square Radians), of a Phase Angle Determined from Known Values of Other Phase Angles. The Variance is Expressed as a Function of α Defined in Equation (32) (28)

VARIATIONS ON THE SYMBOLIC ADDITION METHOD

Two papers have recently appeared dealing with procedures for avoiding extensive use of the approximate sigma-2 relationship. The first, by Germain and Woolfson (29), describes a systematic, multisolution symbolic addition procedure based on the tangent formula and the use of several different starting sets of phases. The authors described a computer program which carries out their procedure.

The second paper, by Oh and Maslen (30), was concerned with the structure determination of iso-eremolactone, space group $P2_12_12_1$. In this work, the authors defined twenty phases, associated with very large $|E_{hk\ell}|$ values, by the sigma-2 formula. They next systematically expanded the starting set by recycling the tangent formula. A total of 200 $|E_{hk\ell}|$ greater than or equal to 1.50 were obtained. E-maps based on these phases revealed 20 of the 22 atoms in the structure.

This worker attempted, unsuccessfully, to apply the second method to the structure determination of cis-pinocarvyl-p-nitrobenzoate, as described on pages 149-52.

EXPERIMENTAL APPLICATION OF THE SYMBOLIC ADDITION METHOD

A detailed discussion of the application of the symbolic addition method to a crystal in space group $P2_12_12_1$ is included in the Data Analysis section. Therefore, the discussion here will be limited to an outline of the steps involved in phase determination.

Preparation of Data Listings

Certain data listings are necessary for the application of the sigma-2 formula. These listings involve the combinations of $\overline{h}$, $\overline{k}$, and $\overline{h-k}$ which satisfy the relationship $\overline{h} = \overline{k}+\overline{h-k}$ and the κ associated with each addition triple.

Specification of Origin and Specification of Enantiomorph

A certain number of reflections are arbitrarily assigned phases according to the rules of Hauptman and Karle (31) for the purpose of defining the unit cell origin.

Specification of the enantiomorph is necessary due to the nature of acentric data. In general, the enantiomorph is determined by the assignment of a sign to a particular linear combination of phases which satisfies the definition of an invariant[4]. Examples of enantiomorph specification in space groups $P2_12_12_1$ and $P2_1$ are given on pages 67 and 144.

Hand Generation of Phases

The sigma-2 formula and variance criteria are used to generate phases. The origin and enantiomorph phases serve as a starting set.

[4] A structure invariant is a phase or linear combination of phases, whose value depends only on the structure and is independent of the choice of origin.

Tangent Formula Reiteration and Expansion

The tangent formula is used to refine the hand-generated phases, and then to expand the set to a lower minimum $|\underline{E}_{\underline{hk\ell}}|$.

Computation of E-Maps

Fourier maps are computed using the $|\underline{E}_{\underline{hk\ell}}|$'s and their associated symbolic addition phases as coefficients.

THE INFLUENCE OF TEMPERATURE

As previously mentioned, the atomic scattering power decreases for reflections of increasing $(\sin \theta)/\lambda$. This fall-off was attributed to the finite size of the electron cloud around the nucleus. The larger the cloud for a given number of electrons, the more rapid the decline in scattering effectiveness.

The atomic scattering factors ($\underline{f}_{o,\underline{j}}$) are calculated on the basis of the electron density in a stationary atom. The atoms in a crystal are always vibrating about their rest point, however. The magnitude of the vibration depends on the temperature, the mass of the atom, and the firmness with which it is held in place through its association with other atoms.

In general, the higher the temperature, the greater the thermal motion. The effect of greater motion is to spread the electron cloud over a greater volume, thereby increasing the rate of scattering power fall-off for the real atom relative to the stationary atom. Figure 12 illustrates this effect. It has been shown (23) that the change in scattering power can be given by

$$q_r = \exp\left(-B(\sin^2\theta)/\lambda^2\right). \qquad (33)$$

$\underline{B}$ is called the overall isotropic temperature factor — an experimentally-determined quantity for a given set of data. $\underline{B}$ is related to the mean-square amplitude ($\overline{\underline{U}^2}$)

of atomic vibration by

$$B = 8\pi^2 \overline{U^2} \ . \qquad (34)$$

During the various stages of structure refinement, individual isotropic temperature factors or individual anisotropic temperature factors can be given to each atom. The latter gives a temperature correction of the form

$$q_r = \exp\left[-(B_{11,r}h^2 + B_{22,r}k^2 + B_{33,r}\ell^2 + 2B_{12,r}hk + 2B_{13,r}h\ell + 2B_{23,r}k\ell)\right], \qquad (35)$$

where the $B_{ij,r}$ are the individual anisotropic temperature factors for atom r. Thus, the six $B_{ij,r}$ serve to help describe the ellipsoidal electron distribution of the anisotropically vibrating atom.

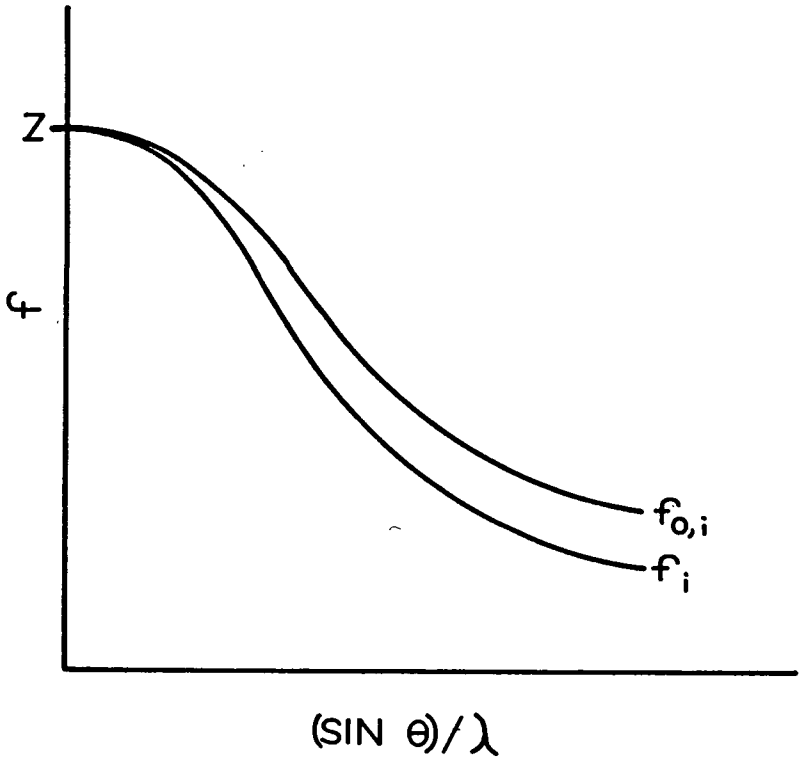

Figure 12. Effect of Temperature on the Atomic Scattering Power of Atom i, Having Atomic Number Z. $f_{o,i}$ = Atomic Scattering Power for Atom i at rest. f_i = Atomic Scattering Power for Atom i at a Finite Temperature

From the foregoing discussion, it can be seen that there are definite advantages to collecting intensity data at low temperatures (e.g., liquid nitrogen). Decreasing the temperature will result in a shrinkage of the atomic electron clouds, and the $\underline{f}_j$-curve will more closely resemble the $\underline{f}_{o,j}$-curve (see Fig. 12). Thus, the high $(\sin \theta)/\lambda$ reflections can be collected more effectively.

Another benefit of low temperatures is a significant decrease in exposure times. Under room temperature conditions, exposure times of 100 hours are quite common with light atom problems. The average exposure time for the work reported in this thesis was 13 hours — an improvement which clearly speaks for itself.

Low-temperature photographs have a lower average background intensity which makes the visual estimation of intensities easier.

Finally, the overall improvement in the intensity data coupled with the low temperature factors facilitates the location of hydrogen atoms by difference Fourier methods.

EXPERIMENTAL SECTION

SYNTHESIS OF trans-2-METHYLENE-5-(2-ISOPROPYLOL)-CYCLOHEXANOL

INTRODUCTION

The purpose of the experiments reported here was to confirm the original synthesis work discussed in the introductory section of this thesis. The previous reactions were run under conditions essentially identical to those of Matsubara (13) and Sato (15). Both of these workers reported trans-sobrerol diacetate to be a major product. This worker found no trace of a sobrerol derivative. Instead, a substantial yield of a crystalline material believed to be trans-2-methylene-5-(2-isopropylol)-cyclohexanol was obtained. The existence of such a compound had never been reported in the literature, and, therefore, it was decided that the experiment should be repeated. The results of the repeat experiments are presented on the following pages.

In order to simplify the discussions, trans-2-methylene-5-(2-isopropylol)-cyclohexanol will be referred to as trans-MIC, whenever it is convenient to do so. It is believed that no ambiguity or misunderstanding will arise from this practice.

GENERAL PROCEDURES

Reagent and Solvent Purification

β-Pinene

β-Pinene (96% pure) was obtained from commercial β-pinene (K and K Laboratories, 75% β-pinene) by fractional vacuum distillation on a spinning band column (32).

Lead Tetraacetate

Reagent-grade lead tetraacetate (K and K Laboratories, slurry in glacial acetic acid) was analyzed by the method suggested by Kharasch (33). The slurry was found to be 85% lead tetraacetate by weight (average of three determinations).

Dry Methanol

Dry methanol was prepared by the procedure of Lund and Bjerrum (34). Magnesium turnings (5 g.), iodine (0.5 g.), and reagent-grade methanol (900 ml.) were placed in a 2-liter, round-bottomed flask. The mixture was warmed until the iodine color disappeared or the reaction became vigorous. After refluxing four hours, the mixture was distilled, with the exclusion of moisture, through a Vigreux column. The initial 100, or so, ml. of distillate were discarded. Approximately 600 ml. of dry methanol were collected and stored in an air-tight container.

Physical Methods of Analysis

Infrared spectra were run on a Perkin-Elmer Recording IR Spectrophotometer, Model 21. Solid samples were run in potassium bromide pellets. Liquid samples were run neat between sodium chloride plates.

Nuclear magnetic resonance spectra were run on a Varian Analytical Spectrometer, Model A-60 A. Solid samples were dissolved in deuterated chloroform. Tetramethylsilane (TMS) was used for an internal standard. Hydroxyl protons were located by addition of deuterium oxide (D_2O) to the solution, and observing the disappearance of the hydroxyl peak.

Gas chromatography was carried out on an Aerograph Autoprep, Model A-700, gas chromatograph. A 5% FFAP (Free Fatty Acid Prep) on 70/80 acid-washed, DMCS-treated Chromosorb G column was used for all analyses. The column temperature was held at 175°C., and a He carrier gas flow rate of 60 ml./min. was maintained.

Melting points were measured on a Thomas Hoover Unimelt capillary melting point apparatus. All melting points were uncorrected.

Elemental analyses (C,H,O) were carried out by Geller Laboratories, Saddle River, New Jersey.

X-ray powder diffractograms were run on a North American Phillips water-cooled x-ray diffraction unit equipped with a wide-range goniometer and a Minneapolis-Honeywell strip chart recorder.

OXIDATION OF β-PINENE WITH LEAD TETRAACETATE

Oxidation Procedure

Matsubara's procedure (13) was followed with two modifications. Lead tetraacetate was substituted for red lead, and ether extractions were made during the workup of reaction products. Matsubara used benzene extracts.

β-Pinene (75 g., 0.55 mole), glacial acetic acid (707 ml.), and acetic anhydride (280 ml.) were mixed together in a two-liter flask which was equipped as shown in Fig. 13.

Lead tetraacetate slurry (331 g., 0.65 mole), was added to the stirred mixture in the flask in small portions over a period of two hours. During this time, the temperature of the solution stayed between 55 to 65°C. due to the heat given off by the reaction. Stirring was continued for one hour after all the lead tetraacetate had been added. The reaction solution was then poured into cold water and allowed to remain overnight.

Workup of Reaction Products

The water-oil mixture was extracted with three 600-ml. portions of ether. The combined extracts were neutralized by washing with saturated sodium bicarbonate solution. The neutralized extracts were then washed with three 1000-ml. portions of water and dried over anhydrous magnesium sulfate. Removal of the ether by distillation left a yellow, sweet-smelling oil, yield 101.8 g. Gas chromatographic analysis indicated that the oil consisted of five major components and a number of lesser ones.

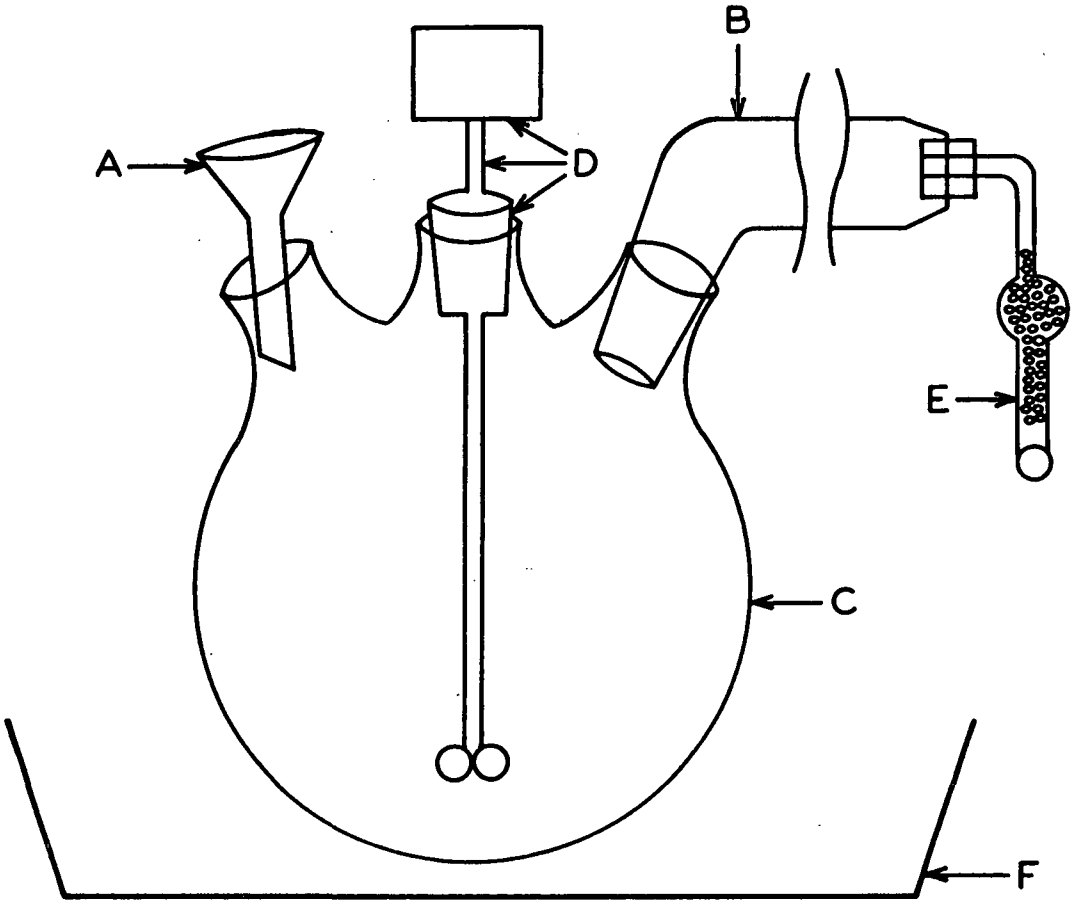

Figure 13. Experimental Apparatus

A. Powder funnel
B. Condenser
C. Two-liter flask
D. Stirring motor, propeller, and seal
E. Calcium chloride drying tube
F. Catch pan

Isolation of trans-MIC Diacetate

The product mixture was separated into six fractions by vacuum distillation over a spinning band column. Table IV shows the results of the distillation.

TABLE IV

FRACTIONAL DISTILLATION OF REACTION MIXTURE

Fraction	Weight, g.	Boiling Range, °C.	Pressure, mm. Hg
1	35.4	47-74	0.20
2	9.1	74-77	0.20
3	11.2	77-85	0.15
4	7.7	85-95	0.15
5	4.9	96-98	0.10
6	16.5	98-100	0.10
Loss through handling and residue	17.0		

Previous work (16) had shown Fraction one to contain trans-pinocarvyl acetate, myrtenyl acetate, and perilla acetate. Gas chromatographic analyses of Fractions two through six revealed that Fraction three contained a single major component whose retention time was 0.59 hour. Fractions five and six consisted principally of a single substance whose retention time was 1.7 hours. Fractions two and four were mixtures.

The infrared spectra of Fractions three and six were similar in the region 950-2000 $cm.^{-1}$. Fraction three showed strong absorption at 908 $cm.^{-1}$ and 1660 $cm.^{-1}$, indicative of a disubstituted alkene grouping. Fraction six showed strong absorption at 810 $cm.^{-1}$ and 1652 $cm.^{-1}$, suggesting the presence of a trisubstituted alkene grouping. Fraction three was believed to be trans-MIC diacetate on the basis of the infrared spectrum.

trans-2-Methylene-5-(2-isopropylol)-cyclohexanol (trans-MIC)

A dilute solution of sodium methoxide in methanol was prepared by adding sodium (0.4 g.) to dry methanol (350 ml.). Fraction three was added to the methanol solution and the mixture heated to the boiling point. Methyl acetate, formed in the transesterification, and methanol were distilled from the solution over a period of twenty-four hours. Additional dry methanol was added during this time. The distillation was stopped when the distillate gave a negative ferric hydroxamate test (35), indicating the absence of methyl acetate.

The solution remaining in the pot was poured into water (180 ml.), and the water solution was extracted four times with ether (40-ml. portions). The combined extracts were dried over anhydrous magnesium sulfate.

The ether was removed with a rotary evaporator, leaving a light yellow, crystalline solid. Recrystallization from benzene gave 2.8 g. white crystals, m.p. 129.5-130.0°C.

An additional 1.0 g. of crystals were obtained by evaporating the water-methanol solution which had previously been extracted with ether. This step was carried out because trans-MIC was known to be soluble in water.

Identification of the Crystals

A detailed comparison of the crystals obtained in the above reaction and the trans-MIC crystals used in the x-ray experiments was carried out. To simplify the following discussion, the crystals obtained by the present synthesis will be referred to as (II).

A mixture of trans-MIC and (II) melted at 129.0-130.0°C.

The infrared and NMR spectra of trans-MIC and (II) were identical. The same was true of their x-ray powder diffractograms.

Acetylation of trans-MIC produced a substance whose gas chromatographic retention time was 0.57 hour.

The conclusion drawn from the above results was that (II) and trans-MIC were identical. Therefore, the original synthesis work (16) was confirmed.

REACTION OF trans-MIC WITH BROMINE

The procedure of Wallach (36) was followed.

trans-MIC (0.45 g.) was dissolved in chloroform by warming. The solution was cooled, and a solution of bromine in chloroform (about 10% Br_2) was added dropwise. The bromine color disappeared with no accompanying evolution of gases. The addition of bromine solution was stopped when the color first persisted. No crystals formed during the addition, although small globules of a liquid which was not soluble in chloroform could be seen in the beaker. The beaker was set in a hood to allow the chloroform to evaporate.

Evaporation of the chloroform left a white crystalline mass. Recrystallization from chloroform gave white crystals, m.p. 116.0-117.0°C. Bromine analysis was run. Calculated for $C_{10}H_{18}O_2Br_2$: Br 48.6. Found: Br 48.7.

X-RAY EXPERIMENTAL STUDIES

INTRODUCTION

Crystal structure analyses follow a standard pattern in most cases which may be divided into several stages.

1. A suitable crystal must be selected. Two main requirements must be met: (a) it must have uniform internal structure, and (b) it must be of proper size and shape.

To satisfy the first requirement, a crystal must be pure at the molecular level. It must be a single crystal, i.e., not twinned or composed of microscopic subcrystals. It does not have to have particularly well-formed faces.

The choice of a suitably sized crystal depends upon a number of counter-balancing factors. The x-ray beam passes through a circular collimator, 1 mm. in diameter. According to Stout and Jensen (24), the beam intensity is uniform in a 0.5 x 0.5 mm. plateau in the center of the beam. Since it is necessary for all portions of the crystal to be exposed to the same radiation intensity, crystal dimensions should not exceed 0.5 x 0.5 mm. In practice, crystals with linear dimensions of 0.1 mm. to 0.3 mm. are preferred due to alignment difficulties encountered with larger crystals.

It is important that the crystal be shaped as uniformly as possible. There are at least two reasons for this. First, a crystal whose dimensions differ greatly will produce widely-varying spot shapes on the film which are difficult to estimate visually. Second, an absorption problem may arise if the incident and reflected rays have different average path lengths for different reflections. Thus, a systematic error may be introduced into the intensity data which is extremely difficult to correct. The point of this lengthy discourse on crystal selection was to emphasize the importance of selecting proper crystals. If one does not start with appropriate crystals, then the labor that follows may well be in vain.

2. The unit cell parameters and space group are determined.

3. The intensity data are collected.

4. The intensity data are converted to structure factor amplitudes by correction for Lorenz and polarization effects and other physical or geometrical factors.

5. An arrangement of atoms is found which is consistent with the experimental data. The successful completion of this step usually depends on the solution of the phase problem.

6. The structure is refined.

7. The refined structure is analyzed for pertinent structural characteristics. Step (5) is the only part of the pattern which cannot be carried out in a more-or-less routine fashion. The solution of a structure will fail, however, if this step is not successfully completed.

Steps (1), (2), and (3) are discussed in this section of the thesis. Steps (4), (5), and (6) can be found in the Data Analysis section which follows. The results of Step (7) are included in the Results and Discussion section.

CRYSTAL SELECTION

The crystals of trans-MIC on hand had been recrystallized from benzene. They were long, thin needles which were unsuitable for x-ray studies. Water was found to be a more suitable recrystallization solvent, producing skewed prisms of the approximate shape shown in Fig. 14. The needle axis was arbitrarily chosen to be the a axis. The crystals grew quite large. It was necessary to trim them to size with a razor blade. All cutting and mounting of crystals were carried out with the aid of a binocular microscope. The internal uniformity of a crystal was estimated simply by looking at it through the microscope. The final check on the suitability of a crystal involved the quality of the diffraction pattern it produced. If the reflections were diffuse or separated into several parts, the crystal was rejected. The two crystals selected for the collection of intensity data had the properties listed in Table V.

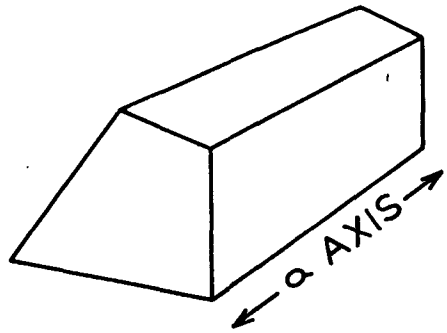

Figure 14. Approximate Crystal Shape of trans-MIC Crystals Recrystallized from Water

TABLE V

PROPERTIES OF TWO CRYSTALS SELECTED FOR INTENSITY DATA COLLECTION

Crystal	Axes of Rotation	Dimensions, mm.	Linear Absorption Coefficient, $\mu cm.^{-1}$	μR
1	c	0.58x0.41x0.20	6.11	0.18
2	a	0.50x0.30x0.20	6.11	0.15

The linear absorption coefficient, μ, was calculated by the formula given by Buerger (21, p. 181),

$$\mu = f \{P_C(MA)_C + P_H(MA)_H + P_O(MA)_O\} \qquad (36)$$

where

f = experimentally-determined density of crystals;

P_i = fraction by weight of element i;

$(MA)_i$ = mass absorption coefficient for element i;

$(MA)_C$ = 4.60 $cm.^2/g.$;

$(MA)_H$ = 0.43 $cm.^2/g.$; and

$(MA)_O$ = 11.5 $cm.^2/g.$

DETERMINATION OF CRYSTAL DENSITY

The density of trans-MIC was determined by the flotation method (37). Benzene (sp. gr. 0.88) and 1,1,2,2-tetrabromoethane (sp. gr. 2.9) were chosen for the

determination because their respective densities bracketed that of trans-MIC. In addition, the crystals were not highly soluble in either of the two liquids.

Benzene (50 ml.) was placed in a 100-ml. beaker. Three or four crystals of trans-MIC were placed in the beaker and allowed to settle to the bottom. 1,1,2,2-Tetrabromoethane was added dropwise, with stirring, until the crystals became "suspended" in the liquid mixture. The crystals never were truly suspended in the sense of being stationary. Rather, a condition was reached where the moving crystals displayed no tendency to rise completely to the liquid surface or sink to the bottom of the beaker and remain there. The liquid density was then measured with the aid of a calibrated pycnometer. The crystal density was assumed to equal that of the liquid.

The density of trans-MIC was found to be 1.123 g./cm.^{3} (average of three determinations).

CRYSTAL MOUNTING

The crystal was mounted on the end of a glass fiber by the following procedure. The selected crystal was placed on a clean microscope slide. A glass fiber was chosen whose end diameter was smaller than that of the crystal face to which the fiber would be glued. The fiber end was dipped into freshly-prepared epoxy glue. Excess glue was removed from the fiber end so that a ball of epoxy remained which was slightly smaller than the fiber end. The crystal was mounted by touching the fiber end to the desired face of the crystal. The crystal and fiber were then allowed to stand for one hour while the glue cured. The opposite end of the fiber was then inserted into a clay-filled chuck which fit into the goniometer head on the Weissenberg camera. Figure 15 illustrates the relationship between the mounted crystal, x-ray beam collimator, and cryostat nozzle when they all are in position.

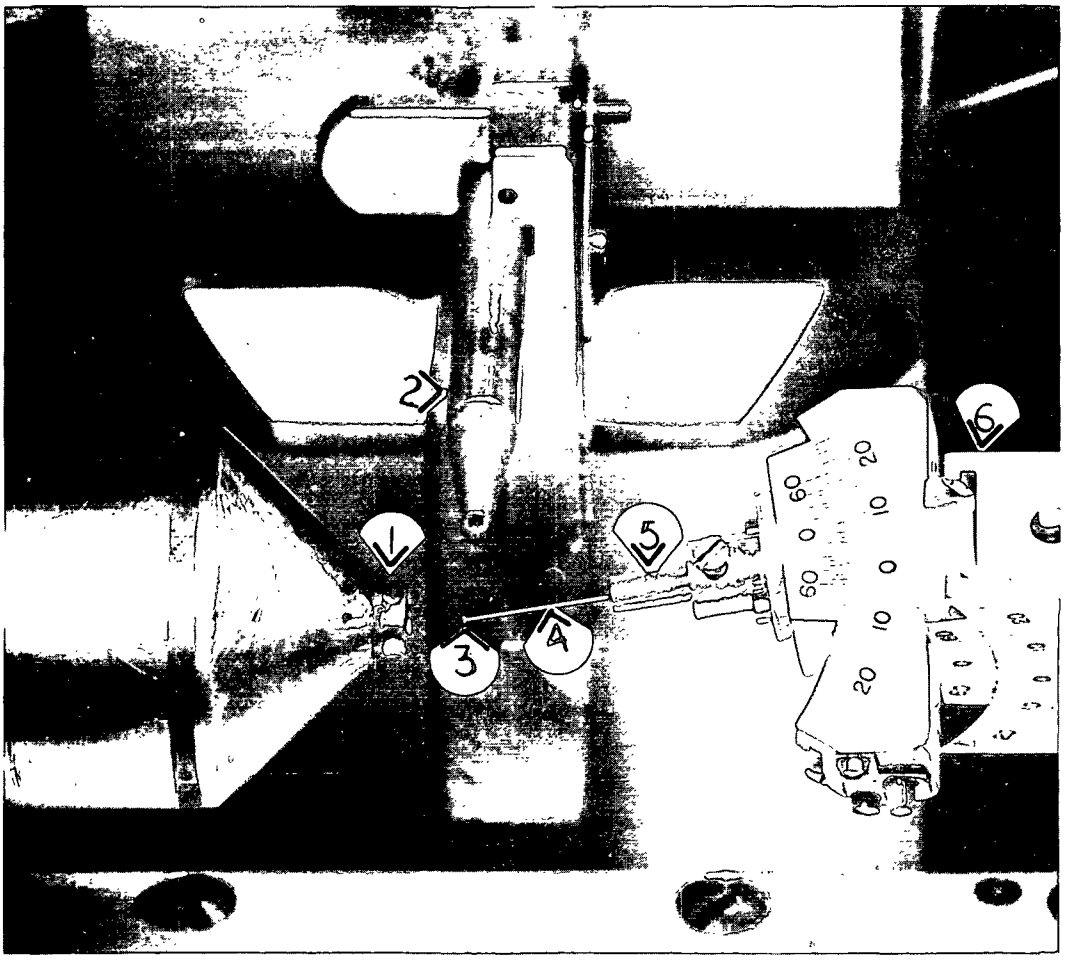

Figure 15. Photograph of Mounted Crystal

1. Liquid Nitrogen Cryostat Nozzle
2. X-ray Beam Collimator
3. Crystal
4. Glass Fiber
5. Chuck
6. Goniometer Head

As previously mentioned, all crystal mounting procedures were carried out with the aid of a binocular microscope.

CRYSTAL ALIGNMENT

The crystal rotation axis was lined up parallel to the desired unit cell axis by the method described in Bunn (22).

SPACE GROUP DETERMINATION

The space group was determined from preliminary photographs. An oscillation photograph around the c axis indicated the reciprocal lattice possessed a mirror plane perpendicular to the axis of rotation ($\underline{m}_x$ symmetry). Only crystals belonging to the monoclinic class or higher possess this symmetry (Fig. 16a).

A zero-layer Weissenberg photograph around the c axis contained two axes, ninety degrees apart, which divided the film into distorted mirror images (mm symmetry) (Fig. 16b).

The preliminary photographs indicated that the requirements of mm symmetry were met, and the crystal had orthorhombic (or higher) symmetry. Consideration of the systematic extinctions in the a axis and c axis zero-level Weissenberg photographs (0k0, k odd; h00, h odd; 00l, l odd) showed the crystal to belong to space group $P2_12_12_1$.

LOW TEMPERATURE APPARATUS

The liquid nitrogen cryostat had been constructed for earlier x-ray studies. Figure 17 contains a diagram of the cryostat which illustrates the important features. The liquid nitrogen reservoir (A) is filled to a level just below the top of the copper tubing (B). Some of the evaporating nitrogen flows into the copper tubing at (C). This gas then flows down through the tubing and out the nozzle onto the

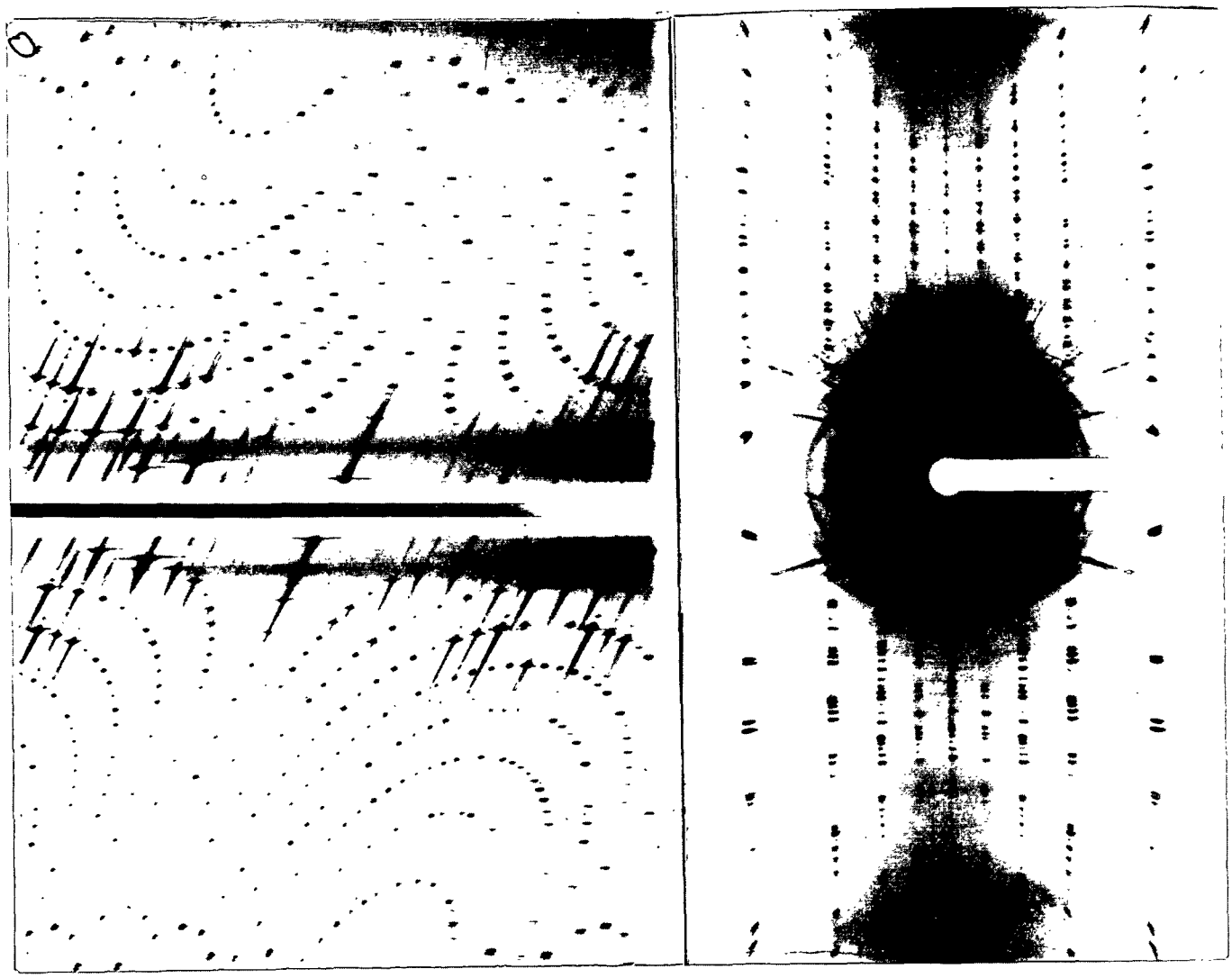

(b) (a)

Figure 16. Preliminary c Axis Exposures of trans-MIC: (a) Rotation Photograph, $\frac{m}{x}$ Symmetry; (b) Zero-Layer Weissenberg Photograph, $\frac{mm}{}$ symmetry

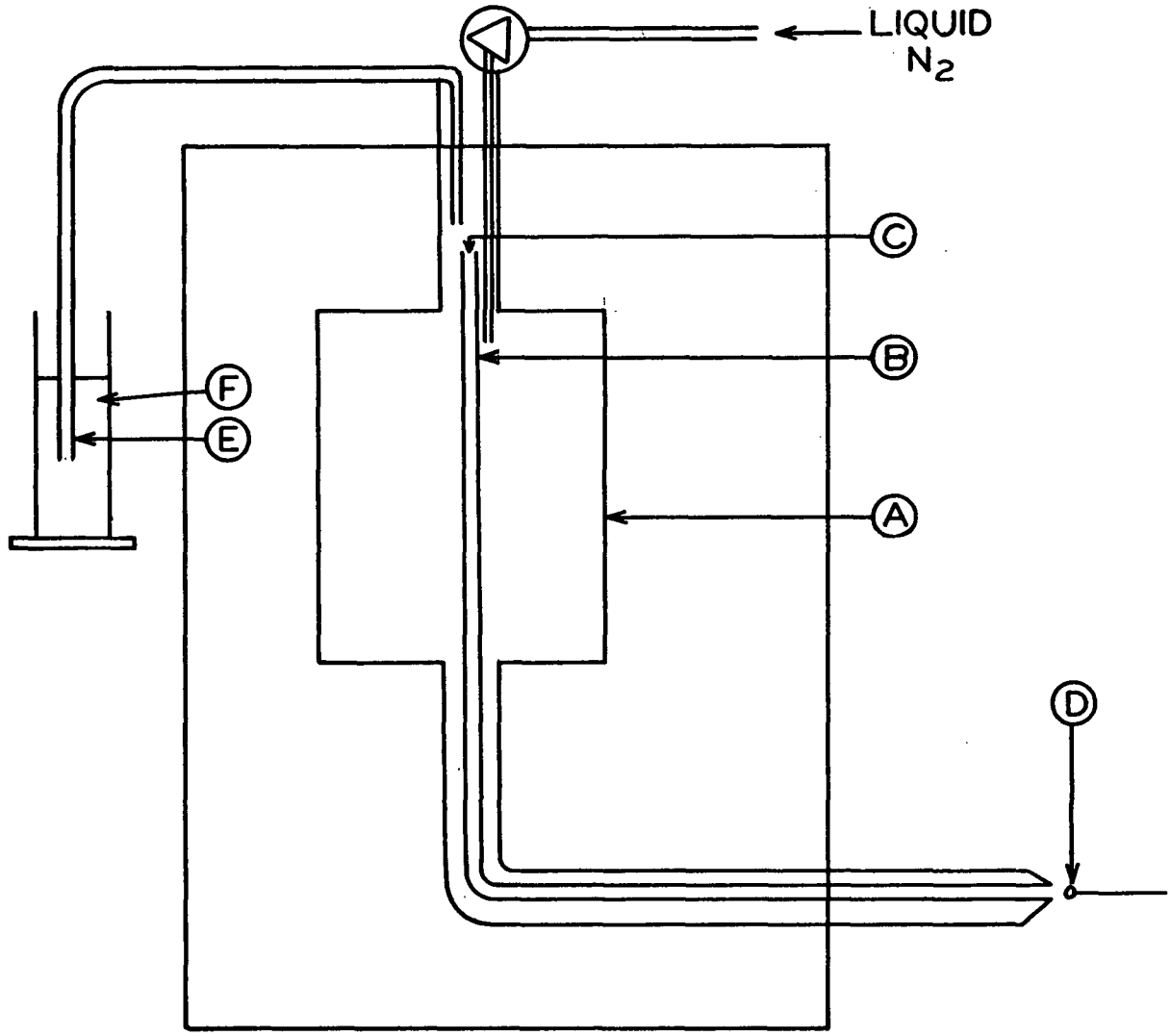

Figure 17. Diagram of Liquid Nitrogen Cryostat

A. Liquid Nitrogen Cryostat
B. Copper Tubing
C. Entrance to Copper Tubing
D. Crystal
E. Vent Tubing
F. Oil Reservoir

crystal (D). The gas temperature is maintained at nearly that of liquid nitrogen during its pass through the cryostat. A slight warming occurs in the space between the nozzle and the crystal ($\sim$ 1 mm.). The rate of gas flow through the nozzle can be varied somewhat by pushing the vent tubing (E) beneath the surface of the oil (F) to a greater or lesser extent. The actual rate of gas flow was never measured.

The cryostat had a capacity of 5.75 liters and a running time of about five hours. Exposures requiring longer than five hours were made by refilling the cryostat at regular intervals during the course of the run. A practice of adding 6.5 pounds of liquid nitrogen every three hours was found to be satisfactory.

It was necessary to enclose the crystal, cryostat nozzle, and x-ray camera in a dry-box to prevent the formation of ice on the crystal and apparatus during a low temperature exposure.

It was also necessary to maintain the photographic film at near room temperature during a low temperature exposure because the rate of film blackening decreases with a decrease in temperature. The control system is shown in Fig. 18.

A thermistor probe (A) was connected to a Thermistep Heating Controller (B). The signal from the controller operated the heating mantle (C) on the film holder (D). The temperature of the outer surface of the film holder was maintained at 20 $\pm$ 1.5°C. during exposures.

For detailed discussions of the specifications and construction of the low temperature apparatus, see Ham (38) and Richards (39).

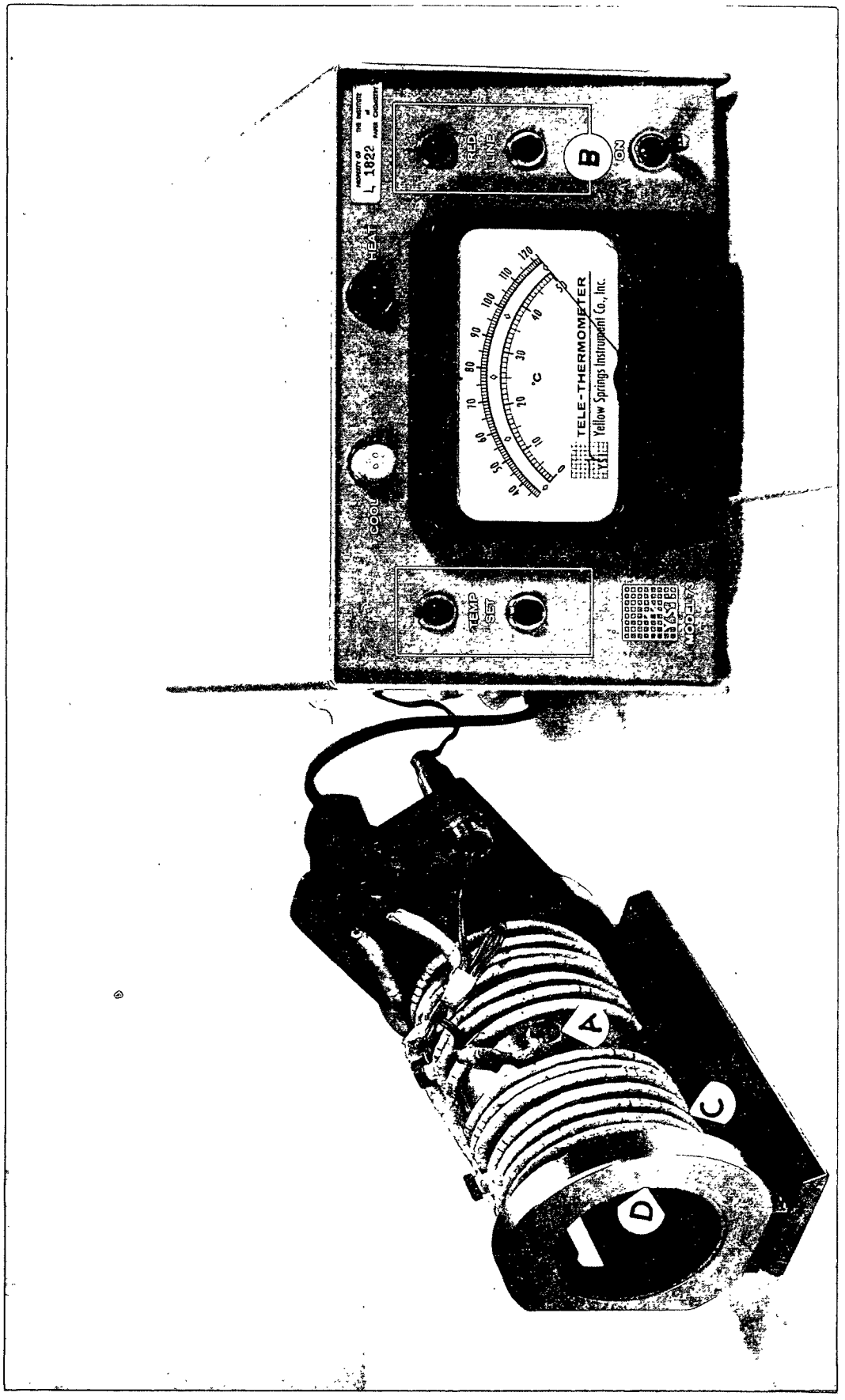

Figure 18. Temperature Control System for Film Holder
A. Thermistor Probe; B. Thermistep Heating Controller; C. Heating Mantle; D. Film Holder

GEOMETRIC DATA COLLECTION

UNIT CELL PARAMETERS

Back Reflection Photographs

Data for the unit cell parameters were collected by means of zero-layer, back-reflection Weissenberg photographs. A detailed discussion of back-reflection techniques can be found in Chapter 21 of Buerger (21).

In order to use an ordinary Weissenberg camera for back-reflection exposures, one must alter the film by cutting a slot in the center. This enables the x-ray beam collimator to be introduced through the center of the moving film (see Fig. 19).

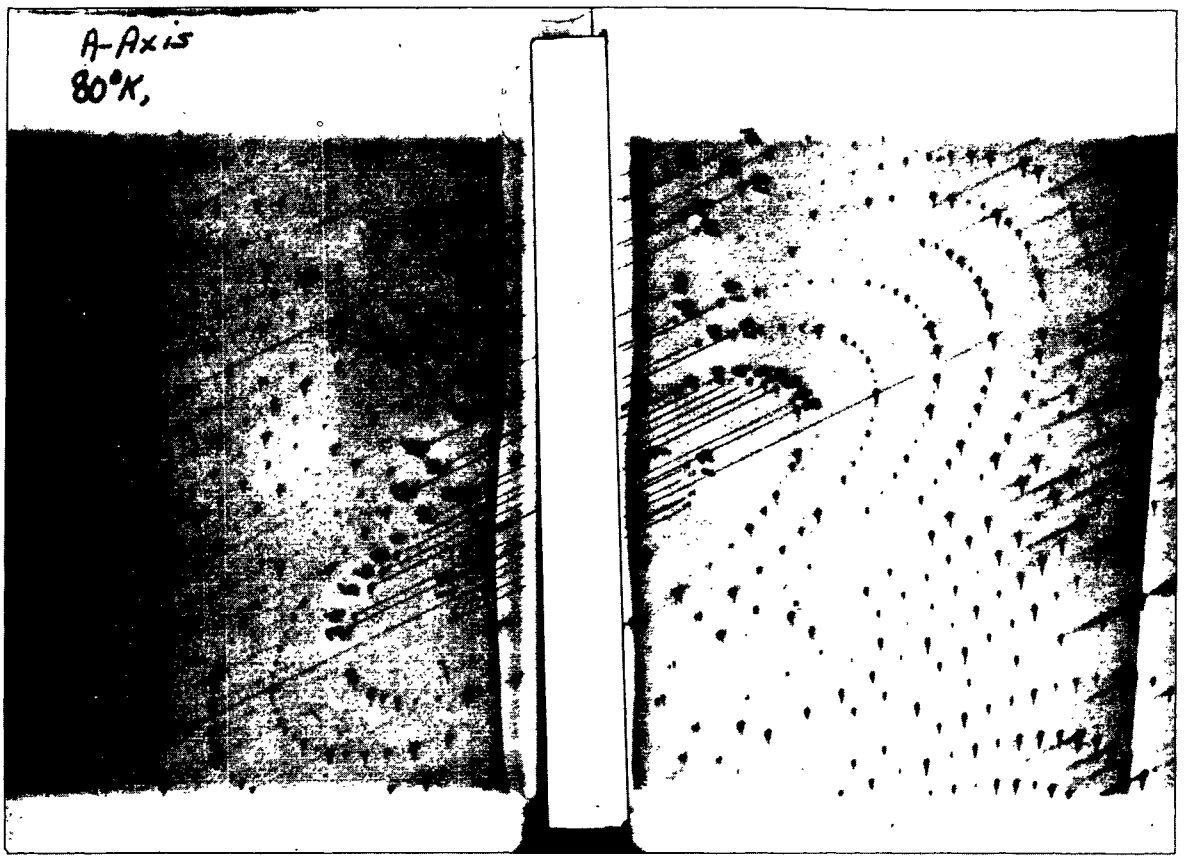

Figure 19. Back-Reflection Photograph. The Equivalent, High-Angle Reflections Are Numbered Alike

The film was enclosed in an envelope to prevent exposure to daylight during the course of the x-ray exposures. The envelope was constructed out of black paper (B.W. 73/80, caliper 0.0045-0.0050 inch, Knowlton Brothers, Watertown, N.Y.).

In order to load the film holder for a back-reflection exposure, the two end clamps were removed. The film packet was fitted into the holder so that the film slot coincided with the collimator slot. Two side rings held the film packet in place against the walls of the holder.

Back-reflection photographs were taken at both room temperature and approximately 80°K. around the a and c axes. The respective exposure periods for the two temperatures were 48 hours and 14 hours. Copper radiation of weighted average wavelength 1.5418 A. ($K\alpha_1$ = 1.5405 A. and $K\alpha_2$ = 1.5443 A.) was used.

Evaluation of Back-Reflection Photographs

The back-reflection data consisted of the Cartesian coordinates of several pairs of equivalent high-angle reflections. The members of each pair were located on opposite sides of the film slot, as illustrated in Fig. 19. These coordinates were used to calculate diffraction angles for the reflections (see Data Analysis section). The reflection coordinates were measured with a Model DY 7092 Automatic Recording Microcomparator. Both the copper $K\alpha_1$ and $K\alpha_2$ reflections were measured whenever possible. A sample of the data is shown in Table VI. Four independent measurements were made per reflection.

Table VII summarizes the number of reflections measured per unit cell dimension.

TABLE VI

BACK-REFLECTION DATA, LOW TEMPERATURE, A AXIS, COPPER $K\alpha_2$ RADIATION

Reflection	Film Side One		Film Side Two	
	X[a]	Y[a]	X[a]	Y[a]
0,1,10	21759	02774	37744	02964
	21773	02772	37736	02973
	21715	02695	37688	03070
	21769	02722	37747	02945
0,2,10	21730	03756	37000	03780
	21751	03642	37024	03700
	21719	03780	37003	03780
	21713	03724	37017	03756

[a]Coordinates in X·12,000 in. or Y·12,000 in.

TABLE VII

SUMMARY OF NUMBER OF REFLECTIONS MEASURED PER BACK-REFLECTION FILM

Film	No. $CuK\alpha_1$	No. $CuK\alpha_2$
a axis, (room temp.)	16	16
a axis, (low temp.)	18	18
c axis, (room temp.)	13	13
c axis, (low temp.)	19	19

EQUI-INCLINATION WEISSENBERG CAMERA SETTINGS

The equi-inclination angles and layer-line screen settings (Table VIII) were derived from the heights, y, of the layer lines as they appeared on a low temperature oscillation photograph. The appropriate settings were found in Buerger (21), Fig. 155 and 156.

TABLE VIII

EQUI-INCLINATION WEISSENBERG CAMERA SETTINGS

Axis of Rotation	Layer	Height, mm.	Equi-inclination Angle, °	Layer Line Screen, mm.
c	0	0.0	0.0	0.0
c	1	5.5	5.4	2.4
c	2	11.5	10.8	4.9
c	3	20.0	16.3	7.4
c	4	34.0	22.2	10.4
c	5	99.0[a]	29.6	14.5
a	0	0.0	0.0	0.0
a	1	6.3	6.1	2.7
a	2	13.5	12.3	5.5
a	3	24.5	19.0	8.8
a	4	55.0	26.4	12.6

[a]The layer line was off the film. The above height value, H, was calculated from $d = n\lambda/\sin(\tan^{-1}2H/2r)$, where d = 8 A., n = 5, and r = 57.3 mm.

INTENSITY DATA COLLECTION

The equi-inclination Weissenberg method was chosen for the collection of intensity data. The experimental apparatus consisted of a water-cooled x-ray tube and power supply manufactured by the North American Phillips Company, Inc., Mount Vernon, N. Y. A standard Weissenberg camera, purchased from the Charles Supper Company, Watertown, Massachusetts, was mounted on the x-ray unit. Copper radiation containing $K\alpha_1$ (wavelength = 1.5404 A.) and $K\alpha_2$ radiation (wavelength = 1.5443 A.) was used. The weighted average wavelength was 1.5418 A.

MULTIPLE-FILM PACKET

A range of one to one thousand or more is often needed for the blackening scale in recording reflection intensities (24). Ordinary photographic film cannot provide

this range, and it is almost impossible to distinguish between varying degrees of blackness for very dark spots. The multiple-film technique was used to overcome the lack of range of a single film.

A packet of four films (Kodak No-Screen Medical X-ray Film, 4-15/16 in. x 6-7/16 in.) was used for each intensity exposure. Each film in the packet acted as a uniform absorber and reduced the x-ray reflection intensities that arrived at the film underneath it by a constant factor. By this arrangement, the limited range of one film was supplemented by the ranges of others in the packet. The intensities of the strong reflections were estimated by examining the third and fourth films of the packet, and the weak reflections were estimated on the first film. In order to prevent exposure to daylight, the four films were enclosed in a black paper envelope.

FILM DEVELOPMENT

It was critical that each film in the packet be developed by the same procedure. This was accomplished by developing them simultaneously. A rack was used to hold the films. Up to ten films could be treated at one time.

The films were immersed in freshly-prepared Kodak X-Ray Developer (68°F.) for five minutes. Next, they were placed in Kodak Indicating Stop Bath for two minutes and then in Kodak X-Ray Fixer for ten minutes. The films were then removed from the rack and washed with water for thirty to sixty minutes. The washed films were dipped in a solution of Kodak Photo-Flo and hung in a forced-air oven to dry at room temperature. The dry, developed films were stored in polyethylene bags.

ESTIMATION OF REFLECTION INTENSITIES

Preparation of Standard Intensity Scale

The relative intensities of the individual reflections were measured by visual comparison to a standard scale. The scale was prepared by selecting an intense

reflection from crystal one (c axis rotation) and taking repeated oscillation photographs of it at exposure times which were in the ratios desired for the final density scale. The crystal oscillation was limited to just the amount needed to obtain the selected reflection (± 2 1/2°), and the film was shifted between exposures to be sure that succeeding reflections did not overlap. The exposure times were selected according to the geometric series, $t = \gamma r^2$, where t equalled the exposure time in seconds, r was an integer of value one to twenty, and γ was a constant chosen so that the blackness of spots from successive exposures was just distinguishable. A scale containing sixteen distinguishable spots was obtained with γ equal to 0.63.

Visual Estimation of Intensities

The films were placed on a light box (Truvision Illuminator, Model 11FV1, General Electric Company) for the intensity measurements, and the scale was placed over them. The individual reflection was viewed through any background on the scale strip, while the comparison spot was placed on the most representative film background. The reflection was compared with various reference spots until a match was found or until it was determined to fall between two values. The appropriate value was then assigned as the observed intensity on an arbitrary scale. The values on the scale ran from 9 to 324 (i.e., $3^2, 4^2, 5^2, \ldots 18^2$).

All quadrants of the Weissenberg photograph are equivalent in a crystal belonging to the orthorhombic class. For convenience, the exposures were made so that one axis crossed the center line at the left edge of the film. The unique data were contained between that axis and one ninety degrees away to the right. The two equivalent quadrants shown in Fig. 19a were estimated, giving two independent estimations per reflection. All reflections were assigned three positive indices.

The total number of measurements per reflection varied from two to twelve, depending on the number of films on which the reflection appeared and whether or

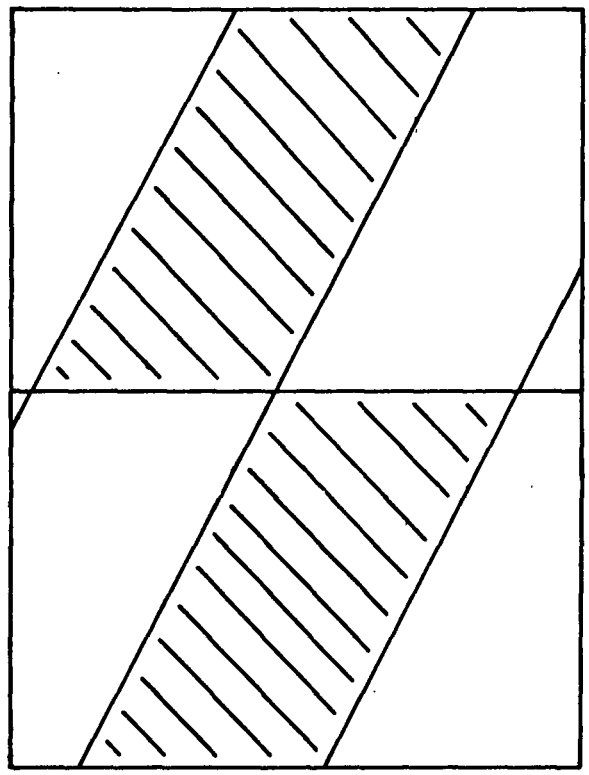

Figure 19a. Unique Reflections in the Orthorhombic System Lie Within the Shaded Area on Either the Top or Bottom Half of the Weissenberg Film

not it was common to both crystals. Table IX contains a summary of the intensity data collection.

TABLE IX

SUMMARY OF INTENSITY DATA COLLECTION

Axis	Layer	No. Observed	No. Unobserved	Total
c	0	122	48	170
c	1	142	23	165
c	2	150	10	160
c	3	143	13	156
c	4	141	6	147
c	5	114	12	126
		812		924
a	0	155	41	196
a	1	180	14	194
a	2	163	18	181
a	3	160	14	174
a	4	139	11	150
		797		895

Approximately 8000 individual estimations were made.

DATA ANALYSIS

UNIT CELL CONSTANTS

In determining unit cell constants with high precision, one must:

1. utilize reflections which lie in the sensitive region (theta values near 90°);
2. eliminate the systematic errors inherent in the recording of reflections and the measurement of reflection angles.

The systematic errors are due to eccentricity of the crystal, lack of knowledge of the exact camera radius, shrinkage during film development, and x-ray absorption by the crystal. A detailed discussion of these errors can be found in Buerger (21), pages 399-434.

It has been shown that the systematic errors tend to vanish as theta approaches 90°. To take advantage of this fact, one takes back-reflection photographs. In these exposures, the high-theta reflections fall near the center of the film, where film shrinkage errors are negligible.

Appendix II contains a detailed discussion of the mathematical treatment of the back-reflection film data. Tables X and XI contain a summary of the results.

TABLE X

BACK-REFLECTION FILM DATA SUMMARY

	Total Reflections Measured	Range of Theta, °	Axis of Rotation
Low temperature	36	60.8-81.4	a
	38	62.9-82.9	c
Room temperature	32	62.7-80.5	a
	26	68.0-81.2	c

TABLE XI

UNIT CELL CONSTANTS FOR trans-2-METHYLENE-5-(2-ISOPROPYLOL)-CYCLOHEXANOL

	a Axis (sigma), A.	b Axis[a] (sigma), A.	c Axis (sigma), A.	Unit Cell Volume, A.^{3}
Low temperature	6.952(.002)	17.527(.005)	8.016(.001)	994.86
Room temperature	7.181(.002)	17.873(.005)	8.053(.001)	1033.50
Percent change on cooling	-3.2	-1.9	-0.5	-3.7

[a]Average from two films.

An estimate of the number of molecules, Z, occupying a unit cell was obtained by comparing the experimental flotation density (see page 42) with a density calculated from the x-ray results.

$$\left(\rho_{x\text{-}ray}\right)_Z = \left(\frac{Z \text{ molecules}}{\text{unit cell}}\right)\left(\frac{\text{unit cell}}{V\ A.^3}\right)\left(\frac{Mg.}{\text{mole}}\right)\left(\frac{\text{mole}}{N \text{ molecules}}\right)\left(\frac{10^{24} A.^3}{cm.^3}\right) \qquad (37)$$

$$\left(\rho_{x\text{-}ray}\right)_4 = \frac{(4)(170)(10^{24})}{(1033.5)(6.02\times10^{23})} \frac{g.}{cm.^3} \qquad (38)$$

$$\left(\rho_{x\text{-}ray}\right)_4 = 1.093 \text{ (g./cm.)} \qquad (39)$$

The close agreement between $\rho_{x\text{-}ray} = 1.093$ g./cm.^{3} and $\rho_{flotation} = 1.130$ g./cm.^{3} indicated four molecules per unit cell.

REDUCTION OF INTENSITY DATA TO NORMALIZED STRUCTURE FACTORS

MULTIPLE-FILM SCALING

As discussed previously, the intensity data were collected by multiple-film techniques. It was necessary to place the intensity estimates from the four films

on the same scale by correcting for x-ray absorption by the films. This process is known as multiple-film scaling and was carried out with a set of IBM 1620 computer programs (see Appendix III). The programs calculated film-to-film scaling factors for the four films in the envelope. The average of the scaled estimates was accepted as the uncorrected relative intensity for each reflection. Table XII contains the film-to-film scaling constants obtained for the c axis setting. The a axis constants were essentially identical with those listed.

TABLE XII

FILM-TO-FILM SCALING CONSTANTS

(c-Axis Setting)

Layer	Films	Constant
0	1:2	4.414
	2:3	4.469
	3:4	4.294
1	1:2	4.428
	2:3	4.482
	3:4	4.752
2	1:2	4.494
	2:3	4.566
	3:4	4.353
3	1:2	4.378
	2:3	4.585
	3:4	4.473
4	1:2	4.585
	2:3	4.585
	3:4	4.707
5	1:2	4.631
	2:3	4.747

LORENTZ AND POLARIZATION CORRECTIONS

The Lorentz-polarization correction was carried out with an IBM 1620 computer program. Each observed intensity was multiplied by the factor $2\cos\theta(\cos^2\mu-\cos^2\theta)^{1/2}/(1+\cos^2 2\theta)$ (see Appendix III). Inasmuch as the intensity measurements were taken

from both the upper and lower quadrants of the films, no spot-shape corrections were made. It was believed that the elongations and contractions would offset one another in this case.

No correction for x-ray absorption was made at either crystal setting.

INTERLAYER SCALING

Due to different experimental conditions, crystal size, exposure time, etc., the layers of intensities collected from the two crystal settings were on different relative scales. This situation made it necessary to modify the intensities so as to put them on a common scale. A procedure to do this has been devised by Rollett and Sparks (40). Their approach utilizes the fact that many reflections are common to both crystal settings.

The following relationship should be true for a reflection which is found on both layers A and B.

$$K_A I_{A,hk\ell} = K_B I_{B,hk\ell} \qquad (40)$$

K_J = interlayer scale factor for layer J

$I_{J,hk\ell}$ = intensity of reflection hkℓ, found on layer J

This expression would hold exactly were there no experimental error involved in the collection and measurement of the intensities. Rollett and Sparks consider all possible expressions (40) in a given set of data and arrive at a least-squares best fit to provide the interlayer scale constants, K_J.

The interlayer scaling constants obtained for trans-2-methylene-5-(2-isopropylol)-cyclohexanol are shown in Table XIII. Layer five of the c axis data was discarded because those reflections were much weaker than seemed reasonable compared to the

remainder of the data. The scaled intensities were referred to as the "observed relative intensities."

TABLE XIII

INTERLAYER SCALING CONSTANTS

Axis	Layer	Scaling Constant
c	0	1.0753
c	1	1.0386
c	2	1.0595
c	3	1.0626
c	4	1.0633
a	0	0.9156
a	1	0.9415
a	2	0.9475
a	3	0.9389
a	4	0.9372

A total of 440 reflections was common to the a and c axes. The discarded hk5 layer contained 122 reflections.

NORMALIZED STRUCTURE FACTORS

The final step in the data reduction involved converting the observed relative intensities to normalized structure factors, $|E_{hk\ell}|$, for use in symbolic addition procedures. The modified K-curve method of Karle and Hauptman (27, 41) was used. The following quantities were defined:

$$\sigma_2 = \sum_{j=1}^{N} f_j^2(hk\ell), \qquad (41)$$

where

$f_j(hk\ell)$ = atomic scattering factor for atom j and direction $hk\ell$

N = number of atoms in unit cell

$$\varepsilon(hk\ell) = 2 \quad \text{if } h=k=0 \text{ or } k=\ell=0 \text{ or } \ell=h=0; \qquad (42)$$

$$= 1 \quad \text{otherwise;}$$

and

$$s = \sin^2\theta/\lambda^2. \qquad (43)$$

The data were arranged according to $(\sin\theta)/\lambda$ and separated into groups of like s, each containing approximately 200 reflections. The quantities K and $\bar{s}$ were computed for each group from Equations (44) and (45).

$$K = \sum_n \varepsilon(hk\ell)\ \sigma_2 / \sum_n |F_{rel,hk\ell}|^2 \qquad (44)$$

n = number reflections in the group

$$\bar{s} = \left|\sum_{j=1}^{n} s_j\right|/n \qquad (45)$$

All reflections (observed and unobserved) were included in the calculations. Table XIV shows the set of values obtained.

TABLE XIV

K-CURVE INPUT VARIABLES

K	$\bar{s}$	Number Reflections
1.5263	0.0620	200
1.4327	0.1460	200
1.6362	0.2113	200
2.7465	0.2735	200
2.3066	0.3343	200
2.2646	0.3865	153

Normalized structure factors are defined by Equation (46).

$$|E_{hk\ell}|^2 = \frac{|F_{rel,hk\ell}|^2 K_{hk\ell}}{\epsilon(hk\ell) \sum_{j=1}^{N} f_j^2(hk\ell)} \qquad (46)$$

The value of $\underline{K}_{hk\ell}$ can be obtained from a plot of $\underline{K}$ versus $\underline{\bar{s}}$. In order to facilitate the computations, the $\underline{K}$-curve input variables were fitted to an equation of form (47) (see Fig. 20).

$$\ln (K) = A + B\,(\sin^2\theta/\lambda^2)^x \qquad (47)$$

The best values of $\underline{A}$, $\underline{B}$, and $\underline{x}$ were found to be $\underline{A}$ = 0.245, $\underline{B}$ = 1.743, and $\underline{x}$ = 1.0.

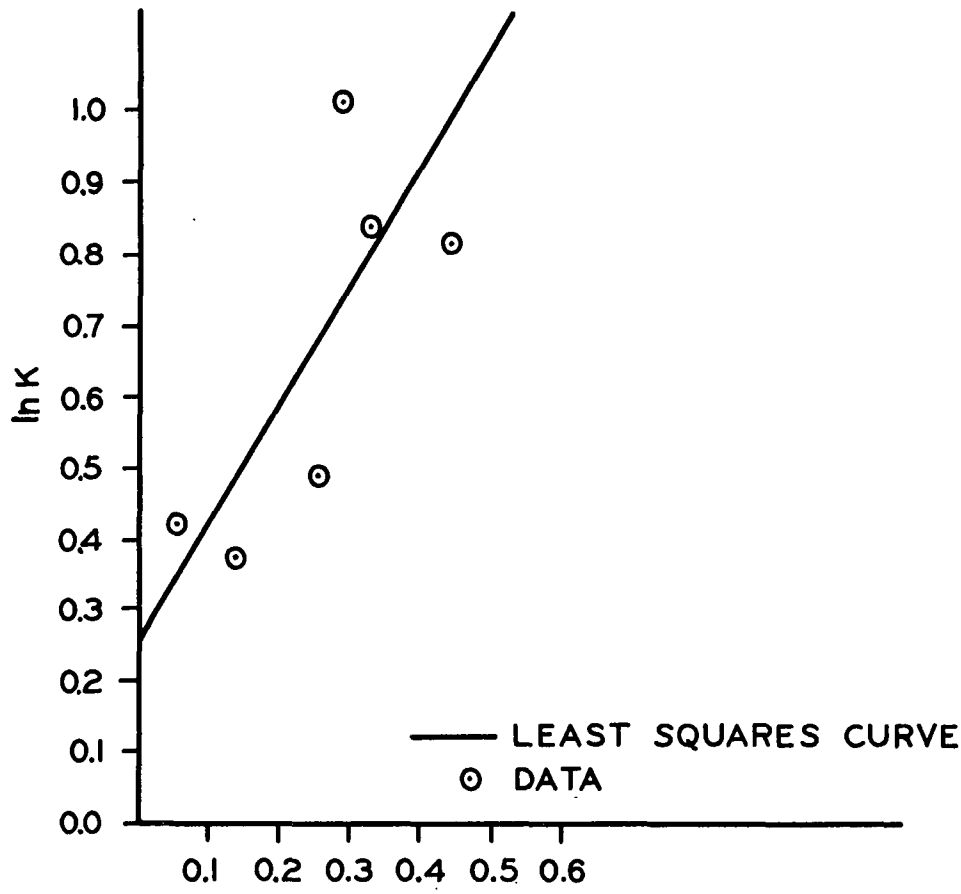

Figure 20. K-Curve Plot

Equation (46) was rewritten in the following form for computational purposes.

$$|E_{hk\ell}|^2 = \frac{|F_{rel,hk\ell}|^2 \exp(0.245 + 1.743\ (\sin^2\theta/\lambda^2))}{\varepsilon(hk\ell) \sum_{j=1}^{N} f_j^2(hk\ell)} \qquad (48)$$

Table XV shows a comparison of the experimental E-statistics with the theoretical distributions published by Karle and Hauptman (27) for crystals with atoms in random positions.

TABLE XV

COMPARISON OF EXPERIMENTAL E-STATISTICS AND THEORETICAL DISTRIBUTIONS

	$/\overline{E}/$	$/\overline{E/^2}$	$\overline{\lvert/E/^2-1/\rvert}$
Centered (theor.)	0.798	1.000	0.968
Acentric (theor.)	0.886	1.000	0.736
Total data (1153)	0.846	1.000	0.840
Acentric data (728)	0.852	1.015	0.848
Centric data (425)	0.812	1.003	0.912

SYMBOLIC ADDITION PHASE GENERATION

PREPARATION OF DATA LISTINGS

The normalized structure factors greater than 1.5 were separated into eight subgroups according to the parity of their three indices — namely: GGG[5], GGU, GUG, UGG, GUU, UGUG, UUG, and UUU. In each of these subgroups the $|E_{hk\ell}|$ were arranged in the order of decreasing magnitude. This listing facilitated the selection of origin reflections.

[5] G denotes even; U denotes odd.

Another useful listing consisted of all the combinations of $\bar{k}$ and $\overline{h-k}$ for a given $\bar{h}$ to be used in the generation of phases by hand[6]. It is called a sigma-2 listing. A FORTRAN program was prepared which computes the listing for orthorhombic and monoclinic space groups. All of the symmetry mates of $\underline{hk\ell}$ available for a given space group are included in the values of $\bar{k}$ and $\overline{h-k}$. The following symmetry relationships exist in space group $P2_12_12_1$: $\underline{hk\ell}=\underline{\bar{h}\bar{k}\ell}=\underline{\bar{h}k\bar{\ell}}=\underline{h\bar{k}\bar{\ell}}=\underline{hk\bar{\ell}}=\underline{h\bar{k}\ell}=\underline{\bar{h}k\ell}=\underline{\bar{h}\bar{k}\bar{\ell}}$. These relationships express the equivalence of all quadrants in the $P2_12_12_1$ diffraction pattern.

Along with each $(\bar{h}=\bar{k}+\overline{h-k})$ interaction, the value of kappa = $\sigma_3\sigma_2^{-3/2}|\underline{E}_{\bar{h}}||\underline{E}_{\bar{k}}||\underline{E}_{\overline{h-k}}|$ was listed[7]. This function was used in finding the variance during phase generation.

Two separate sigma-2 listings were made. The first listing involved only the 135 $|\underline{E}_{hk\ell}|$ greater than 1.5 and was used for bookkeeping during the hand generation of phases. The second listing involved $|\underline{E}_{hk\ell}|$'s whose values ranged down to 1.3 and was used with the tangent formula to expand the set of phases generated by hand.

It should be noted that two separate printouts of the first sigma-2 listing ($|\underline{E}_{hk\ell}|>1.5$) were made in order to facilitate the hand generation of phases. The first printout contained all $\bar{h},\bar{k},\overline{h-k}$ interactions sorted into groups of identical $\bar{k}$, which proved to be advantageous during the early stages of phase generation when

---

[6] When $\bar{h}$ and $\bar{k}$ are found alone, they refer to two different index triples, $h_1\ k_1\ \ell_1$ and $h_2k_2\ell_2$. $\overline{h-k}$ refers to the reflection whose indices are $h_3k_3\ell_3$, where $h_3 = h_1-h_2$, $k_3 = k_1-k_2$, $\ell_3 = \ell_1-\ell_2$. The use of $\bar{h}$ and $\bar{k}$ to mean index triples will be used often throughout this thesis.

[7] $\sigma_m = \sum_{j=1}^{N} Z_j^m$; N = number atoms in unit cell and Z_j = atomic number of jth atom.

only a few phases had been defined (20-30). As the number of accepted phases increased, it became apparent that a printout with all interactions sorted into groups of like $\underline{h}$ would increase the efficiency of the phase-determining process. Therefore, the sigma-2 listing cards were sorted into groups of identical $\underline{h}$ and printed out. See Appendix I for an example of the second sigma-2 listing.

SPECIFICATION OF ORIGIN AND SELECTION OF ENANTIOMORPH

The method for specifying origin and enantiomorph for space group $P2_12_12_1$ has been reported by Hauptman and Karle (31). Three linearly independent, two-dimensional reflections which have large $|E_{\underline{nk\ell}}|$'s are chosen. In addition, the selected reflections should enter into as many of the sigma-2 interactions as possible. Table XVI shows the reflections which were selected.

TABLE XVI

PHASE ASSIGNMENTS FOR SPECIFYING THE ORIGIN

$\underline{h}$	$\lvert E_{\underline{h}} \rvert$	$\phi_{\underline{h}}$, °	Parity	Number Sigma-2 Interactions
320	2.73	-90	UGO	64
203	2.72	90	GOU	49
037	2.61	90	OUU	43

A noncentrosymmetric set of intensity data always has two possible molecular structures associated with it, S and S'. These two structures are related by a center of symmetry located so that inversion of S through the center produces S'. S and S' are called enantiomorphs and one must specify one of the enantiomorphs when utilizing a direct method for phasing. If the enantiomorph assignment is ignored, the phase values appropriate to S and S' will be obtained, and both structures will appear in the electron density maps.

In space group $P2_12_12_1$, it is possible to choose an enantiomorph by specifying the value of a phase whose magnitude is known to be $\pi/2$. In the present case, the value of ϕ_{043}[8] was taken as zero, which fixed the value of structure invariant[9] 246 at + $\pi/2$.

$$\underset{(0)}{\phi_{043}} + \underset{(\pi/2)}{\phi_{203}} = \underset{(\pi/2)}{\phi_{246}} \qquad (48a)$$

GENERATION OF PHASES BY HAND

After the specifications which determined the origin and enantiomorph were made, Formula (49) (sigma-2 formula) was employed to determine the phases of most of the remaining large $|\underline{E}_{\underline{h}}|$

$$\phi_{\underline{h}} = \langle \phi_{\underline{k}} + \phi_{\underline{h}-\underline{k}} \rangle_{\underline{k}_r} \qquad (49)$$

($\underline{k}_r$ implies that the average is restricted to $\underline{k}$'s and $\underline{h}-\underline{k}$'s associated with large $|\underline{E}_{\underline{h}}|$).

Since $\underline{k}$ and $\underline{h}-\underline{k}$ include all of the available symmetry mates, it was advantageous to construct a table for evaluating the phases of $\underline{k}$ and $\underline{h}-\underline{k}$. Table XVII illustrates the need for such an aid in space group $P2_12_12_1$.

---

[8] $\phi_{\underline{hk\ell}}$ means the "phase of structure factor $\underline{hk\ell}$."

[9] A structure invariant is a phase, or linear combination of phases, whose value depends only on the structure and is independent of the choice of origin. Any reflection of the form GGG is a structure invariant in space group $P2_12_12_1$ (31).

TABLE XVII

SYMMETRY RELATIONSHIPS BETWEEN PHASES,
SPACE GROUP $P2_12_12_1$ ($\underline{4}2$)

Parity	$+\phi(\underline{hk\ell})$	$-\phi(\underline{hk\ell})$	$\pi-\phi(\underline{hk\ell})$	$\phi(\underline{hk\ell})-\pi$
	$\phi(\underline{h\bar{k}\ell})$	$\phi(\underline{\bar{h}\bar{k}\ell})$		
UUU	$\phi(\underline{\bar{h}k\ell})$	$\phi(\underline{\bar{h}k\ell})$		
GGG	$\phi(\underline{\bar{h}\bar{k}\ell})$	$\phi(\underline{h\bar{k}\ell})$		
		$\phi(\underline{hk\bar{\ell}})$		
UUG	$\phi(\underline{h\bar{k}\bar{\ell}})$	$\phi(\underline{\bar{h}\bar{k}\bar{\ell}})$	$\phi(\underline{h\bar{k}\ell})$	$\phi(\underline{\bar{h}k\bar{\ell}})$
GGU		$\phi(\underline{\bar{h}k\ell})$	$\phi(\underline{hk\bar{\ell}})$	$\phi(\underline{\bar{h}\bar{k}\ell})$
GUU	$\phi(\underline{\bar{h}k\bar{\ell}})$	$\phi(\underline{\bar{h}\bar{k}\bar{\ell}})$	$\phi(\underline{\bar{h}k\ell})$	$\phi(\underline{h\bar{k}\bar{\ell}})$
UGG		$\phi(\underline{h\bar{k}\ell})$	$\phi(\underline{hk\bar{\ell}})$	$\phi(\underline{\bar{h}\bar{k}\ell})$
GUG	$\phi(\underline{\bar{h}\bar{k}\ell})$	$\phi(\underline{\bar{h}\bar{k}\bar{\ell}})$	$\phi(\underline{\bar{h}k\ell})$	$\phi(\underline{h\bar{k}\bar{\ell}})$
UGU		$\phi(\underline{hk\bar{\ell}})$	$\phi(\underline{h\bar{k}\ell})$	$\phi(\underline{\bar{h}k\bar{\ell}})$

To initiate phase generation, one searches the sigma-2 listing for interactions where $\phi_{\underline{\bar{k}}}$ and $\phi_{\underline{\overline{h-k}}}$ are known. Table XVIII shows six interactions where this was true in the present problem. The interaction defining the phase of $0\bar{7}4$ will serve as an example.

TABLE XVIII

RESULTS OF FIRST SEARCH THROUGH SIGMA-2 LISTING

$\underline{\bar{h}}$	$\underline{\bar{k}}$	$\underline{\overline{h-k}}$	Kappa
$0\bar{7}4$	$0\bar{3}7$	$04\bar{3}$	1.68
$\bar{3}6\bar{3}$	$0\bar{4}3$	$\bar{3}20$	2.05
$\bar{4}00$	$\bar{2}03$	$20\bar{3}$	3.52
$\bar{4}43$	$20\bar{3}$	$\bar{2}46$	2.73
$\bar{5}23$	$\bar{2}03$	$\bar{3}20$	5.30
$\bar{2}71$	$0\bar{3}7$	$24\bar{6}$	2.24

ϕ_{074} is defined by adding the phases of 037 and $04\bar{3}$. The phase of 037 is known; however, one needs the aid of the symmetry table to find $\phi_{04\bar{3}}$. The parity is GGU, and we obtain the following phase.

$$\phi(04\bar{3}) = \pi - \phi(043) \qquad (50)$$

$$\phi(04\bar{3}) = \pi \ .$$

Applying the sigma-2 formula,

				ϕ
$\bar{k}$	0	3	7	$\pi/2$
$\overline{h-k}$	0	4	$\bar{3}$	π
$\bar{h}$	0	7	4	$3\pi/2$

(51)

During the phase determination, the phases, $\phi_{\underline{h}}$, are kept within the range $-\pi<\phi_{\underline{h}}\leq\pi$. Thus, one often must add $\pm$ 2π to the $\phi_{\underline{h}}$ obtained from the sigma-2 formula. Applying this restriction, the phase of 074 becomes $-\pi/2$.

Since the sigma-2 formula is not an exact relationship, it is necessary to apply a probability criterion to each phase indication (28) (see page 27). The criterion states that the variance of a phase indication must be less than 0.5 (Kappa greater than or equal to 2.5) before the phase is accepted. The phases for 074, 363, and 271 in Table XVIII would not be accepted on this basis. ϕ_{400}, ϕ_{443}, and ϕ_{453} satisfy the probability criterion and would be accepted.

Caution should be exercised in accepting ϕ_{400}, however. Interactions in which all three reflections, $\underline{\bar{h}}$,$\underline{\bar{k}}$, and $\underline{\overline{h-k}}$, have one or two indices zero are ordinarily avoided because such combinations often indicate an incorrect phase (28). One cannot easily avoid such interactions in the early stages of phase development in space group $P2_12_12_1$, due to the nature of the origin phases. It is necessary, therefore, to watch the behavior of such a phase during the ensuing operations.

Phase generation is continued by repeating the search through the sigma-2 listing based on the five original phases plus the three new ones. This process is reiterated, each time adding some new phases, until all of the phases with $|\underline{E}_{\underline{h}}| \geq 1.5$ are defined (or rejected for some reason) or no new phases are accepted during one of the searches. If the latter occurs, an unknown symbol is assigned to a reflection which is known to occur in many interactions. Phase determination is them continued in terms of the unknown symbol and known phases. It is not uncommon to assign two or three symbols during the phasing process.

It will be noted that contradictory indications sometimes occur as an increasing number of interactions arise which define a particular phase (see Table XIX). A rule of thumb is to accept the particular indication which is in the clear majority and also has the greatest sum of Kappas — i.e., the highest probability. If an ambiguity exists about which indication to accept, the phase should be ignored until the uncertainty disappears.

TABLE XIX

EXAMPLE OF CONTRADICTORY PHASE INDICATIONS

$\underline{h}$	Indication	Number	$\sum$ Kappa
2,14,4	$\underline{a}-\pi/2$	14	25.8
	$\underline{a}$	4	9.4
	π	2	4.2
	$\pi/2$	2	4.7
	0	1	1.8

A detailed discussion of centrosymmetric symbolic addition can be found in Stout and Jensen (24). Many of the points covered are common to both centric and acentric cases. In addition, Karle and Karle discuss phasing procedures in their review of the symbolic addition method (28).

In the present problem, phases were determined for 112 of the original 135 $|\underline{E}_{\underline{h}}|$ greater than 1.5 in terms of 0, π, $\pi/2$, $-\pi/2$, and an unknown symbol, $\underline{a}$. Assignment of the symbol to reflection 066 had been necessary in order to carry out the phase determination. Of the original 135 $|\underline{E}_{\underline{h}}| \geq 1.5$, 23 gave ambiguous phase indications and were discarded. Reflection 066 is centrosymmetric; therefore, $\underline{a}$ could be either π or 0, giving two sets of phases. The two sets of phases were refined by means of the tangent formula (52) and the list of phases expanded to include those down to $|\underline{E}_{\underline{h}}| \geq 1.3$.

TANGENT FORMULA PHASE REFINEMENT AND EXPANSION OF LIST OF PHASES

The 112 phases were refined by reiteration of the tangent formula (52) (see page 24).

$$\tan \phi_{\underline{h}} \approx \frac{\left\langle \sum_{\underline{k}} |E_{\underline{k}}| \, |E_{\underline{h-k}}| \sin(\phi_{\underline{k}} + \phi_{\underline{h-k}}) \right\rangle_{\underline{k}}}{\left\langle \sum_{\underline{k}} |E_{\underline{k}}| \, |E_{\underline{h-k}}| \cos(\phi_{\underline{k}} + \phi_{\underline{h-k}}) \right\rangle_{\underline{k}}} \qquad (52)$$

The sums in the numerator and denominator are derived from the sigma-2 interactions which define each particular $\underline{h}$.

The initial cycle utilized the 112 symbolic addition phases. Each subsequent cycle used the set of phases produced by the previous cycle. Three cycles were required to produce convergence[10] of the phases with $\underline{a} = \pi$. Four cycles converged the set with $\underline{a} = 0$. Nine phases were rejected from each set based on the following criterion.

---

[10] "Convergence" was defined as the point where each $\phi_{\underline{h}}$ in the set changed by less than 10° between two successive cycles with the tangent formula.

1. A phase was rejected if its value changed greatly on successive cycles.

2. A phase was rejected if its calculated $|\underline{E}_{\underline{c},\underline{h}}| = \left[(\sigma_2^{3/2}\sigma_3^{-1} \sum_{\underline{k}} |\underline{E}_{\underline{k}}| |\underline{E}_{\underline{h}-\underline{k}}| \sin(\phi_{\underline{k}}+\phi_{\underline{h}-\underline{k}}))^2 + (\sigma_2^{+3/2}\sigma_3^{-1} \sum_{\underline{k}} |\underline{E}_{\underline{k}}| |\underline{E}_{\underline{h}-\underline{k}}| \cos(\phi_{\underline{k}}+\phi_{\underline{h}-\underline{k}}))^2\right]^{1/2}$ was less than 0.5.

An $\underline{R}$ index, defined by

$$R = \frac{\sum_{\underline{h}} \left[\left||E_{o,\underline{h}}| - |E_{c,\underline{h}}|\right|\right]}{\sum_{\underline{h}} |E_{o,\underline{h}}|} \qquad (53)$$

was computed for the two sets of phases. The values of $\underline{R}$ are given in Table XX.

TABLE XX

TANGENT FORMULA $\underline{R}$ INDEX, $|\underline{E}_{\underline{h}}| \geq 1.5$

$\underline{a}$	Number of Phases	$\underline{R}$
0	103	0.424
π	103	0.440

The tangent formula was used next to extend the set of phases down to $|\underline{E}_{\underline{h}}| \geq 1.3$. This was a two-step process. First, the sets of phases were expanded by running a cycle of the tangent formula where $\underline{k}$ and $\underline{h}-\underline{k}$ corresponded to $|\underline{E}_{\underline{h}}|$ and $|\underline{E}_{\underline{h}-\underline{k}}|$ greater than 1.5, and $\underline{h}$ referred to $|\underline{E}_{\underline{h}}|$ in the range $1.5 \; |\underline{E}_{\underline{h}}| \geq 1.3$. Ninety-three new, unrefined phases were added in this step for a total of 196.

The 196 phases were then refined in two cycles of the tangent formula. Table XXI shows the final results for the two sets of phases.

TABLE XXI

FINAL RESULTS OF TANGENT FORMULA REITERATION

a	Number of Phases	R
0	176	0.424
π	181	0.350

COMPUTATION OF E-MAPS

The last step in the symbolic addition method is the computation of E-maps. These are Fourier electron-density maps based on $E_{\underline{h}}$ as coefficients. The general expression for electron density in space group $P2_12_12_1$ is

$$\rho(XYZ) = \frac{8}{V}\left\{\sum_{h=0}^{\infty}\sum_{k=0}^{\infty}\sum_{\ell=0}^{\infty} /F/_{hk\ell}\left[\begin{matrix} h+k=2n,\ k+\ell=2n \\ A(1)\cos\phi_{hk\ell} - B(1)\sin\phi_{hk\ell}\end{matrix}\right]\right.$$

$$-\sum_{h=0}^{\infty}\sum_{k=0}^{\infty}\sum_{\ell=0}^{\infty} /F/_{hk\ell}\left[\begin{matrix} h+k=2n,\ k+\ell=2n+1 \\ A(2)\cos\phi_{hk\ell} - B(2)\sin\phi_{hk\ell}\end{matrix}\right] \qquad (54)$$

$$-\sum_{h=0}^{\infty}\sum_{k=0}^{\infty}\sum_{\ell=0}^{\infty} /F/_{hk\ell}\left[\begin{matrix} h+k=2n+1,\ k+\ell=2n \\ A(3)\cos\phi_{hk\ell} - B(3)\sin\phi_{hk\ell}\end{matrix}\right]$$

$$\left.-\sum_{h=0}^{\infty}\sum_{k=0}^{\infty}\sum_{\ell=0}^{\infty} /F/_{hk\ell}\left[\begin{matrix} h+k=2n+1,\ k+\ell=2n+1 \\ A(4)\cos\phi_{hk\ell} - B(4)\sin\phi_{hk\ell}\end{matrix}\right]\right\},$$

where

$\rho(\underline{XYZ})$ = electron density at $(\underline{X},\underline{Y},\underline{Z})$ in the unit cell;

$\underline{V}$ = volume of unit cell, $A.^3$;

$\underline{A}(1)$ = $\cos 2\pi\ \underline{hX} \cos 2\pi\ \underline{kY} \cos 2\pi\ \underline{\ell Z}$;

$\underline{B}(1)$ = $\sin 2\pi\ \underline{hX} \sin 2\pi\ \underline{kY} \sin 2\pi\ \underline{\ell Z}$;

$\underline{A}(2)$ = $\cos 2\pi\ \underline{hX} \sin 2\pi\ \underline{kY} \sin 2\pi\ \underline{\ell Z}$;

$\underline{B}(2)$ = $\sin 2\pi\ \underline{hX} \cos 2\pi\ \underline{kY} \cos 2\pi\ \underline{\ell Z}$;

$\underline{A}(3)$ = $\sin 2\pi\ \underline{hX} \cos 2\pi\ \underline{kY} \sin 2\pi\ \underline{\ell Z}$;

$\underline{B}(3) = \cos 2\pi \underline{hX} \sin 2\pi \underline{kY} \cos 2\pi \underline{\ell Z}$;

$\underline{A}(4) = \sin 2\pi \underline{hX} \sin 2\pi \underline{kY} \cos 2\pi \underline{\ell Z}$;

$\underline{B}(4) = \cos 2\pi \underline{hX} \cos 2\pi \underline{kY} \sin 2\pi \underline{\ell Z}$ (42).

It is customary to combine $|\underline{F}_{hk\ell}|$ and $\sin \phi_{hk\ell}$ or $\cos \phi_{hk\ell}$ to define two new coefficients, FC and FS.

$$FC = |F_{hk\ell}| \cos \phi_{hk\ell} \tag{55}$$

$$FS = |F_{hk\ell}| \sin \phi_{hk\ell} \tag{56}$$

The substitution of $|\underline{E}_{hk\ell}|$ for $|\underline{F}_{hk\ell}|$ in Equations (55) and (56) yields coefficients for an E-map.

E-maps based on the two sets of refined phases were computed at intervals of 0.02 a (0.141 A.) and 0.02 c (0.160 A.) in sections at constant b. The sections were computed at intervals of 0.01 b (0.176 A.). These grid spacings fell within the limits suggested by Cochran and Lipson (69). The maps from the phases with a = 0 contained no recognizable chemical structure. Most of the peaks were located in one end of the unit cell and were quite asymmetric in shape.

The maps based on the phases with a = π revealed eight distinct symmetrical peaks in sections one through twenty (0.00-0.20 b) and four more peaks in sections thirty-six through forty-four (0.36 b - 0.44 b). Bond length and bond angle calculations indicated that the two sets of peaks were not members of a single molecule. However, within each of the two groups of peaks, the bond angles and peaks made chemical sense. Figure 21 shows the two fragments.

A three-dimensional model was constructed containing the two fragments and their $P2_12_12_1$ symmetry mates. It was immediately obvious that operation on fragment (a) with the symmetry operation (1/2 + x, 1/2 - y, - z) positioned the two fragments so as to form a structure which made chemical sense (Fig. 22).

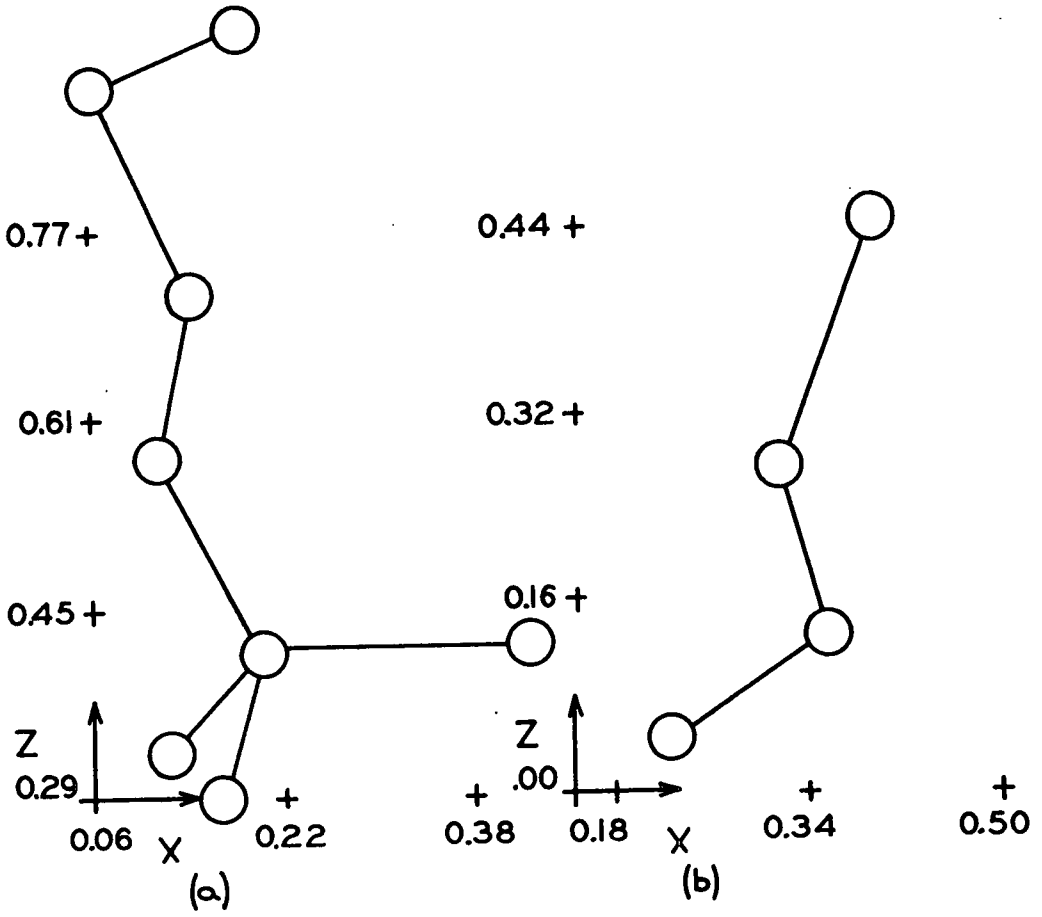

Figure 21. (a) Molecular Fragment Present in Sections 0.00 to 0.20 b. (b) Molecular Fragment from Sections 0.36 b to 0.44 b. Both Fragments Seen in Projection on the 010 Plane. Connecting Lines Drawn Between Atoms Which Calculated Sensible Three-Dimensional Bond Lengths and Angles

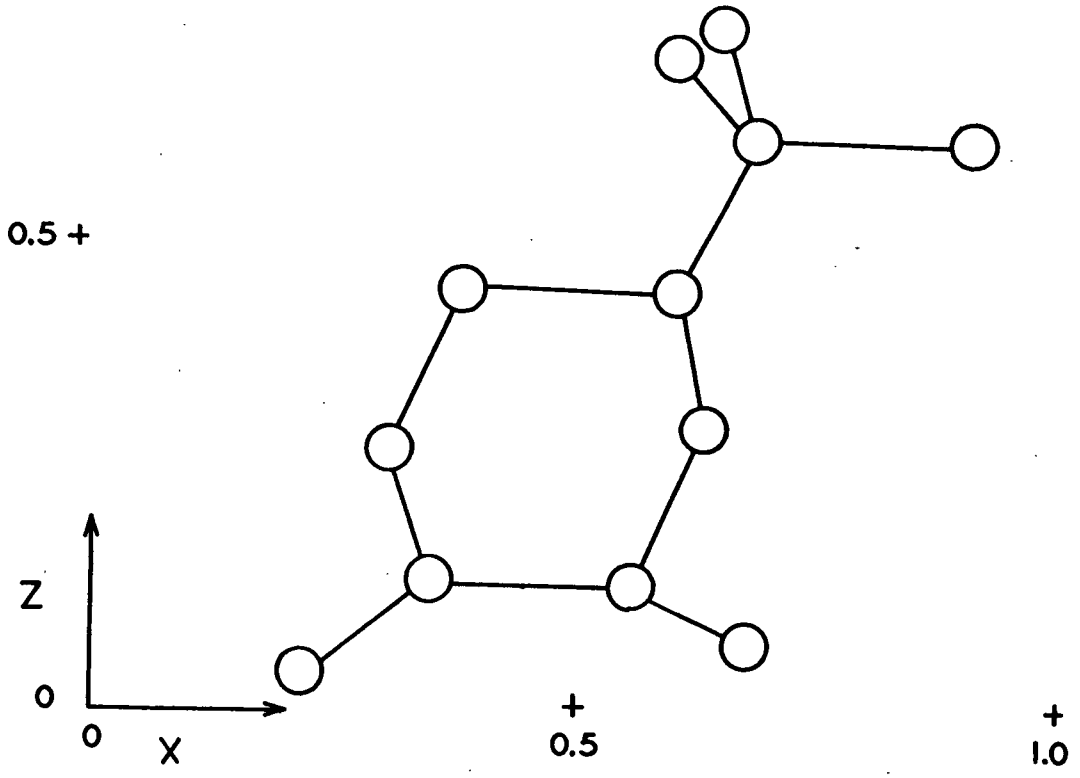

Figure 22. 010 Projection of Structure Revealed in E-Map Corresponding to a = π

STRUCTURE REFINEMENT

Structure refinement involves finding a set of atomic positions (model) whose calculated structure factors duplicate those observed as closely as possible. The effectiveness of a particular refinement operation was judged by its effect on the R index.

$$R = \frac{\sum_{\bar{h}} \left[\left| |F_{o,\bar{h}}| - |F_{c,\bar{h}}| \right| \right]}{\sum_{\bar{h}} |F_{o,\bar{h}}|} \qquad (57)$$

If a particular operation produced a decrease in R, the operation was considered to be successful.

Initially, the R factor for the twelve atoms from the E-map was 0.27 (observed data only). This was encouraging. Usually, a structure can be refined smoothly

beginning with R values in the range 0.3 to 0.4 (63). Occasionally, structures with lower R values may possess wrong features and fail to refine satisfactorily, however.

FOURIER REFINEMENT

A set of higher-resolution electron-density maps were computed with all the observed data. The Fourier coefficients were calculated from the positions of the twelve atoms found in the E-maps. An isotropic temperature factor of 1.743 was used. This value had been obtained from the K-curve plot.[11]

The new coordinates gave an R index of 0.21. Least squares refinement was begun at this point.

LEAST SQUARES REFINEMENT (44)

The diffraction data are subject to errors of observation so that refinement involves finding the most acceptable fit of the set of calculated structure factors with the set of observed structure factors. The problem comes into the general realm of finding the values of a set of variables which best satisfy a set of somewhat inconsistent observations. The solution to this problem is based on the hypothesis that the most acceptable values of the variables are such as to make the sum of the squares of the errors a minimum.

The quantity to be minimized in a crystallographic least squares refinement is

$$Q = \sum_{\bar{h}} W_{\bar{h}} (|F_{o,\bar{h}}| - K|F_{c,\bar{h}}|)^2 = \sum_{\bar{h}} W_{\bar{h}} \Delta^2 \quad , \qquad (58)$$

[11] It is important to realize that the coefficient of $(\sin^2\theta/\lambda^2)^{\underline{x}}$ from the K-curve is equal to the overall isotropic temperature factor only if $\underline{x} = 1.0$. The K-curve is then identical with a Wilson plot (70). If x is not 1.0, it is necessary to compute an additional K-curve, setting $\underline{x} = 1.0$, in order to obtain the overall isotropic temperature factor.

where

Q = residual;

$F_{o,\bar{h}}$ = observed structure factor;

$F_{c,\bar{h}}$ = calculated structure factor;

$\sum_{\bar{h}}$ = summation over all recorded reflections;

$W_{\bar{h}}$ = weighting term, theoretically equal to reciprocal of variance for a given reflection;

K = scale factor (overall).

If p_j ($j = 1,\ldots N$) are the N parameters in $|F_{c,\bar{h}}|$, Q is a minimum when these parameters satisfy the N equations

$$\partial Q/\partial p_j = 0 \qquad j = 1,\ldots,N \tag{59}$$

or

$$\sum_{\bar{h}} W_{\bar{h}} \Delta(\partial|F_{c,\bar{h}}|/\partial p_j) = 0 \qquad j = 1,\ldots,N. \tag{60}$$

Equations (59) and (60) are nonlinear and, therefore, difficult to solve. Linear expressions can be obtained by taking the first two terms in Taylor's series. We get

$$\Delta(\underset{\sim}{p} + \underset{\sim}{\varepsilon}) = \Delta(\underset{\sim}{p}) - \sum_{i=1}^{N} \underset{\sim}{\varepsilon}_i \, 2|F_{c,\bar{h}}|\underset{\sim}{\partial p}_i, \tag{61}$$

where

$\underset{\sim}{p}$ = set of trial parameters;

$\underset{\sim}{p+\varepsilon}$ = set of parameters in the refined structure;

$\underset{\sim}{\varepsilon}_i$ = shift in parameter i.

Substituting (61) into (60), we arrive at the linear Normal Equations,

$$\sum_{i=1}^{N} \left\{ \sum_{\bar{h}} W_{\bar{h}} \frac{\partial|F_{c,\bar{h}}|}{\partial \underset{\sim}{p}_i} \frac{\partial|F_{c,\bar{h}}|}{\partial \underset{\sim}{p}_j} \right\} \underset{\sim}{\varepsilon}_i = \sum_{\bar{h}} W_{\bar{h}} \Delta \frac{\partial|F_{c,\bar{h}}|}{\partial \underset{\sim}{p}_j}, \tag{62}$$

where the Δ on the right side is calculated with the trial parameters p_j. Thus, we have N equations in N unknowns, and the ε_i's can be found by the proper mathematical operations.

The solution of Equation (62) for a structure the size of the one under consideration would require the storage of at least one array of dimensions 109 x 109 in the computer. Such a solution, known as a full matrix solution, cannot be carried out with an IBM 1620 computer due to limitations in core storage.

In order to reduce the amount of computation and allow a large number of parameters to be refined simultaneously, the block diagonal approximation to the full matrix is often used. In this approximation, interactions between the parameters of different atoms are neglected.

No loss of accuracy is involved with the block diagonal approximation to the full matrix solution. However, the results do not converge nearly so rapidly as those from the full matrix, and there is sometimes a tendency to overcorrect, resulting in oscillation from one cycle to the next. To eliminate such behavior, and to improve the rate of convergence, damping factors can be applied; i.e., the shifts in parameters are multiplied by a factor other than 1.0. Initially, in the present work, a set of damping factors was tried based on the paper by Hodgson and Rollett (45). These factors proved unsatisfactory. The parameter values oscillated badly from cycle to cycle, and no convergence occurred. Satisfactory convergence was attained by using a constant factor of 0.67 (46).

Two computer programs written for the IBM 1620 computer by G. Mair of the National Research Council, Ottawa, Canada, were used to carry out the least squares computations. The main program, SFLS, calculated structure factors and accumulated least squares totals for any space group. An additional program, SFLS RESULTS, calculated the shifts to the parameters from the least squares totals, new

parameters, new bond distances and their standard deviations, and new bond angles and their standard deviations.

Atoms could be given either anisotropic or isotropic temperature factors and their respective corrections, $\underline{q_r}(\underline{hk\ell})$, were expressed as

$$q_r(hk\ell) = \exp[-(B_{11}h^2+B_{22}k^2+B_{33}\ell^2+B_{23}k\ell+B_{13}h\ell+B_{12}hk)_r], \tag{63}$$

and

$$q_r(hk\ell) = \exp[-B_r(\sin\theta/\lambda)^2]. \tag{64}$$

The $\underline{B_{ij}}$'s in (63) can be calculated from the isotropic $\underline{B_r}$ by the relations

$$B_{11} = Ba^{*2}/4, \tag{65}$$

$$B_{22} = Bb^{*2}/4, \tag{66}$$

$$B_{33} = Bc^{*2}/4, \tag{67}$$

$$B_{23} = (Bb^*c^*\cos\alpha^*)/2, \tag{68}$$

$$B_{13} = (Ba^*c^*\cos\beta^*)/2, \tag{69}$$

and

$$B_{12} = (Ba^*b^*\cos\gamma^*)/2. \tag{70}$$

The block diagonal approximation was used in the least squares calculation. The block sizes were 3 x 3 for positional parameters and either 6 x 6 or 1 x 1 for thermal parameters.

The interaction between the scale factor and the individual thermal parameters was neglected in the program. An approximate correction for the omission was made, however. If $\Delta\underline{B}'$ is the overall isotropic temperature factor change calculated from a 2 x 2 matrix when interaction with the scale factor is allowed for, and if $\Delta\underline{B}''$ is the overall isotropic temperature factor change calculated from a 1 x 1 matrix, then:

$$\Delta B_{\text{corrected}} = \Delta B_{\text{apparent}} + (\Delta B' - \Delta B'') \tag{71}$$

$$\Delta B_{ij\ \text{corrected}} = \Delta B_{ij\ \text{apparent}} + (\Delta B' - \Delta B'')R_{ij}/\lambda^2 \tag{72}$$

where the $\underline{R}_{ij}$'s are defined such that

$$\sin^2\theta = h^2R_{11} + k^2R_{22} + \ell^2R_{33} + k\ell R_{23} + h\ell R_{13} + hkR_{12}. \tag{73}$$

The estimated standard deviations were calculated in the program according to the following formula in which the weights are assumed to be relative.

$$\sigma^2(p_j) = [(a^{-1})_{jj}(\textstyle\sum\omega\cdot\Delta^2)]/(m-n), \tag{74}$$

where

$(\underline{a}^{-1})_{\underline{jj}}$ = diagonal element in the matrix inverse to the coefficient matrix of the Normal Equations;

$\underline{m}$ = number of reflections included in the refinement;

$\underline{n}$ = number of variable parameters in the structure.

Seven cycles of refinement with individual isotropic temperature factors and unit weights lowered $\underline{R}$ to 0.12. Two additional cycles of anisotropic refinement with unit weights lowered $\underline{R}$ to 0.11, at which time an attempt was made to locate the hydrogen atoms.

Although data from Cu Kα radiation provide resolution more than adequate to separate hydrogen atoms from other atoms to which they are bonded, in practice the contrast is not sufficient, and they appear as bulges on the electron density of the nonhydrogen atoms. A difference ($\Delta\underline{F}$)[12] synthesis provides a means for locating them by subtracting out the electron density of other atoms in the structure.

[12] $\Delta\underline{F} = (|\underline{F}_o,\underline{h}| - |\underline{F}_c,\underline{h}|)$, used as Fourier coefficients in conjunction with calculated phases.

Thus, hydrogen atoms not included in the calculated structure factors will appear in a ΔF map based on these F_c's. Good data are required if the locations are to be unequivocal, since hydrogen atoms are easily obscured by errors. Another factor which affects the ease with which hydrogens are located is the temperature at which the data are collected (47). At higher temperatures, the peaks tend to spread out (large isotropic temperature factors). For room temperature data, peak densities of 0.5 to 0.7 $eA.^{-3}$ are observed, and much higher values are found for low-temperature data (liquid nitrogen and below). Structures with large thermal motion give lower peak values. Extreme cases, such as the rotation of a methyl group, produce a toroid of low electron density.

The positions of all 18 hydrogen atoms were located in the difference maps. Isotropic temperature factors of 1.0 $A.^2$ (48) were assigned to these atoms. One cycle of least squares refinement was run with all 30 atoms. The positions and temperature factors of the hydrogen atoms were held constant. The R values decreased to 0.098.

At this point in the refinement, an indexing error was discovered on the 0 layer, c axis films which affected five 8 k 0 reflections. All the data were rechecked and a number of reflections removed from the observed list because their estimated intensities were too low to be known confidently. The revamped data list included 999 observed reflections and 190 unobserved reflections. Subsequent least squares refinement was carried out with the observed data only.

The atomic scattering factors for the first nine cycles of least squares refinement were taken from the International Tables for X-Ray Crystallography (49). The atomic scattering factors of Hanson and coworkers (50) for carbon and oxygen and the hydrogen scattering factors of Stewart and coworkers (51) were used in the final least squares refinement.

The refinement was resumed with the parameters from the seventh isotropic cycle. The hydrogens were included with their parameters fixed. Each hydrogen was assigned an isotropic temperature factor equal to that of the nonhydrogen atom to which it was attached. Two cycles of isotropic refinement converged at $\underline{R} = 0.095$. The final isotropic temperature factors are shown in Table XXII. Figure 23 contains the number system followed.

TABLE XXII

FINAL ISOTROPIC TEMPERATURE FACTORS

Atom	Isotropic Temperature Factor, $A.^2$
C-1	0.812
C-2	1.103
C-3	1.195
C-4	0.851
C-5	0.656
C-6	0.862
C-7	0.698
C-8	1.045
C-9	1.158
C-10	1.697
O-11	1.839
O-12	1.053

Average isotropic temperature factor = 1.08 $A.^2$

Four additional cycles of anisotropic least squares lowered $\underline{R}$ to 0.084. At this point, the largest shift in an atomic coordinate was less than 0.03 times its estimated standard deviation.

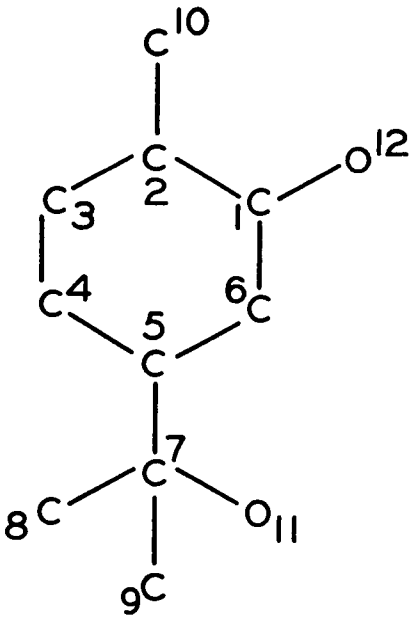

Figure 23. Numbering System for Atoms in trans-2-Methylene-5-(2-Isopropylol)-Cyclohexanol

WEIGHTING SCHEME

The functions minimized in the least squares method carry a weighting factor for each observation. If properly chosen, it has the effect of adjusting the contribution of each observation to the least squares equations in such a way as to produce the most reliable results. In addition, the usual least squares formula for estimating standard deviations is invalid unless the weights are correct.

In the absence of a satisfactory absolute weighting scheme for photograph data, the relative weighting scheme suggested by Cruickshank was used (46). This scheme is effective only after both anisotropic vibrations and hydrogen atoms have been allowed for in the calculated structure factors because the weights, $\underline{W}_{\underline{h}}$ are derived from an analysis of $\Delta^2 = (|\underline{F}_{\underline{c}},\underline{h}| - |\underline{F}_{\underline{o}},\underline{h}|)^2$.

The requirement was that the averages of $\underline{W}_{\underline{h}}\Delta^2$ must be constant when analyzed in groups of increasing $|\underline{F}_{\underline{o}},\underline{h}|$. In the present analysis, $\underline{W}_{\underline{h}}\Delta^2$ was set equal to one in the analysis.

The SFLS computer program utilized a weighting equation of the following form.

$$W_{\bar{h}} = \left(1 + \frac{(|F_{o,\bar{h}}| - b)^2}{a^2}\right)^{-1} \qquad (75)$$

$\underline{a}$,$\underline{b}$ = experimental constants

This expression was expanded into the general quadratic form.

$$\Delta^2 = 1/W_{\bar{h}} = \left(\frac{1}{a^2}\right)|F_{o,\bar{h}}|^2 - \left(\frac{\partial b}{a^2}\right)|F_{o,\bar{h}}| + \left(1 + \frac{b^2}{a^2}\right). \qquad (76)$$

The constants $\underline{a}$ and $\underline{b}$ were evaluated by arranging the $|\underline{F}_{o,\bar{h}}|$'s in increasing order of magnitude, calculating $\bar{\Delta}^2$ for groups of similar $|\underline{F}_{o,\bar{h}}|$ and fitting the sets of $\bar{\Delta}^2$'s and $|\underline{F}_{o,\bar{h}}|$'s to an equation of form (76) (see Fig. 24). The following equation was obtained.

$$\Delta^2 = 0.012\ |F_{o,\bar{h}}|^2 - 0.174\ |F_{o,\bar{h}}| + 1.51 \qquad (77)$$

The values of $\underline{a}$ and $\underline{b}$ were 8.89 and 6.89, respectively.

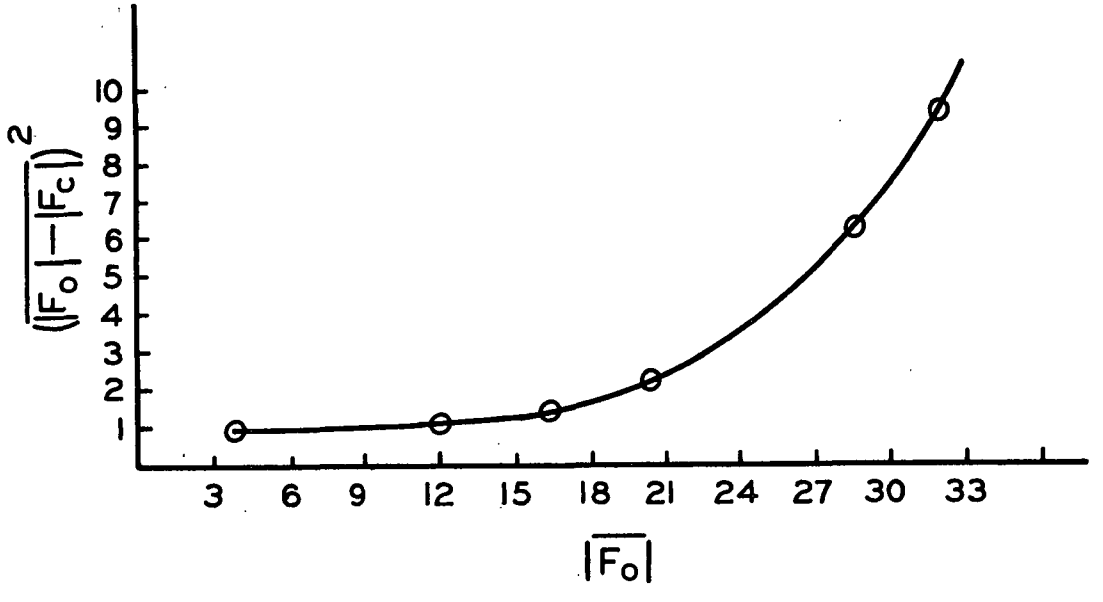

Figure 24. Weighting Scheme Plot of $\bar{\Delta}^2$ Versus $|\underline{F}_o|$

Two cycles of properly weighted least squares refinement reduced R to 0.083. Although the weighting scheme had little effect on the R index, it produced an average decrease in the estimated standard deviations of the coordinates of 0.001 A., a decrease which was considered to be quite significant. Table XXIII contains a summary of the least squares refinement results.

TABLE XXIII

LEAST SQUARES REFINEMENT

Cycle	$\lvert\Delta X\rvert_{max}$	$\lvert\Delta Y\rvert_{max}$	$\lvert\Delta Z\rvert_{max}$	$\lvert\Delta B\rvert_{max}$	Damping Factor	R	ΔK
1[a]	0.01352	0.00416	0.01275	1.509	0.91	0.249	-0.099
2[a]	0.00433	0.00128	0.00188	1.946	0.71	0.175	0.00
3[a]	0.00151	0.00069	0.00199	1.516	1.26	0.152	-0.001
4[a]	0.00107	0.00064	0.00164	1.576	0.59	0.176	0.00
5[a]	0.00006	0.00002	0.00003	0.135	0.50	0.121	0.00
6[a]	0.00005	0.00001	0.00006	0.03	0.50	0.120	0.00
7[b]	0.00111	0.00048	0.00109	0.00898	0.91	0.205	-0.014
8[b]	0.00097	0.00027	0.00067	0.00208	0.71	0.119	0.014
9[b]	0.00027	0.00009	0.00018	0.00109	0.50	0.114	-0.002
10[b]	0.00011	0.00007	0.00010	0.00024	0.50	0.113	0.00
11[b]	0.00005	0.00003	0.00003	0.00016	0.50	0.112	0.00
12[b,c]	0.00076	0.00041	0.00120	0.00160	0.50	0.098	0.038
13[a,d]	0.00051	0.00019	0.00049	0.164	0.67	0.097	0.002
14[a]	0.00011	0.00007	0.00009	0.028	0.67	0.095	0.00
15[b]	0.00069	0.00018	0.00043	0.00124	0.67	0.090	+0.012
16[b]	0.00031	0.00007	0.00020	0.00109	0.67	0.087	0.00
17[b]	0.00025	0.00005	0.00012	0.00103	0.67	0.087	0.00
18[b,e]	0.00064	0.00010	0.00013	0.00203	0.67	0.086	0.00
19[b]	0.00026	0.00005	0.00010	0.00054	0.67	0.084	0.00
20[b]	0.00006	0.00002	0.00005	0.00020	0.67	0.084	0.00
21[b,f]	0.00214	0.00022	0.00052	0.00062	0.67	0.084	0.02
22[b]	0.00079	0.00011	0.00019	0.00043	0.67	0.083	0.001
23[b]	0.00035	0.00005	0.00011	0.00029	0.67	0.083	0.00

[a] Isotropic.
[b] Anisotropic.
[c] First cycle with fixed hydrogen parameters.
[d] First cycle with 999 observed reflections plus hydrogens.
[e] First cycle with corrected 8,4,0 to 8,10,0 indices.
[f] First cycle with proper relative weights.

A weighting scheme was devised for the 190 unobserved reflections. A constant weight was computed such that the average $\underline{W}_{\underline{h}}\Delta^2$ equalled one. An $\underline{R}$-index of 0.10 was calculated for all the data.

Tables XXIV and XXV show the final parameters.

TABLE XXIV

FINAL FRACTIONAL COORDINATES AND THEIR ESTIMATED STANDARD DEVIATIONS

Atom	$\underline{X}$, $\sigma_{\underline{x}}$x10^{3}A.	$\underline{Y}$, $\sigma_{\underline{y}}$x10^{3}A.	$\underline{Z}$, $\sigma_{\underline{z}}$x10^{3}A.
C1	0.0597 (5)	0.1362 (4)	0.8786 (4)
C2	0.3496 (5)	0.3889 (4)	0.1345 (4)
C3	0.3098 (5)	0.4452 (5)	0.2728 (5)
C4	0.3899 (5)	0.4162 (4)	0.4382 (5)
C5	0.1073 (4)	0.0992 (4)	0.5744 (4)
C6	0.1419 (5)	0.1600 (4)	0.7092 (5)
C7	0.2005 (4)	0.1184 (4)	0.4050 (4)
C8	0.4229 (5)	0.1240 (5)	0.4227 (5)
C9	0.1236 (6)	0.1907 (5)	0.3234 (5)
C10	0.2162 (5)	0.3613 (6)	0.0355 (5)
O11	0.1591 (3)	0.0567 (3)	0.2892 (3)
O12	0.1803 (4)	0.0752 (3)	0.9416 (3)

TABLE XXV

FINAL ANISOTROPIC TEMPERATURE FACTORS[a]

Atom	B_{11}	B_{22}	B_{33}	B_{23}	B_{13}	B_{12}
C1	0.00507	0.00077	0.00160	-0.00049	-0.00070	0.00074
C2	0.00554	0.00101	0.00313	0.00140	0.00093	0.00006
C3	0.00324	0.00137	0.00332	0.00125	0.00026	0.00179
C4	0.00229	0.00104	0.00211	-0.00097	0.00215	0.00122
C5	0.00122	0.00070	0.00189	0.00073	0.00010	0.00022
C6	0.00232	0.00073	0.00354	-0.00004	0.00028	-0.00036
C7	0.00213	0.00061	0.00245	-0.00071	-0.00050	-0.00024
C8	0.00310	0.00117	0.00420	0.00016	0.00283	-0.00116
C9	0.01055	0.00073	0.00275	0.00047	0.00167	0.00069
C10	0.00628	0.00194	0.00473	0.00003	-0.00251	-0.00232
O11	0.00559	0.00070	0.00163	-0.00055	-0.00062	0.00105
O12	0.00653	0.00092	0.00220	-0.00044	-0.00185	0.00178

[a]The $\underline{B}_{\underline{i}\underline{j}}$ given here are defined by:

$$T = \exp\left\{B_{11}h^2+B_{22}k^2+B_{33}\ell^2+B_{12}hk+B_{13}h\ell+B_{23}k\ell\right\}.$$

Table XXVI contains fractional coordinates of the hydrogen atoms. The hydrogen positions were held constant during the refinement and, consequently, have no estimated standard deviation.

TABLE XXVI

HYDROGEN POSITIONS FOUND IN FOURIER DIFFERENCE MAP

Atom[a]	X	Y	Z
H1(C1)	0.060	0.180	0.945
H1(C3)	0.338	0.486	0.216
H2(C3)	0.195	0.460	0.280
H1(C4)	0.338	0.370	0.500
H2(C4)	0.365	0.455	0.500
H1(C5)	0.160	0.055	0.620
H1(C6)	0.080	0.200	0.670
H2(C6)	0.270	0.165	0.715
H1(C8)	0.318	0.120	0.405
H2(C8)	0.475	0.075	0.485
H3(C8)	0.500	0.138	0.318
H1(C9)	0.000	0.190	0.313
H2(C9)	0.195	0.210	0.233
H3(C9)	0.150	0.230	0.388
H1(C10)	0.235	0.325	0.970
H2(C10)	0.085	0.365	0.030
H1(O11)	0.205	0.015	0.370
H1(O12)	0.110	0.068	0.050

[a] $H_j(nk)$ refers to the jth hydrogen bonded to the ith atom of kind n.

RESULTS AND DISCUSSION

GENERAL MOLECULAR FEATURES

ARRANGEMENT OF ATOMS

The structure was found to contain a six-carbon ring with an exocyclic double bond. Figure 25 illustrates the arrangement of substituents around the ring and the numbering system followed in this discussion.

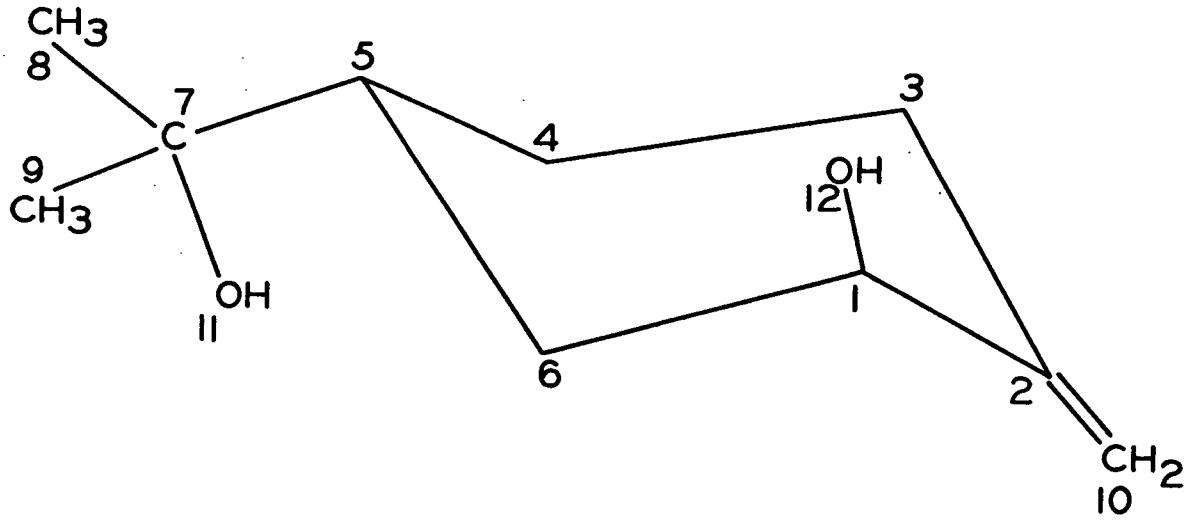

Figure 25. The Arrangement of Atoms and Numbering System Followed

The six-carbon ring takes on the ordinary chair conformation with an axial hydroxyl group located at C1 and an equatorial isopropylol group at C5. The structure was named trans-2-methylene-5-(2-isopropylol)-cyclohexanol, which, for the purposes of discussion, will be abbreviated trans-MIC.

STEREOCHEMICAL FEATURES OF THE METHYLENECYCLOHEXANE SYSTEM

Least Squares Planes

The equation for the mean plane calculated through the four carbon atoms associated with the ethylene bond is

$$-0.171x - 0.751y + 0.638z = -4.83. \quad (78)$$

The respective deviations from this plane for the four atoms are given in Table XXVII.

TABLE XXVII

DEVIATIONS FROM LEAST SQUARES PLANE THROUGH DOUBLE BOND

Atom	Dev. from L.S. Plane, A.
C1	0.0032
C2	-0.0108
C3	0.0034
C10	0.0042

Statistical analysis indicated that the deviations observed were greater than would be expected if the four atoms were truly planar (99% confidence level) (see Appendix V).

A least squares plane was calculated through ring carbons C1, C3, C4, and C6. Table XXVIII lists the respective deviations from the plane.

TABLE XVIII

DEVIATIONS FROM PLANE THROUGH C1, C2, C4, AND C6

Atom	Dev. from L.S. Plane, A.
C1	-0.020
C3	-0.020
C4	-0.020
C6	0.020
C2	-0.586
C5	0.712

These calculations showed that the ring was slightly puckered.

Dihedral Angles of the Six-Membered Ring

In discussions of cyclohexane chemistry, authors (72, 73) many times assume a so-called ideal ring having bond angles of 109°28' and bond lengths of 1.545 A. Recent findings indicate that these assumptions may not be valid.

Davis and Hassel (56) reported an average bond angle of 111.55 ± 0.15° for cyclohexane from electron diffraction studies. Wohl (52) has discussed the fact that ring angles of 111.5° lead to a somewhat flattened molecule which furnishes a better interpretation than the ideal model for numerous physical and chemical data. The extent of flattening can be measured by its effect on the two dihedral angles formed by the chair conformation, as shown in Fig. 26. Table XXIX summarizes some dihedral angles associated with cyclohexane compounds.

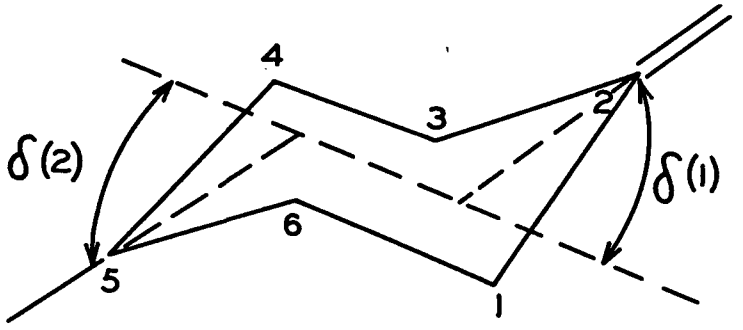

Figure 26. Dihedral Angles, δ(1) and δ(2), Formed by the Chair Conformation of a Six-Membered Ring

The experimental dihedral angles given in the table for cyclohexane, bicyclohexylidene, and trans-MIC provide definite evidence for the nonideality of cyclohexane rings.

As can be seen from Table XXIX, the introduction of an exocyclic double bond with a trigonal angle of 120° produced a large decrease in dihedral angle δ(1),

according to the original calculations of Corey and Sneen (53). Moffitt and co-workers found these calculations to be incompatible with certain optical rotatory dispersion data that they had gathered on cyclohexanone derivatives. Therefore, they repeated the calculations (54), assuming a trigonal angle of 116° and sp^2-sp^3 bond lengths of 1.50 A. All other angles and bond lengths were assumed to be ideal. The results of these later calculations led to the conclusion that the shape of cyclohexanone was much the same as ideal cyclohexane.

TABLE XXIX

DIHEDRAL ANGLES IN CYCLOHEXANE COMPOUNDS

Compound	Trigonal Angle, °	Other Angles, °	δ(1), °	δ(2), °	Ref.
Cyclohexane[a]	--	109.5	60.0	60.0	(52)
Cyclohexane[b]	--	111.5	54.6	54.6	(52)
Methylenecyclohexane[c]	120.0	109.5	40.0[e]	59.5[e]	(53)
Cyclohexanone[c]	116.0	109.5	51.2[e]	54.4[e]	(54)
Bicyclohexylidene[d]	110.6	111.2	49.4	51.1	(55)
trans-MIC[d]	114.5	110.9	45.5	52.6	

[a] Ideal model.
[b] Electron-diffraction.
[c] Vector analysis calculations.
[d] X-ray diffraction.
[e] Calculated from data given by authors.

From the preceding discussion, we see that ring flattening reflects two kinds of variations in the structure of methylenecyclohexane compounds: namely, an increase or decrease in the ring angle at the trigonal carbon and an increase or decrease in the average bond angle around the ring. The experimental dihedral angles found for trans-MIC seem to indicate that these effects can be quite substantial.

One must be cautious in interpreting these results, however. The possibility always exists that molecular packing will affect the shape of the molecule to a greater or lesser extent. For example, the trigonal carbon angle in bicyclohexylidene is 110.6°, and δ(1) equals 49.4° whereas the equivalent values in trans-MIC are 114.5° and 45.5°. It is not unreasonable that the extra flattening in trans-MIC improves the hydrogen bonding in the crystal due to the slight tilting of the hydroxyl on C1. Bicyclohexylidene, on the other hand, would probably not improve its intermolecular bonding enough to offset the amount of ring strain introduced by increasing the trigonal angle.

INTERATOMIC DISTANCES AND ANGLES

BONDING DISTANCES

Carbon-Carbon and Carbon-Oxygen Bond Distances

Figure 27 and Table XXX illustrate the most significant bond distances in the trans-MIC molecule.

The mean sp^3-sp^3 carbon-carbon bond distance in the ring of 1.533 A. agrees within 1 σ with that reported for cyclohexane (56) and within 1.5 σ with the average in bicyclohexylidene (55). Statistical analysis indicated that the four bonds in question are not equivalent, however (see Appendix V).

The difference between the mean sp^3-sp^3 carbon-carbon bond length and the mean sp^2-sp^3 carbon-carbon bond length (C1-C2, C2-C3) is significant at the 99% confidence level. Taken individually, however, bond C1-C2 is approximately equal to the mean sp^3-sp^3 bond length. No conclusions were drawn concerning the quantum mechanical prediction that sp^2-sp^3 carbon-carbon bonds should be shorter than sp^3-sp^3 carbon-carbon bonds (57).

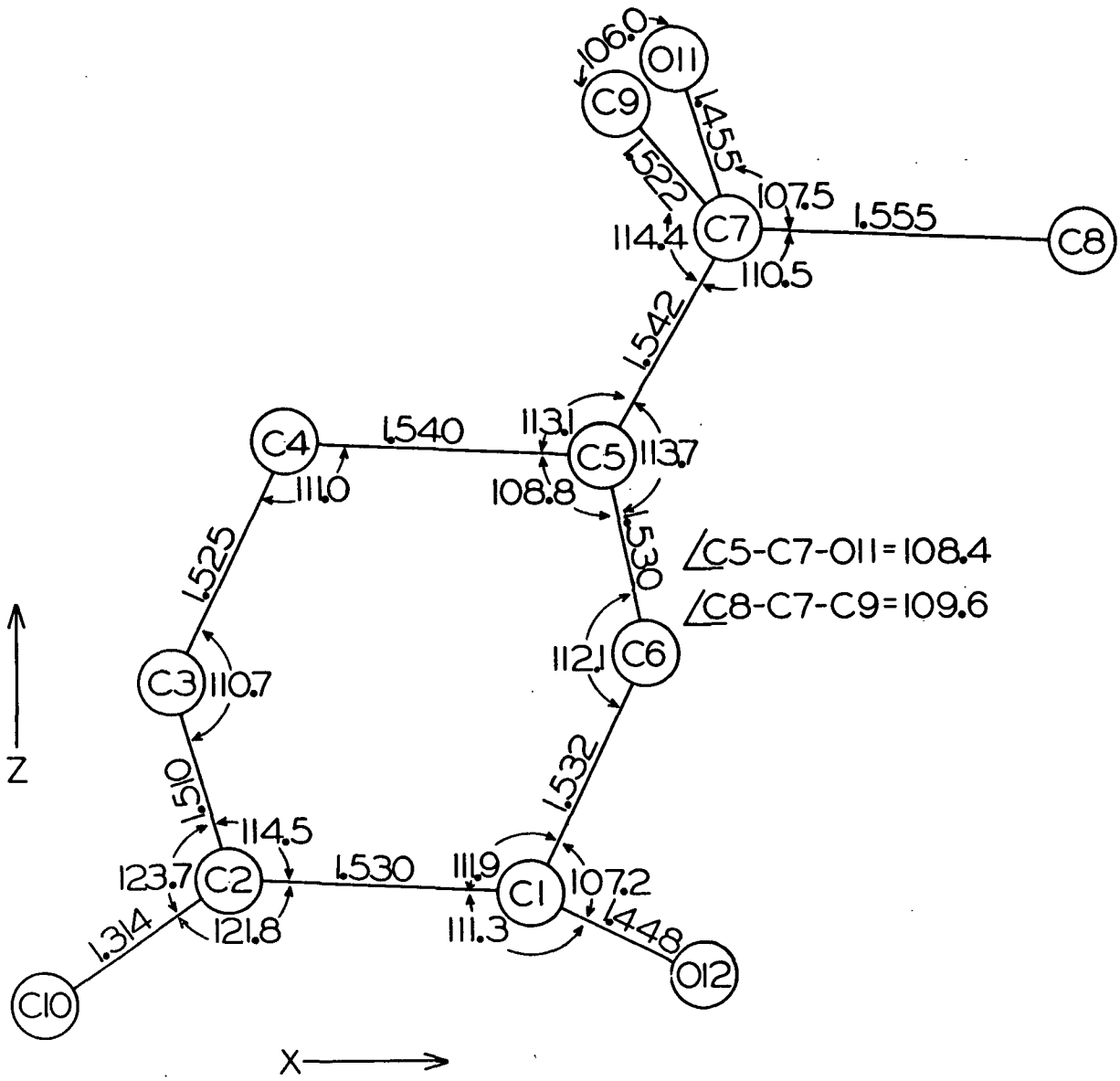

Figure 27. The Most Significant Atomic Distances and Bond Angles in the Molecule of trans-MIC Given in the Orthogonal Projection on the Plane (010)

TABLE XXX

BOND LENGTHS AND THEIR ESTIMATED STANDARD DEVIATIONS

Atom 1	Atom 2	Distance (1-2)[a], A.
C2	C10	1.314 (6)
C2	C1	1.530 (6)
C1	C6	1.532 (6)
C6	C5	1.530 (6)
C5	C4	1.540 (6)
C4	C3	1.525 (6)
C3	C2	1.510 (6)
C5	C7	1.542 (5)
C7	C8	1.555 (6)
C7	C9	1.522 (6)
C7	O11	1.455 (5)
C1	O12	1.448 (5)

[a]The number in parentheses is the estimated standard deviation of the last decimal place.

The two carbon-oxygen bonds in trans-MIC are slightly longer than the value of 1.430 A. generally accepted for a carbon-oxygen single bond (48).

The C2-C10 double bond (1.314 A.) is shorter than those reported in ethylene (1.334 A.) (58) and bicyclohexylidine (1.332 A.) (55).

Carbon-Hydrogen and Oxygen-Hydrogen Bond Distances

The carbon-hydrogen and oxygen-hydrogen bond distances are given in Table XXXI. It is evident that the distances are all shorter than the value of 1.10 A. which is usually given for a carbon-hydrogen bond. The discrepancy arises from the nature of x-ray diffraction. With x-rays, the electron density is measured. The distortion

of the electron cloud from a spherically symmetric atom is great enough so that there are systematic errors of large magnitude in bond lengths involving hydrogen as determined by x-ray diffraction (59).

Inasmuch as the hydrogen coordinates are taken from difference electron-density maps, they are greatly influenced by errors in the $|\underline{F}_c,\underline{\bar{h}}|$'s and $|\underline{F}_o,\underline{\bar{h}}|$'s. Consequently, the bond lengths listed in Table XXXI may be greatly in error, as suggested by the wide range of values.

TABLE XXXI

BOND LENGTHS INVOLVING HYDROGENS

Bond	Bond Length, A.
C1-H1	0.93
C3-H1	0.87
C3-H2	0.84
C4-H1	1.02
C4-H2	0.86
C5-H1	0.93
C6-H1	0.88
C6-H2	0.90
C8-H1	0.75
C8-H2	1.03
C8-H3	1.06
C9-H1	0.86
C9-H2	0.94
C9-H3	0.88
C10-H1	0.84
C10-H2	0.92
O11-H1	1.03
O12-H1	1.01

It is desirable to include the hydrogen parameters in the refinement procedures even if they are not known with great accuracy, however, because their presence allows the heavier atoms to assume positions which are more nearly correct.

NONBONDED DISTANCES IN THE MOLECULE

Table XXXII contains a listing of several representative intramolecular, nonbonded distances.

TABLE XXXII

NONBONDED INTERATOMIC DISTANCES WITHIN THE trans-MIC MOLECULE

Atom 1	Atom 2	Distance from Atom 1 to Atom 2, A.
C1	C3	2.557
C1	C4	2.949
C1	C5	2.544
C4	C8	4.830
C4	C6	2.501
C4	C9	5.130
C8	C9	2.516
C8	C6	3.080
C8	O11	2.428
C8	C5	2.545
C9	C6	4.458
C9	C5	2.576
C10	C3	2.491
C10	C4	3.578
C10	C5	4.201
C10	C7	5.619
C10	C8	6.562
C10	C9	5.938
C10	O11	6.398
C10	O12	3.417
O11	C4	2.915
O11	C5	2.432
O12	C3	3.118
O12	C4	3.657
O12	C5	3.016
O12	C6	2.399
O12	C7	4.370
O12	C8	4.569
O12	C9	5.367
O12	O11	5.242

The isopropylol group assumes a staggered arrangement relative to ring atoms C4 and C6, with C9 anti to the hydrogen on C5. There is considerable crowding; as shown by the very short C4-C9 and C6-C8 distances (Table XXXII). This situation probably allows O11 to participate more effectively in hydrogen bonding and improves the overall molecular packing.

The longest dimension of the molecule is 6.562 A. (C10-C8). Comparison of distances C1-C3 (2.557 A.) and C4-C6 (2.501 A.) illustrates the effect of the large trigonal angle on molecular dimensions.

As previously discussed, ring flattening causes the hydroxyl on C1 to tilt slightly outward. In a molecule having the properties assumed by Moffitt and co-workers (see Table XXIX — cyclohexanone), the O12-C3 distance is about 2.9 A. The distance found experimentally in trans-MIC is 3.118 A., illustrating the effects of nonideality in the ring.

BOND ANGLES

Table XXXIII contains a list of the bond angles in trans-MIC.

The average angle in the ring, excluding the trigonal angle, is 110.9°, with a range of 108.8° to 112.1°. This value compares favorably with the average angle of 111.1° reported for bicyclohexylidene (range 110.4 to 111.9°) (55) and the 111.55 ± 0.15° determined for cyclohexane by electron diffraction (56). It is questionable whether one should attach much significance to average bond angles, however. The energy to change bond angles is not great, and bond angles of a given type will be quite variable, depending on packing and other forces in the crystal. The bond angles in the isopropylol group (C5,C7,C8,C9,O11) exhibit a range of 106.0 to 114.4°. These angles are probably influenced by the hydrogen bonding in which O11 participates.

TABLE XXXIII

BOND ANGLES IN trans-MIC

Atoms 1-2-3	Angle(1-2-3), °[a]
C10-C2-C1	121.8
C1-C2-C3	114.5
C10-C2-C3	123.7
C2-C3-C4	110.7
C3-C4-C5	111.0
C4-C5-C6	108.8
C5-C6-C1	112.1
C6-C1-O12	107.2
C2-C1-O12	111.3
C4-C5-C7	113.1
C6-C5-C7	113.7
C5-C7-C8	110.5
C5-C7-C9	114.4
C5-C7-O11	108.4
C9-C7-O11	106.0
C8-C7-O11	107.5
C8-C7-C9	109.6

[a]The standard deviation is 0.3°.

INTERMOLECULAR RELATIONSHIPS

HYDROGEN BONDING

The molecules of trans-MIC are arranged in the crystal so as to permit the maximum amount of hydrogen bonding. Figure 28 and Table XXXIV illustrate the bond distances and angles involved.

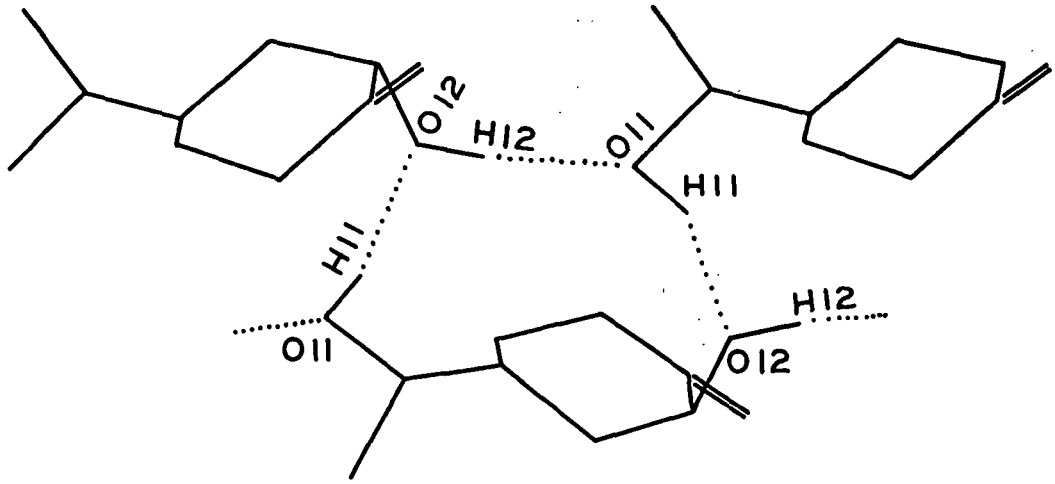

Figure 28. Intermolecular Hydrogen Bonding in trans-MIC

TABLE XXXIV

INTERATOMIC DISTANCES AND ANGLES INVOLVED IN HYDROGEN BONDING

Atom 1	Atom 2	Atom 3	Distance (1-2), A.	Distance (2-3), A.	Angle (1-2-3), °
O12	H11	O11	1.862	1.03	158.7
O11	H12	O12	1.957	1.01	140.7
O11	O12	--	2.809[a]		
O11	O12	--	2.844[b]		

[a] O12 and O11 on molecules related by a unit translation along the c axis.
[b] O12 and O11 on molecules related by the symmetry operation (1/2 -x, -y, 1/2+z).

These values are compatible with values listed by Stout and Jensen (24) for hydrogen bonded alcohols — mean O-O distance = 2.74 A., range = 2.55-2.96 A. The O-H---O bond angles are normal, also.

MOLECULAR PACKING

Eight different molecules contribute atoms to the cell in such a manner as to constitute four complete molecules.

The molecular packing in the crystal is dictated by the intermolecular hydrogen bonding, as shown in Fig. 29. The individual molecules are bonded "heads-to-tails," forming polymerlike chains which extend through the unit cell approximately parallel to the c axis. A secondary chain pairing occurs through the association of two chains by lateral hydrogen bonds. Each unit cell contains one complete chain pair and shares two others with cells located on both sides along the b axis translation. The average distance between chain pairs is approximately 4.3 A.

The extensive hydrogen bonding probably accounts for the readiness with which trans-MIC crystallizes from solution. This property was noticed during the synthesis.

The low density of the crystals (1.123 g./cc.) arises from the large amounts of void space between the chain pairs.

NONBONDED INTERMOLECULAR DISTANCES

Table XXXV gives the distance between each atom in the molecule and its nearest neighbor in another molecule. These distances all lie within a single chain pair and appear to be quite normal.

TABLE XXXV

THE DISTANCE BETWEEN EACH ATOM AND ITS NEAREST NEIGHBOR IN ANOTHER MOLECULE

Atom	Closest Chemical Grouping	Distance, A.
C1	OH	3.640
C2	CH_3	4.101
C3	OH	3.117
C4	CH_3	3.504
C5	OH	3.559
C6	OH	4.094
C7	OH	3.508
C8	CH_2	3.504
C9	OH	3.690
C10	CH_3	3.831
O11	OH	2.809
O12	OH	2.809

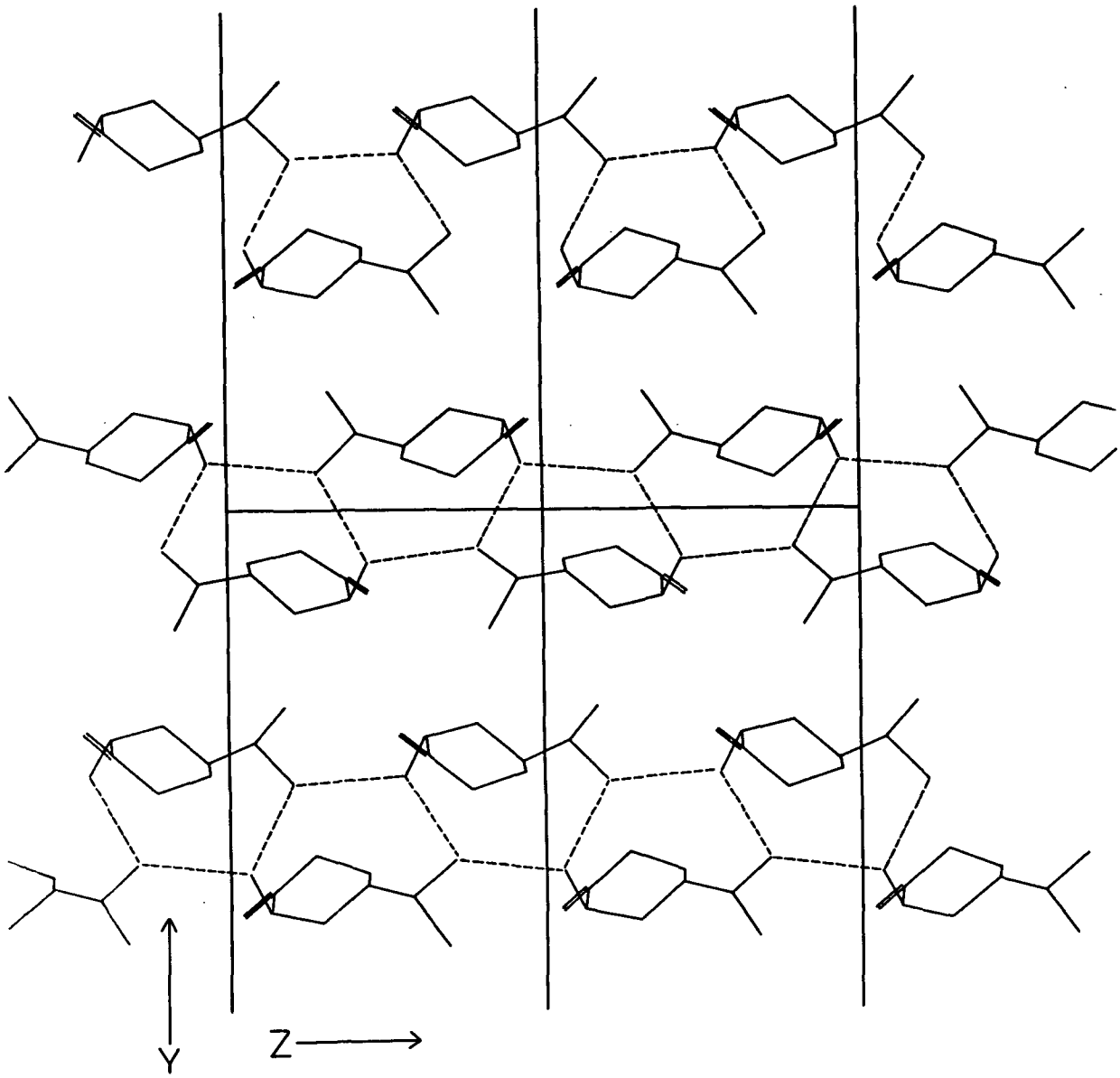

Figure 29. Crystal Packing and Intermolecular Hydrogen Bonding in trans-MIC, Given in Orthogonal Projection on the Plane (100). The Figure Extends Two Unit Cells Along the c Axis and from -0.8 to +0.8 Along the b Axis.

THERMAL ANALYSIS

The general anisotropic temperature correction to the atomic scattering factor is given by Equation (79),

$$q_r = \exp-(b_{11}h^2+b_{22}k^2+b_{33}\ell^2+b_{12}hk+b_{23}k\ell+b_{13}h\ell), \qquad (79)$$

and is often referred to in a general way as representing the thermal ellipsoid for atom $\underline{r}$. In the present case, the $\underline{b_{ij}}$'s were used to calculate the magnitudes and directions of the principal axes of atomic vibrations. The method of Waser (60) as modified by Busing and Levy (61) was chosen for the calculations.

Consider a triclinic crystal with unit cell axes $\vec{\underline{a}}_j$ and corresponding reciprocal axes $\vec{\underline{b}}_j$. The anisotropic temperature factor of a given atom is of the form $\exp(-\sum_{ij} \underline{B_{ij}}\underline{h_i}\underline{h_j})$, where the $\underline{h_i}$ are the indices of a given reflection which has the reciprocal lattice vector $\vec{\underline{H}} = \sum_i \underline{h_i}\vec{\underline{b}}_i$ associated with it. The $\underline{B_{ij}} = \underline{B_{ji}}$ are components of a symmetric tensor describing the temperature effect. More generally, in terms of a continuous reciprocal space vector $\vec{\underline{Q}} = \sum_i \underline{q_i}\vec{\underline{b}}_i$, the temperature factor has the form $\exp(-\sum_{ij} \underline{B_{ij}}\underline{q_i}\underline{q_j})$.

Consider the surface, in reciprocal space, for which the temperature factor is constant, i.e.,

$$\sum_{ij} B_{ij}q_iq_j = \text{const.} = B. \qquad (80)$$

This equation represents an ellipsoid. The problem of finding the principal axes of this ellipsoid is the same as that of finding vectors $\vec{\underline{Q}}$ for which $\underline{Q}^2 = \sum_{ij} \underline{q_i}\underline{q_j}\vec{\underline{b}}_i\cdot\vec{\underline{b}}_j$ is stationary with the extra condition

$$\sum_{ij} B_{ij}q_iq_j = B. \qquad (81)$$

Introducing the Lagrange multiplier $1/\lambda$, we have

$$\delta\left[\sum_{ij}(\vec{b}_i\cdot\vec{b}_j - B_{ij}/\lambda)q_iq_j\right] = 0 \qquad (82)$$

which reduces to

$$\sum_i(B_{ij} - \lambda\vec{b}_i\cdot\vec{b}_j)q_i = 0 \quad j = 1,2,3. \qquad (83)$$

Solution of the secular determinant yields three roots, $\lambda(\underline{r})$, corresponding to the three principal axis directions. Substitution of $\lambda(\underline{r})$ in (83) gives a vector $\vec{\underline{Q}}(\underline{r}) = \sum_{\underline{i}} \underline{q_i}(\underline{r})\vec{\underline{b}}_{\underline{i}}$ which defines the direction of the $\underline{r}$th principal axis.

Busing and Levy (61) recast (83) into the form

$$\sum_k\left[\sum_j B_{ij}(\vec{a}_j\cdot\vec{a}_k) - \lambda\delta_{ki}\right] p_k = 0. \qquad (85)$$

Here the $\vec{\underline{a}}_{\underline{j}}$ represent the direct lattice vectors, and the $\underline{p_k}$ are the components of $\vec{\underline{Q}}$ in terms of these vectors.

$$\vec{Q} = \sum_k q_k\vec{b}_k = \sum_k p_k\vec{a}_k. \qquad (86)$$

Solution of (85) for the three $\lambda(\underline{r})$ enables one to determine the values of $\underline{p_k}(\underline{r})$ for the $\underline{r}$th principal axis vector. The root mean square displacement, $\overline{\underline{U}}$, of the given atom along the $\underline{r}$th principal axis is given by

$$\overline{U_r} = (\lambda(r)/2\pi^2)^{1/2}. \qquad (87)$$

The isotropic temperature factor, $\underline{B}(\underline{r})$, related to each $\overline{\underline{U^2}}(\underline{r})$ was calculated by

$$B(r) = 8\pi^2\,\overline{U}_r^2 \qquad (88)$$

and the volume of the thermal ellipsoid for a given atom was calculated by

$$4 = (4\pi/3)\,\overline{U}_1\cdot\overline{U}_2\cdot\overline{U}_3. \qquad (89)$$

Table XXXVI contains the results of the thermal analysis of trans-MIC. The information contained in Table XXXVI should be analyzed from a qualitative viewpoint. The temperature factors obtained in a least squares refinement may include various non-random errors of observation or neglected corrections for absorption, dispersion, etc. In order to determine the magnitudes of these errors, one must collect two or more sets of intensity data and refine them separately (62). The results from one set of data can be used for making qualitative comparisons between various atoms or molecules, however.

Terminal groups ($-CH_3$, $=CH_2$, etc.) would be expected to exhibit greater thermal motion than atoms or groups which are "locked-in" by the structure. The results agree with this reasoning. The terminal methylene carbon shows the largest amount of thermal vibration (largest thermal ellipsoid volume). The two methyl carbons in the isopropyl group also exhibit relatively large thermal motion. The smallest volumes are found in the ring, with C4 and C5 appearing to be the most restricted. In general, the results agree with what would be expected.

PHASE COMPARISON

A comparison of the values of the 131 three-dimensional phases produced by the tangent formula with the corresponding phase values associated with the refined structure was made. Figure 30 shows the distribution of phase differences. The average phase difference was 22°.

An additional 50 centrosymmetric phases had been determined exactly by the symbolic addition process. The overall average phase error for the 181 reflections used to compute the initial electron density maps was 16°.

TABLE XXXVI

THERMAL MOTION ANALYSIS OF trans-MIC

Atom	r	B(r), A.^{2}	$\bar{U}_r$, A.	θ(r,a), °a	θ(r,b), °a	θ(r,c), °a	Volume, A.$^3 10^3$	$\bar{U}_3/\bar{U}_1$	$\bar{U}_3/\bar{U}_2$	$\bar{U}_2/\bar{U}_1$
C1	1	0.38	0.070	91.9	103.4	13.5	3.61	1.76	1.21	1.45
	2	0.80	0.101	132.5	43.8	81.4				
	3	1.19	0.122	42.6	49.2	79.5				
C2	1	0.57	0.085	79.7	61.5	30.5	5.68	1.61	1.18	1.37
	2	1.07	0.120	165.3	75.8	86.2				
	3	1.49	0.140	100.3	147.6	59.7				
C3	1	0.43	0.073	149.6	66.9	71.4	4.86	2.14	1.56	1.37
	2	0.80	0.100	66.1	80.9	25.6				
	3	1.94	0.157	107.6	155.0	72.9				
C4	1	0.10	0.036	42.4	108.3	53.3	1.97	3.69	1.37	2.97
	2	0.75	0.098	129.4	91.4	39.4				
	3	1.40	0.134	76.8	18.4	77.3				
C5	1	0.24	0.055	175.9	86.1	88.9	1.79	1.99	1.58	1.26
	2	0.39	0.070	87.4	66.7	23.4				
	3	0.97	0.110	93.1	156.3	66.6				
C6	1	0.43	0.073	8.9	82.1	85.6	3.59	1.49	1.03	1.45
	2	0.90	0.107	86.7	140.1	50.3				
	3	0.95	0.110	98.3	51.2	39.9				
C7	1	0.36	0.067	151.9	106.6	68.1	2.50	1.59	1.28	1.24
	2	0.55	0.083	62.0	118.7	42.2				
	3	0.90	0.107	91.9	34.0	56.0				
C8	1	0.35	0.067	29.1	75.6	65.2	4.83	2.09	1.12	1.87
	2	1.23	0.125	110.7	105.3	26.2				
	3	1.53	0.139	109.4	21.2	81.7				

TABLE XXXVI (Continued)

THERMAL MOTION ANALYSIS OF *trans*-MIC

Atom	r	B(r), A.	$\bar{U}_r$, A.	θ(r,a), °[a]	θ(r,b), °[a]	θ(r,c), °[a]	Volume, A.$^3 10^3$	$\bar{U}_3/\bar{U}_1$	$\bar{U}_3/\bar{U}_2$	$\bar{U}_2/\bar{U}_1$
C9	1	0.64	0.09	85.8	66.6	23.7	6.62	1.83	1.53	1.19
	2	0.91	0.11	78.3	154.7	67.9				
	3	2.12	0.16	167.5	99.1	81.6				
C10	1	0.75	0.10	142.9	105.7	57.4	9.89	1.87	1.37	1.36
	2	1.40	0.13	61.8	74.1	33.0				
	3	2.63	0.18	67.9	157.3	84.8				
O11	1	0.39	0.07	89.6	107.0	17.0	3.53	1.82	1.35	1.34
	2	0.70	0.09	126.0	39.4	76.0				
	3	1.29	0.13	36.0	55.6	80.3				
O12	1	0.51	0.08	105.1	90.5	15.1	4.90	1.82	1.45	1.25
	2	0.80	0.10	53.4	142.0	81.2				
	3	1.68	0.15	40.6	52.0	77.7				

[a] θ(r,n) = angle that rth principal axis makes with unit cell axis n (n = a,b,c).

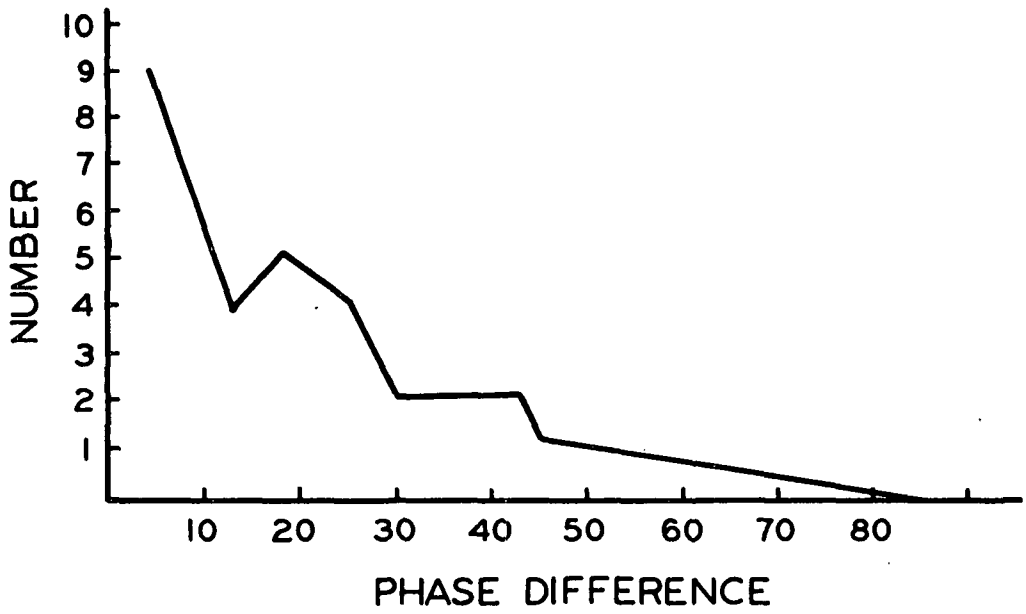

Figure 30. The Distribution of the Difference Between the Values of the Phases for the 3-D Reflections as Determined by the Tangent Formula and the Final Values Calculated from the Refined Structure

CONCLUSIONS

The symbolic addition method was successfully applied to a noncentrosymmetric crystal in this work. The average three-dimensional phase error of 22° is one of the smallest reported up to this time. It is believed that the high-quality data obtained by low temperature techniques contributed directly to the success of the structure determination. This was especially noticeable in the ease with which the hydrogen atom positions were located.

A new compound, trans-2-methylene-5-(2-isopropylol)-cyclohexanol (trans-MIC) has been isolated from the products of the oxidation of β-pinene with lead tetra-acetate in glacial acetic acid. Previous workers had found sobrerol, instead. The two compounds differ only in the position of the double bond.

Investigation by this worker showed that many of the physical properties of the two compounds are similar. It is unlikely, however, that the two could be mistakenly identified to be the same due to the differences in their infrared and NMR spectra, their behavior on a gas chromatograph column, and their addition products with bromine.

No reasons have been found for the unique results obtained by this worker. The synthesis experiments were carried out under the same conditions as previously reported, and it is believed that the reaction products should have been the same.

Single crystal, x-ray studies reveal that the six-membered ring contains ordinary carbon-carbon single bond distances which are in agreement with those reported for cyclohexane and bicyclohexylidene. The same is true for all the bond angles except the trigonal angle at C2. This angle is 114.9°.

The x-ray work indicates that cyclohexane rings found in real chemical structures differ from the ideal six-membered ring discussed in chemistry texts. Other workers have been led to the same conclusion.

The average ring angle found experimentally is about 111°, considerably greater than the 109.5° usually assumed. These larger angles flatten the ring slightly, which, in turn, causes the axial substituents to tilt outwardly to a greater extent than in the ideal situation. Ring flattening is enhanced in methylenecyclohexane rings if the trigonal angle is much greater than 111°.

The individual trans-MIC molecules are held in the crystal by an efficient system of hydrogen bonding. Both hydroxyls participate in two linkages to other molecules. This intermolecular bonding accounts for the readiness with which trans-MIC crystallizes from solution, even in the presence of impurities. The molecular packing arrangement leaves a large amount of void space in the cell, and consequently, the crystal density is low.

These studies have served to indicate that the reaction between lead tetraacetate and β-pinene may be even more complex than previous workers have believed. It is unlikely that diacetates containing exocyclic double bonds would result from the same intermediates that produce diacetates with endocyclic double bonds, because any endocyclic-exocyclic equilibrium which arises would be expected to greatly favor the endocyclic structure.

It appears that two reaction mechanisms may exist — one for endocyclic products and another for exocyclic products. Changing the reaction solvent from acetic acid to benzene probably affects the two pathways differently, thereby influencing the relative yields of exocyclic and endocyclic products.

FUTURE WORK

Structure solutions of the following terpenes would contribute greatly to the interpretation of much of the chemical information which already exists relative to this important class of compounds.

ISOPINOCAMPHEOL

There has been speculation in the literature concerning the exact structure of isopinocampheol. The four-membered ring introduces considerable strain into the system, and the cyclohexane portion of the structure probably will be flattened in order to relieve this strain.

Preliminary work in this laboratory indicates that isopinocampheol crystallizes in space group $P2_1$ with six molecules per unit cell. The approximate room temperature unit cell constants are: $\underline{a}$ = 17.5 A., $\underline{b}$ = 6.5 A., $\underline{c}$ = 14.1 A., β = 110°.

The information from this study could be applied to all compounds having the pinene configuration.

cis-PINOCARVYL-p-NITROBENZOATE

The solution of this structure will provide quantitative information about the structure of β-pinene. A complete set of three-dimensional intensity data has already been collected in this laboratory (Appendix VI). The structure remains to be solved.

α-PINENE DERIVATIVE

A crystalline, light atom derivative of α-pinene should be solved.

SOBREROL

An x-ray structure determination of the structure of trans-sobrerol would provide information for comparison with the work reported in this thesis.

Preliminary experiments in this laboratory showed that sobrerol crystallizes nicely from water.

NOMENCLATURE

A = absorption correction

a = unit cell axis

B = overall isotropic temperature factor

b = unit cell axis

b_{ij}, $B_{ij,r}$ = individual anisotropic temperature factor for atom r

$\vec{b}_j$ = reciprocal cell axis

$B(r)$ = individual isotropic temperature factor

C = length of unit cell axis

d = spacing between equivalent lattice planes

$d_{hk\ell}$ = spacing between equivalent lattice planes

$|E_{c,\bar{h}}|$ = calculated normalized structure factor

$|E_{\bar{h}}|$ = normalized structure factor

$|E_{hk\ell}|$ = normalized structure factor

exp = exponential function

f_j = atomic scattering factor at a finite temperature

f_o = atomic scattering factor at absolute zero

$f_{o,j}$ = atomic scattering factor at absolute zero

$|F_{o,hk\ell}|$ = observed structure factor amplitude

$|F_{rel,hk\ell}|$ = relative structure factor amplitude

$|F_{hk\ell}|$ = structure factor amplitude

G = even

$hk\ell$ = general indices associated with a given reflection

h = abbreviation for $hk\ell$

$\overline{h\text{-}k}$ = abbreviation for $hk\ell$

i = $\sqrt{-1}$

$I_{hk\ell}$ = intensity of reflection $hk\ell$

$I_j(x)$ = Bessel function

K = scale factor to put structure amplitude on an absolute scale, or overall least squares refinement scale factor

K_j = interlayer scaling constant for layer j

$K\alpha_1$, $K\alpha_2$ = x-radiation used in structure determination

$\bar{k}$ = abbreviation for $hk\ell$

$\bar{k}_r$ = restricted set of reflections

L = Lorentz correction

$(MA)_j$ = mass absorption coefficient for element j

n = order of reflection in the Bragg equation

N = total number of atoms in the unit cell

p = polarization correction

p_j = weight fraction of atom j in a compound

Q = residual

q_r = temperature correction

R = agreement index

$\vec{r}$ = vector from origin to point (x_r, y_r, z_r) in the unit cell

$\bar{s}$ = average of a group of $(\sin\theta)/\lambda$ values

U odd

U_r = length of rth principal axis of thermal ellipsoid

(u_j, v_j, w_j) = absolute coordinates of atom j, A.

V = variance of a phase indication (rad.^{2}); or volume of unit cell (A.^{3}).

W_h = weighting constant in least squares refinement

(X, Y) = Cartesian coordinates of a reflection based on an arbitrary rectangular coordinate system

(x_j, y_j, z_j) = coordinates of an atom in fractions of unit cell axes

Z_j = atomic number of atom j, or wavelet scattered from atom j

β = monoclinic angle

$\delta(1)$, $\delta(1)$ = dihedral angles in a six-membered ring

$\Delta\underline{F}$, Δ = coefficient in a difference map ($|\underline{F}_o| - |\underline{F}_c|$)

θ = angle between incident x-ray beam and reflecting planes

$\theta(\underline{r},\underline{n})$ = angle between $\underline{r}$th principal thermal ellipsoid axis and unit cell axis $\underline{n}$ ($\underline{n}$ = $\underline{a}$,$\underline{b}$,$\underline{c}$)

κ = kappa function associated with the noncentrosymmetric probability functions in symbolic addition

λ = wavelength of x-radiation

μ = equi-inclination angle, or linear absorption coefficient

$\rho_{\underline{f}}$ = experimentally determined density

$\rho_{x\text{-ray}}$ = density calculated from x-ray unit cell dimensions

$\rho(\underline{r})$ = electron-density distribution function

$\sigma(\underline{p}_j)$ = estimated standard deviation of parameter $\underline{p}_j$

$\sigma_{\underline{n}} = \sum_{\underline{j}=1}^{\underline{N}} \underline{Z}_{\underline{j}}^{\underline{n}}$

$\phi_{\underline{hk\ell}}$ = phase associated with reflection $\underline{hk\ell}$

$\phi_{-\underline{h}}$ = phase associated with reflection $\underline{hk\ell}$

$\phi_{\underline{j}}$ = phase of wavelet scattered from atom $\underline{j}$ relative to the wave scattered by fictitious electrons at the origin of the unit cell

ACKNOWLEDGMENTS

The author wishes to acknowledge his sincere appreciation for the advice and encouragement offered by the members of his thesis advisory committee. More specifically, he thanks Dr. Gerald F. Richards (Chairman) for his guidance pertaining to all matters of this thesis and for his readiness to share his knowledge of x-ray crystallography. He thanks Dr. Dale G. Williams for many fruitful discussions regarding crystallographic techniques and the interpretation of experimental results. And, he thanks Dr. Donald C. Johnson for his suggestions and assistance with regard to the execution and interpretation of the chemistry experiments discussed in this thesis.

The author acknowledges advice given by Drs. Jerome and Isabella Karle of the Naval Research Laboratories relative to the application of the symbolic addition method.

The author thanks Dr. George A. Jeffrey, of the University of Pittsburgh, for providing the computer programs used for data reduction, Fourier synthesis, and structure analysis; Dr. Farid R. Ahmed of the Canadian Research Council for the least squares refinement computer programs; John Bachhuber of the I.P.C. computer center for his advice and assistance in the writing of many of the computer programs.

The author especially thanks his fellow student, John T. Ham, for his assistance in writing most of the FORTRAN programs and for participating in many enlightening discussions with the author in the course of this work.

The author wishes to express his sincere appreciation to his wife, Ginny, for her assistance in preparing this manuscript and for keeping her sense of humor throughout the course of this work.

LITERATURE CITED

1. Simonsen, J. L., and Owen, L. N. The terpenes. 2nd ed. Vol. I. Cambridge, University Press, 1947.

2. Simonsen, J. L., and Owen, L. N. The terpenes. 2nd ed. Vol. II. Cambridge, University Press, 1952.

3. Simonsen, J. L., and Barton, D. H. R. The terpenes. 2nd ed. Vol. III. Cambridge, University Press, 1952.

4. Simonsen, J. L., and Ross, W. C. J. The terpenes. 2nd ed. Vols. IV and V. Cambridge, University Press, 1957.

5. Wallach, O., Ann. 227:300(1885).

6. Webb, R., U. S. pat. 3,264,362(Aug. 2, 1966); C.A. 65:15436e.

7. Glidden Co., Neth. Appl. pat. 6,501,986(Aug. 20, 1965); C.A. 64:3619a.

8. Buchanan, M. A. Extraneous components of wood. In Browning's The chemistry of wood. New York, Interscience, 1963.

9. Matsubara, Y., J. Chem. Soc. Japan Pure Chem. Sect. 78:907(1957); C.A. 49:22056.

10. Ward, K., et al. Unpublished work, The Institute of Paper Chemistry, 1962.

11. Whitham, G. H., J. Chem. Soc. 1961:2232.

12. Criegee, R., Angew. Chem. 70:171(1958).

13. Matsubara, Y., J. Chem. Soc. Japan Pure Chem. Sect. 75:809(1954).

14. Gruenewald, L., and Johnson, D., J. Org. Chem. 30:1673(1965).

15. Sato, T., J. Chem. Soc. Japan Pure Chem. Sect. 86, no. 2:252(1965).

16. Scott, W. E. Unpublished work, The Institute of Paper Chemistry, 1966.

17. Williams, P. P., Chem. and Ind. 1964:1583.

18. MacDonald, A., Trotter, J., Acta Cryst. 19:456(1965).

19. Weibenga, E., and Krom, C., Rec. Trav. Chim. 65:663(1946).

20. Constitution of the American Crystallographic Association, Article I, Adopted April 11, 1950.

21. Buerger, M. J. X-ray crystallography. New York, John Wiley and Sons, 1942.

22. Bunn, C. W. Chemical crystallography. London, England, Oxford at the Clarendon Press. 173 p.

23. Buerger, M. J. Crystal structure analysis. New York, John Wiley and Sons, 1960. 668 p.

24. Stout, G., and Jensen, L. X-ray structure determination, a practical guide. p. 315-38. New York, The MacMillan Company, 1968.

25. Karle, J. The determination of phase angles. In R. Brill's Advances in structure research by diffraction methods. Vol. 1. p. 55-89. New York, Interscience, 1964.

26. Harker, D., and Kasper, J., J. Chem. Phys. 15:882(1947).

27. Karle, J., and Hauptman, H., Acta Cryst. 9:635(1956).

28. Karle, I. L., and Karle, J., Acta Cryst. 21:860(1966).

29. Germain, G., and Woolfson, M., Acta Cryst. B24:91(1968).

30. Oh, Y., and Maslen, E., Acta Cryst. B24:883(1968).

31. Hauptman, H., and Karle, J., Acta Cryst. 9:45(1956).

32. Gruenewald, L. E. Solvolysis of cis-pinocarvyl brosylate and related esters. Doctor's Dissertation. Appleton, Wis., The Institute of Paper Chemistry, 1965.

33. Kharasch, M. S., et al., J. Org. Chem. 16:533(1951).

34. Lund, H., and Bjerrum, J., Ber. 64:210(1931).

35. Cheronis, N. D., and Entrikin, J. B. Semimicro qualitative organic analysis. 2nd ed. New York, Interscience, 1957. 774 p.

36. Wallach, O., Ann. 291:353(1896).

37. MacGillavry, C., and Rieck, G., eds. International tables for x-ray crystallograph. Vol. III. Birmingham, England, Kynoch Press, 1962. 201 p.

38. Ham, J. The crystal and molecular structure of methyl beta-cellobioside·methanol. Doctor's Dissertation. Appleton, Wis., The Institute of Paper Chemistry, January, 1969.

39. Richards, G. Some structures of metal-olefin complexes. Doctor's Dissertation. Iowa City, Iowa, University of Iowa, Feb., 1964.

40. Rollett, J., and Sparks, R., Acta Cryst. 13:273(1960).

41. Norment, H. G. Naval Research Laboratory Report 5739, 1962.

42. Henry, N. F. M., and Lonsdale, K., eds. International tables for x-ray crystallography. Vol. I. Birmingham, England, Kynoch Press, 1952. 386 p.

43. Karle, J. Personal communication to John Ham, 1968.

44. Ahmed, F. R., et al. NRC Crystallographic Programs for the IBM-360 System, Divisions of Pure Physics and Pure Chemistry, National Research Council, Ottawa, Canada.

45. Hodgson, L. I., and Rollett, J. S., Acta Cryst. 16:329(1963).

46. Cruickshank, D. W. J., et al. Crystallographic calculations on PEGASUS and Mark I. In Pepinsky, Robertson, and Speakman's Computing methods and the phase problem in x-ray crystallography. p. 44. New York, Pergamon Press, 1961.

47. Ref. (24), p. 381.

48. Hordvik, A., Acta Chem. Scand. 20:1943(1966).

49. Ref. (37), p. 201.

50. Hanson, H., et al., Acta Cryst. 17:1040(1964).

51. Stewart, F., J. Chem. Phys. 42:3175(1965).

52. Wohl, R., Chimia 18:219(1964).

53. Corey, E., and Sneen, R., J. Am. Chem. Soc. 77:2505(1955).

54. Moffitt, W., Woodward, R. B., Moscowitz, A., Klyne, W., and Djerassi, C., J. Am. Chem. Soc. 83:4013(1961).

55. Sasvari, K., and Low, M., Acta Cryst. 19:840(1965).

56. Davis, M., and Hassel, O., Acta Chem. Scand. 17:1181(1963).

57. Dewar, M. J. S., and Schmeising, H., Tetrahedron 11:96(1960).

58. Bartell, L., and Bonham, R., J. Chem. Phys. 27:1414(1957).

59. Hamilton, W. C., J. Chem. Ed. 45:296(1968).

60. Waser, J., Acta Cryst. 8:731(1955).

61. Busing, W., and Levy, H., Acta Cryst. 8:731(1955).

62. Lonsdale, K., and Mellege, J., Acta Cryst. 14:59(1961).

63. Ref. (24), p. 369.

64. Hauptman, H., and Karle, J. Solution of the phase problem I. The Centrosymmetric Crystal, ACA Monograph Number 3. Ann Arbor, Mich., Edwards Brothers, Inc., 1953. 88 p.

65. Schomaker, V., Waser, J., Marsh, R. E., and Bergman, G., Acta Cryst. 12:600(1959).

66. Schmidt, H., Ber. 77:167(1944).

67. Karle, I. L. Personal communication, Aug. 6, 1968.

68. Karle, I. L., and Karle, J., Acta Cryst. B24:81(1968).

69. Cochran, W., and Lipson, H. The determination of crystal structures. p. 88. London, G. Bell and Sons, Ltd., 1953.

70. Wilson, A. J. C., Nature 150:151(1942).

71. Watson, G. N. A treatise on the theory of Bessel functions. 2nd ed. p. 77. Cambridge, England, University Press, 1958.

72. Eliel, E. Stereochimstry of carbon compounds. New York, McGraw-Hill, 1962. 486 p.

73. Eliel, E., Allinger, N., Angyal, S., and Morrison, G., Conformational analysis. New York, Interscience, 1965. 524 p.

APPENDIX I

SIGMA-2 LISTING

H			K			H-K			KAPPA
1	5	3	-2	5	8	3	0	-5	2.69
1	5	3	2	5	-8	-1	0	11	3.86
1	5	3	2	6	1	-1	-1	2	1.59
1	5	3	-1	2	11	2	3	-8	5.25
1	5	3	-1	3	1	2	2	2	1.41
1	5	3	1	-1	2	0	6	1	2.14
1	5	3	-1	-1	1	2	6	2	2.51
1	5	3	-1	1	-2	2	4	5	1.73
1	5	3	-1	-1	0	2	6	3	2.25
1	5	3	-2	1	1	3	4	2	2.37
1	5	3	-2	1	-5	3	4	8	2.46
1	5	3	-2	1	6	3	4	-3	2.64
1	5	3	0	8	0	1	-3	3	3.35
1	5	3	-2	7	-5	3	-2	8	3.23
1	5	3	-3	3	11	4	2	-8	3.36
1	5	3	-3	4	3	4	1	0	3.41
1	5	3	-3	5	-9	4	0	12	3.81
1	5	3	-3	5	10	4	0	-7	3.59
1	5	3	-4	0	1	5	5	2	3.53
1	5	3	-4	3	11	5	2	-8	2.90
1	5	3	-4	7	5	5	-2	-2	2.97
1	5	3	-5	0	-4	6	5	7	3.67
1	5	3	-5	-1	-2	6	6	5	3.71
1	5	3	-5	6	-6	6	-1	9	3.22
1	5	3	-6	4	-1	7	1	4	3.36
1	5	3	6	4	-2	-5	1	5	2.54
1	5	3	-6	5	-5	7	0	8	4.36
1	5	3	-6	7	4	7	-2	-1	3.44
1	5	3	-7	3	2	8	2	1	3.61
1	6	2	-5	7	1	6	-1	1	.63
1	6	2	4	1	8	-3	5	-6	.95
1	6	2	-4	3	2	5	3	0	.65
1	6	2	4	3	-6	-3	3	8	1.03
1	6	2	-3	7	2	4	-1	0	.90
1	6	2	-4	4	10	5	2	-8	.89
1	6	2	4	5	2	-3	1	0	1.26
1	6	2	-4	5	-6	5	1	8	1.35
1	6	2	-4	5	9	5	1	-7	1.33
1	6	2	4	5	-10	-3	1	12	.72
1	6	2	0	0	2	1	6	0	2.38
1	6	2	0	1	-3	1	5	5	1.76
1	6	2	0	3	9	1	3	-7	2.19
1	6	2	0	3	10	1	3	-8	1.99
1	6	2	-5	5	5	6	1	-3	.94
1	6	2	5	4	0	-4	2	2	1.15
1	6	2	7	2	10	-6	4	-8	.93
1	6	2	-4	5	-1	5	1	3	.52
1	6	2	-5	5	5	6	1	-3	.94
1	6	2	-5	7	1	6	-1	1	.63
1	6	2	5	7	2	-4	-1	0	1.02
1	6	2	6	0	-6	-5	6	8	.55
1	8	0	-1	4	-7	2	4	7	5.69
1	8	0	0	4	6	1	4	-6	3.03
1	8	0	0	4	-6	1	4	6	3.56
1	8	0	0	5	-3	1	3	3	3.32
1	8	0	-3	0	-1	4	8	1	3.15
1	8	0	-3	1	1	4	7	-1	4.43
1	8	0	-3	5	-1	4	3	1	4.02
1	8	0	-3	6	8	4	2	-8	4.49
1	8	0	-4	1	0	5	7	0	4.52
1	8	0	-4	3	-1	5	5	1	6.46
1	8	0	-4	4	9	5	4	-9	5.28
1	8	0	-4	7	5	5	1	-5	2.69
1	8	0	0	2	-8	1	6	8	.70
1	8	0	0	6	-7	1	2	7	.70
1	8	0	-5	7	1	6	1	-1	.52
1	8	0	6	2	-8	-5	6	8	.52
1	8	0	6	3	8	-5	5	-8	.89
1	8	0	6	4	-8	-5	4	8	1.11
1	8	0	-6	5	0	7	3	0	.61
1	8	0	-6	7	-4	7	1	4	.86
1	8	0	3	2	2	-2	6	-2	.78
1	8	0	4	3	9	-3	5	-9	.72
1	8	0	7	3	-3	-6	5	3	.73
1	8	0	4	4	-3	-3	4	3	.92
1	8	0	-4	4	8	5	4	-8	1.18

APPENDIX II

DERIVATION OF UNIT CELL EXPRESSIONS

Beginning with the usual statement of Bragg's Law, one can develop an analytical expression which takes the systematic errors in reflection positions into account,

$$\frac{n\lambda}{2d} = \sin\theta \tag{90}$$

where

θ = reflection angle;

$\underline{d}$ = reflection plane spacing;

$\underline{n}$ = order of the reflection;

λ = wavelength of the radiation.

Since one determines θ from x-ray reflection positions which are subject to error, one actually determines $\theta + \Delta\theta$, and the expression becomes

$$\frac{n\lambda}{2d} = \sin(\theta+\Delta\theta). \tag{91}$$

Squaring Equation (91), expanding the right side by Taylor's expansion, and neglecting terms involving powers of $\Delta\theta$, we obtain

$$\left(\frac{n\lambda}{2d}\right)^2 = \sin^2\theta + \Delta\theta\sin 2\theta. \tag{92}$$

The term $\Delta\theta$ is composed of several systematic errors, due respectively to eccentricity, shrinkage, and absorption.

$$\left(\frac{n\lambda}{2d}\right)^2 = \sin^2\theta + \Delta\theta_{ecc}\sin 2\theta + \Delta\theta_{shr}\sin 2\theta + \Delta\theta_{abs}\sin 2\theta \tag{93}$$

The $\Delta\theta$'s have been found to be the following, where the shrinkage and eccentricity errors are grouped together (12),

$$\Delta\theta_{abs} = - E\cos^2\theta \tag{94}$$

$$\Delta\theta_{shr,ecc} = - D\sin 2\theta. \tag{95}$$

D and E are experimental constants. The error equation then becomes

$$\left(\frac{n\lambda}{2d}\right)^2 = \sin^2\theta - D\sin^2 2\theta - E\cos^2\theta\sin 2\theta. \tag{96}$$

The general expression for the d-spacings in an orthorhombic crystal is given by (97).

$$d_{h'k'\ell'} = \frac{1}{\sqrt{\frac{h'^2}{a^2} + \frac{k'^2}{b^2} + \frac{\ell'^2}{c^2}}} \tag{97}$$

a, b, and c are the lengths of the respective axes. Substituting (97) into (96) and letting $nh' = h$, $nk' = k$, and $n\ell' = l$ we obtain (98).

$$\frac{h^2\lambda^2}{4a^2} + \frac{k^2\lambda^2}{4b^2} + \frac{\ell^2\lambda^2}{4c^2} + D\sin^2 2\theta + E\cos^2\theta\sin^2\theta = \sin^2\theta. \tag{98}$$

One of the first three terms in (98) will be zero, depending on the axis of rotation of the back-reflection exposure. Equation (98) can be written in the following useful form,

$$Y = AX_2 + BX_3 + DX_4 + EX_5 \tag{99}$$

where

$A = 1/4m^2$;

$B = 1/4n^2$;

m,n = lengths of nonrotation unit cell axes;

$Y = \sin^2\theta$;

$X_2 = H^2\lambda^2$;

$X_3 = H^2\lambda^2$;

$\underline{H}_m, \underline{H}_n$ = Miller indices associated with a given reflection;

$\underline{X}_4 = \sin^2 2\theta$;

$\underline{X}_5 = \cos^2\theta \sin 2\theta$.

In order to use Equation (99), one needs to know $\underline{h}, \underline{k}, \underline{\ell}$, and θ for a given reflection; $\underline{h}$, $\underline{k}$, and $\underline{\ell}$ were obtained directly from indexing the back-reflection film. θ was calculated from the Cartesian coordinates of the equivalent reflections lying on opposite sides of the film slot. See Fig. 31.

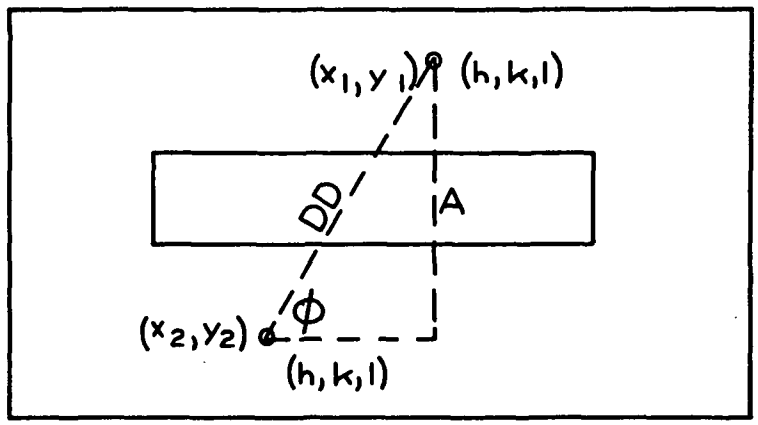

Figure 31. Diagram of Geometry of Equivalent High-Theta Spots on a Back-Reflection Film (ϕ = 63° 27')

$\underline{A}$ is related to theta by the following expression,

$$\theta = 90 - F/2. \tag{100}$$

$\underline{A}$ is also related to the Cartesian coordinates of the equivalent reflections in the following manner.

$$A = \sin(63°27')(DD) \tag{101}$$

$$DD = \sqrt{(x_1-x_2)^2 + (y_1-y_2)^2}\ . \tag{102}$$

Combining Equations (100), (101), and (102), we obtain an expression for θ in terms of reflection Cartesian coordinates.

$$\theta_{hk\ell} = 90 - 0.45 \sqrt{(x_1-x_2)^2 + (y_1-y_2)^2} \quad . \tag{103}$$

In practice, several high-angle reflections were chosen from a given back-reflection photograph. The corresponding values of $\underline{Y}$, $\underline{X}_2$, $\underline{X}_3$, $\underline{X}_4$, and $\underline{X}_5$ in Equation (99) were calculated for each reflection. These sets of variables were then fitted to Equation (99) by the least squares computer program 921-A (I.P.C. Utility Program Library, written by Dr. R. Nelson and modified by John Ham as to input format).

The unit cell constants were obtained from coefficients $\underline{A}$ and $\underline{B}$ in the least squares equation

$$m = \frac{1}{2A^{1/2}} \quad , \quad n = \frac{1}{2B^{1/2}} \tag{104}$$

where $\underline{m}$,$\underline{n}$ = nonrotation unit cell axes.

The standard deviations of the cell dimensions were calculated with the following formulas.

$$s(m) = \sqrt{\frac{0.0625V(A)}{A^3}} \tag{105}$$

$$s(n) = \sqrt{\frac{0.0625V(B)}{B^3}} \tag{106}$$

APPENDIX III

A LIST OF COMPUTER PROGRAMS USED IN THE STRUCTURE ANALYSIS

UNIT CELL PARAMETERS

1. Program to convert microcomparator output to Utility 921-A input[1]
2. Utility 921-A[2]
3. Program to calculate unit cell parameters from 921-A output[1]

MULTIPLE FILM SCALING

4. BK1[3]
5. BK2[3]
6. BK3[3]
7. BK4[3]
8. Lorentz and polarization corrections[3]

INTERLAYER SCALING

9. BK7[3]
10. BK8[3]
11. BK8AB[3]
12. BK9[3]
13. BK10[3]
14. IBM 1620 Library No. 5.0.003 — Eigen values of Real Symmetric Matrices

PREPARATION OF NORMALIZED STRUCTURE FACTORS

15. Program to interpolate scattering factor tables[3]
16. Structure factor part I[3]
17. K-curve program[1]
18. Program to prepare input to Utility Program 911-B[1]
19. Utility Program 911-B[2]
20. E-value program[1]

SYMBOLIC ADDITION PROGRAMS

21. Program to convert indices for a given reflection into one word and a sign indicator; input to sigma-2 listing program[1]

22. Program to generate symmetry mates for space groups $P2_1$ and $P2_12_12_1$ and convert to one word and a sign indicator; input to sigma-2 listing program[1]

23. Sigma-2 listing program[1]

24. Tangent formula for space group $P2_12_12_1$[1]

25. Program to convert tangent formula output to Fourier synthesis input[1]

ELECTRON DENSITY MAPS

26. Structure factor part II[3]

27. Three-dimensional Fourier synthesis program[3]

28. Alphabetic print-out program[3]

REFINEMENT

29. Program to prepare SFLS data cards from structure factor part I output[1]

30. SFLS Program[4]

31. SFLS Results Program[4]

DATA ANALYSIS

32. Least squares plane calculation[3]

33. Calculation of interatomic angles and distances[3]

34. Calculation of angle between two planes[1]

35. Calculation of standard deviations of interatomic distances and angles[3]

36. Thermal Vibrations Analysis[1]

37. Program to compare tangent formula phases with final refined phases[1]

---

[1]FORTRAN II-D Programs written by the author and/or John Ham.

[2]I.P.C. Utility Program Library, written by Dr. Richard Nelson.

[3]SPS Program obtained from the Crystallography Laboratory, University of Pittsburgh, Pittsburgh, Pennsylvania.

[4]SPS Program obtained from Dr. F. R. Ahmed, Pure Physics Division, National Research Council, Ottawa, Canada, 1963.

APPENDIX IV

SUMMARY OF F_c, F_o, AND ϕ FOR *trans*-MIC

h	k	ℓ	F_o	F_c	φ
0	2	0	53.5	51.2	0
0	6	0	40.1	37.4	180
0	8	0	20.6	15.4	180
0	12	0	12.8	13.9	180
0	14	0	8.4	9.4	0
0	16	0	21.0	22.8	0
0	1	1	20.7	19.9	270
0	2	1	33.1	36.4	0
0	3	1	16.0	17.7	270
0	4	1	17.8	17.3	0
0	5	1	13.2	12.9	270
0	6	1	30.0	25.5	180
0	7	1	7.6	9.0	90
0	8	1	4.4	6.8	0
0	9	1	9.1	9.7	90
0	10	1	4.2	6.5	180
0	11	1	17.2	19.0	270
0	12	1	8.3	6.5	180
0	13	1	11.7	11.1	270
0	14	1	22.7	23.1	0
0	15	1	12.6	13.0	90
0	17	1	10.3	10.9	90
0	18	1	10.7	10.5	180
0	21	1	3.7	3.6	270
0	22	1	3.0	3.6	180
0	0	2	11.1	11.9	0
0	1	2	59.3	59.0	270
0	3	2	45.3	45.6	90
0	4	2	54.6	52.7	180
0	5	2	28.1	24.0	90
0	6	2	33.0	31.6	180
0	7	2	19.8	20.2	270
0	8	2	38.2	36.9	0
0	9	2	16.1	18.1	270
0	10	2	24.5	23.1	0
0	11	2	22.4	20.9	90
0	12	2	9.1	8.8	0
0	13	2	19.0	18.8	90
0	14	2	6.0	8.2	0
0	15	2	24.9	25.5	270
0	16	2	5.7	5.1	180
0	17	2	15.4	16.1	270
0	18	2	17.1	19.1	180
0	19	2	12.5	12.1	90
0	20	2	16.5	15.4	180
0	21	2	6.0	5.4	90
0	22	2	3.7	3.8	0
0	1	3	32.8	34.3	90
0	2	3	35.1	33.6	0
0	3	3	4.8	4.2	90
0	4	3	38.1	34.9	0
0	5	3	12.1	8.2	90
0	6	3	3.6	6.7	0
0	7	3	37.7	39.0	90
0	8	3	27.0	26.3	180
0	9	3	7.6	8.0	270
0	10	3	22.2	23.2	180
0	11	3	18.6	18.1	270
0	12	3	4.4	5.6	180
0	13	3	10.9	10.9	270
0	14	3	7.8	7.4	0
0	15	3	5.6	6.0	270
0	16	3	15.2	16.4	0
0	17	3	4.6	4.6	90
0	18	3	3.3	3.0	180
0	20	3	14.0	12.7	180
0	21	3	5.5	5.6	90
0	1	4	7.2	7.2	270
0	2	4	13.2	13.9	0
0	3	4	17.0	19.2	90
0	4	4	24.0	23.5	0
0	5	4	8.6	10.1	90
0	6	4	4.2	1.7	0
0	7	4	25.7	27.0	270
0	8	4	38.5	35.3	180
0	10	4	24.1	25.2	180
0	11	4	20.9	19.8	90
0	12	4	13.3	11.4	0
0	13	4	8.7	9.2	270
0	14	4	9.9	10.7	0
0	15	4	7.3	7.8	270
0	16	4	4.1	3.7	180
0	17	4	4.5	4.3	270
0	18	4	5.6	4.3	0
0	19	4	5.8	5.8	90
0	20	4	6.5	6.2	0
0	1	5	13.4	13.1	270
0	2	5	20.6	20.4	0
0	3	5	5.8	5.5	270
0	4	5	11.6	13.1	0
0	5	5	11.6	12.7	270
0	6	5	13.8	14.8	0
0	7	5	36.5	34.3	270
0	8	5	6.8	7.9	180
0	10	5	23.9	25.8	180
0	11	5	21.7	21.9	90
0	13	5	10.1	11.7	90
0	14	5	12.5	13.1	0
0	16	5	13.0	12.6	0
0	18	5	4.4	2.2	180
0	19	5	7.9	1.4	90
0	0	6	28.8	28.6	180
0	2	6	18.5	18.8	180
0	3	6	14.8	14.8	270
0	4	6	19.2	19.6	0
0	5	6	6.2	7.0	270
0	6	6	24.0	24.3	0
0	7	6	15.6	16.0	90
0	8	6	6.2	5.9	180
0	9	6	12.9	13.7	90
0	15	6	15.1	14.5	270
0	17	6	3.7	2.9	270
0	18	6	5.7	5.4	180
0	1	7	23.6	25.6	90
0	2	7	5.1	4.9	0
0	3	7	30.3	31.3	90
0	4	7	4.1	6.6	0
0	5	7	4.7	6.0	270
0	6	7	11.8	11.5	180
0	7	7	7.0	8.0	270
0	9	7	6.8	7.1	90
0	11	7	4.6	3.1	90
0	12	7	3.9	3.6	180
0	13	7	3.3	4.1	270
0	14	7	9.0	8.8	0
0	15	7	13.4	12.3	270
0	16	7	4.2	3.3	0
0	0	8	19.5	20.6	180
0	2	8	4.0	4.3	180
0	3	8	6.5	7.8	90
0	4	8	3.9	4.8	0
0	5	8	5.4	4.5	270
0	6	8	9.3	10.9	0
0	8	8	17.9	17.5	0
0	9	8	6.0	5.9	90
0	10	8	8.9	8.1	180
0	11	8	8.7	6.6	270
0	12	8	16.4	14.1	180
0	13	8	6.7	6.4	270
0	2	9	15.1	16.0	0
0	3	9	9.5	10.7	270
0	5	9	13.2	12.7	270
0	6	9	9.0	8.3	180
0	7	9	10.2	9.3	270
0	8	9	6.0	3.5	0
0	9	9	3.3	3.0	270
0	10	9	14.2	13.6	0
0	1	10	3.8	4.8	270
0	2	10	4.4	3.3	180
1	1	0	39.2	44.2	90
1	3	0	27.9	29.6	270
1	4	0	28.2	25.8	90
1	5	0	3.5	4.6	270
1	6	0	22.6	22.2	90
1	7	0	24.7	22.5	270
1	8	0	14.3	12.7	270
1	9	0	12.1	9.8	270
1	10	0	23.0	22.7	270
1	11	0	7.6	7.6	90
1	15	0	6.3	6.7	90
1	17	0	7.7	8.0	90
1	21	0	7.7	6.6	270
1	22	0	9.0	8.4	90
1	0	1	31.0	37.4	270
1	1	1	28.2	28.5	265
1	2	1	44.3	42.3	349
1	3	1	45.4	39.6	261
1	4	1	56.3	51.5	127
1	5	1	36.5	35.7	256
1	6	1	39.3	36.4	175
1	7	1	18.5	16.8	345
1	8	1	29.5	25.0	291
1	9	1	5.3	2.6	348
1	10	1	33.5	31.8	3
1	11	1	17.0	18.2	223
1	12	1	14.3	14.0	341
1	13	1	18.7	18.4	90
1	14	1	13.3	14.2	192
1	15	1	25.2	25.9	65
1	16	1	16.2	16.7	151
1	17	1	5.7	6.2	331
1	19	1	7.1	8.1	221
1	20	1	6.8	6.5	21
1	21	1	9.9	9.4	221
1	22	1	6.4	7.3	9
1	0	2	45.0	42.3	0
1	1	2	9.4	9.5	1
1	2	2	21.7	20.0	320
1	3	2	34.7	32.7	102
1	4	2	21.9	18.2	93
1	5	2	26.5	23.3	265
1	6	2	19.6	18.9	211
1	7	2	21.5	18.7	302
1	8	2	29.6	25.6	231
1	9	2	16.9	15.2	80
1	10	2	5.8	5.5	233
1	11	2	7.3	7.2	71
1	12	2	8.7	8.1	125
1	13	2	10.2	9.7	198
1	14	2	15.5	16.7	57
1	15	2	6.6	7.3	187
1	16	2	16.7	17.5	20
1	17	2	9.7	9.3	24
1	18	2	5.5	6.3	196
1	20	2	11.8	10.2	211
1	21	2	5.7	5.5	276
1	0	3	46.7	51.4	270
1	1	3	9.6	9.8	293
1	2	3	31.5	32.0	208
1	3	3	17.5	14.3	82
1	4	3	35.5	31.6	111
1	5	3	64.4	57.0	67
1	6	3	31.6	29.1	120
1	7	3	34.1	31.1	129
1	8	3	9.3	8.7	0
1	9	3	32.2	28.9	229
1	10	3	18.1	16.8	325
1	11	3	21.0	20.4	286
1	12	3	5.4	5.9	161
1	13	3	8.1	8.5	262
1	16	3	6.3	7.0	312
1	17	3	4.9	5.5	14
1	18	3	6.8	7.0	118
1	19	3	4.6	4.3	308
1	20	3	7.7	7.4	160
1	21	3	4.2	4.5	94
1	0	4	6.5	8.2	0
1	1	4	16.9	20.8	218
1	2	4	13.6	11.3	261
1	3	4	20.5	20.2	162
1	4	4	20.6	18.6	156
1	5	4	3.8	4.7	146
1	6	4	20.7	19.2	113
1	7	4	13.3	13.3	311
1	8	4	10.2	10.5	31
1	9	4	10.4	10.2	325
1	10	4	14.3	14.3	310
1	11	4	15.7	14.3	138
1	12	4	15.8	16.5	338
1	13	4	4.8	5.4	99
1	14	4	4.4	5.2	22
1	15	4	9.9	10.0	312
1	16	4	5.7	6.8	213
1	19	4	8.8	8.2	50
1	20	4	18.1	16.6	162
1	0	5	16.4	15.6	270
1	1	5	16.9	17.1	175
1	2	5	5.9	5.8	308
1	3	5	12.2	14.5	349
1	4	5	5.8	7.5	162
1	5	5	3.7	3.6	175
1	6	5	18.2	19.3	33
1	7	5	5.8	7.2	219
1	8	5	17.9	17.7	45
1	9	5	20.6	20.1	303
1	10	5	19.8	21.8	205
1	11	5	12.3	12.2	15
1	12	5	17.3	17.2	219
1	13	5	15.3	15.8	75
1	14	5	5.9	5.0	6
1	15	5	10.3	10.3	168
1	16	5	11.5	9.7	11
1	17	5	7.6	6.1	194
1	18	5	5.1	4.5	109
1	0	6	13.8	14.4	0
1	1	6	18.1	18.4	225
1	2	6	21.7	21.9	346
1	3	6	12.2	13.0	140
1	4	6	17.3	17.8	296
1	5	6	27.7	26.9	47
1	6	6	24.6	26.3	178
1	7	6	13.6	14.4	333
1	8	6	23.4	26.4	165
1	9	6	14.3	16.3	231
1	10	6	6.5	6.7	81
1	11	6	5.1	4.8	148
1	14	6	9.7	9.1	270
1	15	6	4.6	5.1	156
1	16	6	11.9	9.9	356
1	17	6	5.3	4.1	294
1	18	6	6.2	6.8	39
1	0	7	7.9	8.2	90
1	1	7	14.0	15.2	357
1	2	7	4.2	5.3	226
1	3	7	7.4	8.9	117
1	4	7	8.9	10.1	334
1	5	7	9.4	11.6	143
1	6	7	8.5	9.7	44
1	7	7	5.7	6.9	239
1	8	7	9.2	10.7	166
1	10	7	6.7	7.2	192
1	12	7	9.6	9.2	277
1	15	7	9.4	7.1	213
1	16	7	9.7	9.9	44
1	0	8	14.0	15.8	180
1	1	8	14.8	15.4	290
1	2	8	9.8	10.7	194
1	4	8	8.6	9.4	322
1	5	8	7.0	7.7	130
1	6	8	14.3	15.3	301
1	7	8	8.2	9.6	97
1	8	8	10.1	10.1	117
1	9	8	4.2	4.3	128
1	10	8	23.2	20.1	64
1	11	8	5.4	4.8	297
1	12	8	20.1	16.4	341
1	13	8	6.6	6.4	30
1	2	9	8.1	7.5	0
1	3	9	7.9	6.8	195
1	4	9	12.0	10.7	342
1	5	9	4.4	4.1	106
1	7	9	3.6	3.9	54
1	8	9	5.5	5.3	143
1	9	9	8.6	8.3	356
1	10	9	7.7	7.7	163
1	0	10	7.0	6.3	180
1	1	10	11.9	11.0	60
1	2	10	6.2	6.6	0
1	3	10	13.8	14.7	328
1	4	10	8.7	9.8	326
2	0	1	20.1	19.7	90
2	1	1	29.7	27.1	208
2	2	1	16.0	15.6	110
2	3	1	29.3	29.0	215
2	4	1	15.2	16.1	255
2	5	1	4.9	5.6	208
2	6	1	11.0	11.8	238
2	7	1	35.2	33.7	10
2	8	1	6.8	6.2	222
2	9	1	14.1	13.1	62
2	10	1	15.7	16.5	297
2	11	1	8.0	7.9	74
2	12	1	6.8	6.3	76
2	13	1	16.0	17.0	354
2	14	1	22.2	23.5	96
2	15	1	11.8	12.2	224
2	16	1	4.7	4.8	75
2	17	1	13.9	14.9	199
2	18	1	14.7	16.1	273
2	19	1	4.8	4.6	151
2	20	1	14.1	13.8	264
2	21	1	6.6	6.9	153
2	0	2	6.6	7.3	0
2	1	2	19.4	20.7	45
2	2	2	16.3	16.6	35
2	3	2	9.8	9.8	128
2	4	2	15.6	14.6	30
2	5	2	16.4	16.5	254
2	6	2	25.3	26.2	102
2	7	2	27.2	23.5	326
2	8	2	15.0	13.1	168
2	9	2	6.6	6.9	86
2	10	2	17.1	16.2	248
2	11	2	10.2	9.5	123
2	12	2	15.1	15.1	260
2	14	2	10.0	9.5	242
2	16	2	15.0	15.5	85
2	18	2	14.2	13.6	45
2	19	2	2.6	2.0	90
2	20	2	12.6	12.2	296
2	21	2	4.5	5.2	289
2	0	3	63.9	61.0	90
2	1	3	41.0	36.8	332
2	2	3	5.8	6.7	48
2	3	3	27.5	24.4	282
2	4	3	17.7	15.7	241
2	5	3	12.3	12.9	184
2	6	3	7.1	6.1	221
2	7	3	15.9	14.1	186
2	8	3	17.6	17.4	287
2	9	3	12.5	11.2	213
2	10	3	6.0	7.0	15
2	11	3	14.6	15.3	140
2	12	3	6.0	6.3	12
2	13	3	10.2	10.7	109
2	15	3	14.7	14.6	351
2	16	3	8.4	9.5	133
2	17	3	7.4	7.4	317
2	18	3	3.9	3.8	135
2	0	4	17.5	18.9	180
2	1	4	20.4	17.9	97
2	2	4	6.0	3.9	122
2	3	4	9.9	9.8	233
2	4	4	5.9	5.3	355
2	5	4	12.5	12.0	280
2	6	4	13.9	13.0	248
2	7	4	4.1	3.9	293
2	8	4	5.6	5.4	336
2	10	4	17.3	17.4	331
2	11	4	4.5	4.2	36
2	12	4	8.9	8.4	293
2	13	4	5.9	6.8	106
2	14	4	21.9	23.1	115
2	16	4	11.8	12.1	103
2	17	4	5.9	6.4	325
2	18	4	4.1	3.8	23
2	19	4	7.6	6.6	205
2	20	4	2.8	3.2	155
2	0	5	17.8	19.1	270
2	1	5	10.5	10.2	339
2	2	5	14.9	15.2	173
2	3	5	17.9	17.9	160
2	4	5	4.0	5.2	171
2	5	5	18.1	17.6	114
2	6	5	8.6	10.3	288
2	7	5	8.4	8.7	60
2	8	5	18.3	17.4	110
2	9	5	12.4	13.7	325
2	10	5	12.6	12.5	93
2	11	5	12.0	12.6	314
2	12	5	12.5	12.8	342

h	k	ℓ	F_o	F_c	φ
2	0	0	43.0	53.1	180
2	1	0	44.2	52.6	180
2	2	0	23.9	27.4	180
2	3	0	14.1	12.1	180
2	4	0	6.8	4.0	0
2	5	0	3.5	2.2	0
2	6	0	16.9	13.8	0
2	7	0	26.6	27.2	180
2	8	0	17.9	14.7	0
2	9	0	8.2	10.4	0
2	10	0	13.9	12.9	0
2	11	0	17.9	18.0	0
2	13	0	6.8	7.0	0
2	16	0	6.3	6.2	180
2	18	0	8.7	10.2	180
2	21	0	6.7	6.8	180
2	0	6	6.0	7.2	0
2	1	6	6.8	7.9	102
2	2	6	12.8	14.5	72
2	3	6	8.7	9.6	350
2	4	6	24.1	26.3	87
2	5	6	6.7	7.7	286
2	6	6	14.1	16.0	108
2	7	6	11.5	11.8	183
2	8	6	12.8	12.7	237
2	10	6	8.9	10.8	260
2	11	6	4.1	4.2	281
2	12	6	3.9	3.3	275
2	13	6	10.4	10.8	57
2	14	6	10.9	10.8	278
2	15	6	10.1	9.3	75
2	16	6	4.3	3.7	344
2	17	6	11.1	11.3	215
2	2	7	12.3	13.0	192
2	4	7	4.2	3.3	34
2	5	7	6.3	8.2	213
2	6	7	15.2	15.8	42
2	7	7	7.2	7.1	281
2	10	7	11.4	11.4	232
2	11	7	4.7	4.8	167
2	12	7	4.1	3.0	0
2	13	7	4.5	4.4	25
2	14	7	3.8	4.2	312
2	15	7	9.0	8.5	101
2	1	8	7.9	9.5	17
2	3	8	6.8	7.9	337
2	4	8	12.7	13.9	264
2	5	8	5.3	5.2	10
2	6	8	6.8	7.5	270
2	7	8	5.9	5.1	32
2	9	8	11.8	11.1	201
2	10	8	5.9	5.8	200
2	11	8	3.9	3.6	270
2	12	8	6.2	5.9	67
2	13	8	5.2	5.6	43
2	0	9	11.0	11.0	270
2	1	9	13.0	12.0	103
2	2	9	9.2	9.2	241
2	3	9	18.1	16.5	77
2	4	9	7.6	7.2	123
2	5	9	8.6	7.9	12
2	6	9	10.4	8.7	78
2	7	9	3.3	3.6	204
2	8	9	3.6	3.6	59
2	9	9	7.2	7.8	171
3	1	0	20.2	24.7	90
3	2	0	68.0	76.7	270
3	3	0	37.0	34.3	270
3	4	0	49.2	52.2	270
3	5	0	4.7	5.1	90
3	6	0	21.6	22.0	270
3	7	0	19.2	16.9	90
3	8	0	15.2	14.5	90
3	9	0	6.0	5.7	270
3	10	0	23.1	20.9	90
3	11	0	15.4	14.1	270
3	13	0	6.4	8.3	270
3	14	0	7.6	7.6	90
3	15	0	6.5	7.5	90
3	16	0	10.3	11.3	90
3	20	0	16.3	15.5	270
3	21	0	11.8	11.3	90
3	1	1	14.5	15.6	12
3	2	1	4.2	5.2	117
3	3	1	17.5	18.8	162
3	4	1	10.5	9.8	290
3	5	1	7.1	6.8	275
3	6	1	4.1	4.9	323
3	7	1	16.7	15.3	352
3	8	1	11.8	11.0	171
3	9	1	12.2	12.1	77
3	11	1	10.3	10.8	194
3	12	1	18.4	18.6	53
3	13	1	7.4	8.3	202
3	15	1	4.1	3.6	79
3	16	1	15.0	15.7	234
3	17	1	5.0	5.5	275
3	18	1	4.3	5.0	113
3	20	1	6.0	5.4	0
3	21	1	3.9	7.5	24
3	0	2	11.3	9.1	0
3	1	2	13.8	12.3	207
3	2	2	12.4	15.1	129
3	4	2	9.6	10.1	234
3	5	2	13.1	13.7	203
3	6	2	17.9	18.4	51
3	7	2	19.9	18.2	69
3	8	2	24.0	24.1	86
3	9	2	15.5	15.7	54
3	10	2	8.7	8.5	174
3	11	2	8.5	9.8	216
3	12	2	13.1	13.6	242
3	14	2	17.4	16.3	310
3	15	2	12.7	12.0	355
3	16	2	11.2	12.8	311
3	17	2	3.9	4.3	191
3	18	2	15.2	14.2	197
3	19	2	10.3	9.9	180
3	20	2	7.8	8.1	126
3	0	3	11.8	9.8	90
3	1	3	16.1	15.5	174
3	2	3	21.1	20.6	124
3	4	3	6.5	6.1	26
3	5	3	13.0	14.3	240
3	6	3	28.9	29.9	249
3	7	3	13.4	13.2	345
3	8	3	19.5	20.4	266
3	9	3	22.3	23.2	19
3	10	3	11.1	11.8	50
3	11	3	8.4	10.3	66
3	12	3	8.8	10.5	103
3	13	3	4.6	5.2	170
3	15	3	8.3	8.5	204
3	17	3	4.5	5.2	222
3	18	3	3.7	3.5	291
3	19	3	5.4	5.7	256
3	0	4	5.3	4.2	0
3	4	4	11.3	11.5	231
3	6	4	17.9	17.9	282
3	8	4	14.4	14.8	302
3	9	4	4.8	4.1	270
3	10	4	16.2	16.4	133
3	11	4	8.1	8.1	0
3	12	4	16.2	17.9	93
3	14	4	8.9	9.5	7
3	15	4	6.6	6.6	203
3	17	4	5.6	4.7	86
3	18	4	3.0	2.9	141
3	19	4	10.4	10.0	146
3	0	5	12.0	12.6	90
3	1	5	15.9	15.3	4
3	2	5	7.1	7.6	46
3	3	5	4.3	5.7	282
3	4	5	4.1	4.4	161
3	5	5	4.5	4.8	323
3	6	5	8.8	10.1	314
3	7	5	9.9	10.7	160
3	8	5	15.2	16.9	291
3	9	5	20.5	22.3	180
3	10	5	4.5	3.7	180
3	11	5	5.5	6.9	135
3	12	5	10.9	12.6	107
3	13	5	4.9	4.9	48
3	14	5	8.8	9.2	118
3	15	5	8.1	6.8	296
3	17	5	11.1	9.2	305
3	18	5	8.3	8.4	285
3	1	6	5.5	5.4	338
3	2	6	10.4	12.0	90
3	4	6	14.4	15.5	94
3	5	6	19.5	18.9	155
3	7	6	7.9	9.2	216
3	8	6	4.7	5.4	278
3	9	6	8.5	9.2	323
3	10	6	5.9	6.5	333
3	11	6	8.6	10.0	29
3	12	6	6.3	5.9	250
3	13	6	10.7	9.7	18
3	15	6	4.1	4.3	98
3	16	6	3.7	2.9	352
3	1	7	15.1	17.4	202
3	2	7	10.1	12.0	172
3	3	7	5.8	6.5	304
3	4	7	5.0	3.6	247
3	6	7	6.2	6.5	319
3	8	7	5.6	5.9	134
3	9	7	6.8	7.0	57
3	11	7	5.1	4.9	330
3	12	7	6.3	5.7	54
3	13	7	7.2	6.9	0
3	14	7	3.7	4.3	41
3	0	8	8.9	9.3	0
3	2	8	10.4	10.6	90
3	3	8	5.5	5.7	66
3	4	8	6.3	6.6	140
3	6	8	5.1	4.2	82
3	7	8	4.9	4.1	214
3	9	8	7.5	7.2	316
3	10	8	11.7	10.9	272
3	11	8	4.2	3.9	311
3	12	8	4.7	4.2	290
3	0	9	4.3	4.0	90
3	1	9	14.6	13.9	15
3	2	9	6.5	5.7	139
3	3	9	4.7	4.0	0
3	4	9	6.3	5.1	5
3	5	9	6.9	6.4	206
3	6	9	8.1	7.8	318
3	7	9	6.3	7.2	145
4	0	0	46.8	50.3	180
4	1	0	15.5	15.8	0
4	2	0	11.4	11.4	180
4	3	0	22.2	23.5	0
4	4	0	13.4	13.2	0
4	5	0	7.4	7.9	0
4	6	0	16.9	16.9	0
4	8	0	16.8	16.8	0
4	9	0	5.1	5.1	180
4	10	0	8.2	8.8	180
4	11	0	9.6	9.5	180
4	12	0	7.1	7.1	180
4	13	0	5.9	6.5	180
4	14	0	6.1	7.8	0
4	17	0	10.2	9.3	0
4	18	0	4.6	4.8	180
4	19	0	11.9	10.7	0
4	20	0	6.9	6.7	180
4	0	1	9.2	9.8	90
4	1	1	31.6	32.3	33
4	2	1	10.6	9.0	204
4	3	1	11.3	11.6	95
4	4	1	12.0	11.3	273
4	5	1	12.2	11.3	198
4	6	1	20.5	19.6	21
4	8	1	18.9	18.7	76
4	11	1	15.0	16.2	190
4	12	1	14.7	15.8	248
4	13	1	12.2	13.4	169
4	14	1	16.8	17.3	202
4	15	1	10.2	10.0	36
4	16	1	7.5	8.2	64
4	17	1	12.9	13.2	5
4	18	1	9.4	8.7	39
4	19	1	11.7	11.4	304
4	0	2	11.7	9.3	0
4	1	2	10.9	10.6	340
4	2	2	17.9	16.4	244
4	3	2	16.6	17.1	6
4	4	2	16.7	17.6	274
4	5	2	9.3	9.7	83
4	6	2	18.4	17.7	351
4	7	2	10.0	9.5	204
4	8	2	9.3	9.7	122
4	10	2	12.7	12.5	175
4	12	2	4.6	5.0	166
4	13	2	12.2	12.6	242
4	14	2	7.2	7.0	90
4	15	2	7.3	6.9	84
4	16	2	5.3	5.4	35
4	17	2	14.7	13.9	42
4	18	2	9.2	7.9	310
4	19	2	3.1	2.5	348
4	0	3	27.1	24.5	270
4	1	3	8.6	7.9	204
4	2	3	17.0	16.1	201
4	3	3	27.2	26.6	163
4	4	3	28.1	27.9	148
4	5	3	7.0	6.5	228
4	7	3	37.7	36.5	331
4	8	3	18.7	19.4	343
4	9	3	27.4	28.1	11
4	10	3	9.4	9.4	39
4	11	3	7.6	7.6	105
4	12	3	7.9	8.6	160
4	13	3	15.3	17.1	169
4	14	3	5.7	5.4	277
4	15	3	7.7	8.6	155
4	16	3	4.5	5.0	317
4	0	4	5.2	3.2	0
4	1	4	19.9	20.1	291
4	2	4	20.5	20.2	258
4	3	4	5.4	3.9	0
4	4	4	7.5	6.1	168
4	5	4	13.3	13.7	125
4	6	4	22.2	21.0	97
4	7	4	14.7	15.5	96
4	8	4	10.3	9.5	50
4	9	4	5.0	5.0	302
4	10	4	9.5	11.0	324
4	11	4	9.0	8.9	248
4	12	4	5.8	5.5	243
4	13	4	6.7	6.5	108
4	14	4	4.7	4.4	217
4	15	4	7.8	6.4	344
4	16	4	5.1	4.3	280
4	18	4	5.6	5.8	250
4	0	5	10.3	11.4	270
4	1	5	10.5	10.8	125
4	2	5	6.2	6.0	138
4	3	5	6.0	6.5	0
4	4	5	13.1	14.3	94
4	5	5	7.7	8.0	329
4	6	5	6.6	6.2	212
4	7	5	12.3	12.8	96
4	8	5	18.9	19.7	293
4	10	5	11.8	11.1	351
4	11	5	5.4	5.0	229
4	12	5	15.8	16.1	110
4	13	5	13.2	11.7	203
4	14	5	8.4	8.0	167
4	15	5	8.7	7.8	235
4	16	5	10.4	10.0	244
4	0	6	5.0	5.5	0
4	1	6	7.8	9.1	205
4	2	6	20.3	21.9	288
4	3	6	13.5	14.1	127
4	4	6	15.4	17.3	248
4	5	6	7.5	8.7	59
4	6	6	8.7	8.8	177
4	7	6	12.4	11.5	316
4	9	6	5.5	6.2	270
4	11	6	7.5	6.9	233
4	12	6	15.5	14.2	67
4	13	6	6.6	5.9	289
4	14	6	12.8	12.4	74
4	15	6	10.3	9.5	77
4	1	7	18.5	21.0	215
4	2	7	4.8	5.5	32
4	3	7	18.1	19.0	299
4	4	7	4.7	5.3	185
4	5	7	12.2	12.7	357
4	6	7	6.3	5.8	270
4	7	7	7.6	6.7	125
4	9	7	5.0	5.9	125
4	10	7	4.3	4.2	36
4	11	7	7.9	6.8	15
4	12	7	6.3	5.6	40
4	13	7	5.5	6.2	278
4	0	8	17.2	15.1	0
4	1	8	12.7	12.0	174
4	2	8	10.2	9.5	80
4	3	8	18.7	18.3	202
4	4	8	15.6	13.1	111
4	6	8	4.7	4.0	160
4	7	8	3.9	3.9	14
4	8	8	10.0	9.0	206
4	9	8	5.0	4.8	118
4	10	8	3.9	4.5	40
4	0	9	13.2	13.7	90
4	1	9	5.9	5.5	223
4	2	9	3.4	3.4	22
4	3	9	3.1	2.7	306
4	4	9	8.9	10.1	264
5	4	0	16.7	15.6	90
5	5	0	11.3	11.9	270
5	6	0	4.8	5.1	90
5	7	0	16.0	16.1	90
5	9	0	24.7	25.6	90
5	10	0	5.1	6.0	90
5	12	0	8.6	10.3	270
5	13	0	10.3	13.0	270
5	14	0	14.6	16.0	270
5	16	0	5.6	6.2	270
5	18	0	12.2	13.2	90
5	0	1	9.8	8.4	90
5	1	1	9.9	9.8	52
5	3	1	13.4	14.3	51
5	4	1	13.2	14.7	296
5	5	1	12.6	13.3	114
5	7	1	22.4	25.9	175
5	8	1	13.4	14.8	99
5	9	1	5.2	5.6	194
5	10	1	5.2	5.9	132
5	11	1	20.4	23.5	14
5	12	1	4.2	4.2	194
5	13	1	12.9	16.4	320
5	15	1	13.3	14.2	235
5	16	1	6.6	7.2	323
5	17	1	11.6	11.6	162
5	18	1	4.0	3.6	23
5	0	2	6.6	7.8	0
5	1	2	13.4	13.7	30
5	2	2	6.0	7.3	238
5	3	2	26.4	24.7	349
5	4	2	22.9	22.0	214
5	5	2	5.8	4.5	42
5	6	2	7.3	7.6	328
5	7	2	17.3	17.8	180
5	8	2	21.1	21.3	3
5	9	2	9.7	10.6	226
5	10	2	3.3	2.7	60
5	11	2	3.3	3.9	324
5	12	2	6.9	8.3	137
5	13	2	5.3	5.8	340
5	14	2	4.6	4.4	193
5	17	2	4.6	4.8	99
5	0	3	28.4	25.6	90
5	1	3	9.1	7.5	5
5	2	3	33.1	28.1	9
5	3	3	16.6	14.7	316
5	4	3	23.9	20.7	276
5	5	3	21.5	20.4	236
5	6	3	6.9	7.1	239
5	7	3	10.1	11.0	201
5	8	3	13.9	15.0	74
5	9	3	5.1	4.6	103
5	10	3	5.5	6.6	96
5	12	3	10.7	11.2	242
5	13	3	8.3	9.4	61
5	14	3	8.3	8.5	229
5	15	3	6.4	6.4	99
5	16	3	3.9	3.3	83
5	17	3	3.7	3.3	290

h	k	ℓ	F_o	$\|F_c\|$	φ
5	0	4	3.9	2.4	0
5	1	4	25.2	21.7	318
5	3	4	29.9	27.1	26
5	4	4	9.5	7.3	49
5	5	4	13.9	13.1	53
5	6	4	11.6	11.9	98
5	7	4	15.1	15.5	213
5	8	4	5.0	3.3	194
5	9	4	15.7	16.5	182
5	11	4	7.8	8.3	59
5	12	4	13.4	13.8	194
5	13	4	5.5	5.4	353
5	15	4	4.5	4.0	242
5	16	4	10.8	10.9	356
6	0	0	13.1	11.9	0
6	2	0	12.6	12.2	0
6	3	0	10.6	12.4	180
6	4	0	6.4	8.3	0
6	5	0	5.6	9.1	0
6	6	0	9.2	7.1	180
6	7	0	14.0	19.8	0
6	8	0	13.4	17.7	180
6	9	0	7.2	8.3	180
6	10	0	9.0	11.3	180
6	11	0	5.2	6.7	180
6	13	0	4.8	5.6	0
6	15	0	6.8	6.6	180
6	16	0	5.5	5.4	0
6	0	1	15.4	16.5	90
6	1	1	4.5	5.9	79
6	3	1	12.5	14.5	98
6	4	1	9.4	10.9	250
6	5	1	5.2	5.0	90
6	6	1	4.7	5.2	141
6	7	1	11.4	13.2	258
6	9	1	10.4	12.2	287
6	11	1	3.5	3.5	68
6	12	1	3.0	3.8	324
6	13	1	5.5	7.0	119
6	14	1	3.2	3.6	50
6	15	1	6.5	7.4	10
6	16	1	2.8	3.2	162
6	0	2	22.1	20.8	180
6	1	2	18.7	18.1	213
6	2	2	21.7	19.9	107
6	3	2	13.8	13.1	203
6	4	2	7.3	7.8	30
6	5	2	8.3	10.3	84
6	6	2	18.1	18.2	272
6	7	2	17.7	17.2	116
6	10	2	11.9	13.2	52
6	11	2	12.8	13.5	314
6	12	2	4.3	4.2	335
6	13	2	6.2	6.3	353
6	14	2	2.5	2.0	296
6	15	2	4.0	3.2	90
6	0	3	12.3	11.6	270
6	1	3	11.7	11.1	26
6	2	3	3.3	1.7	70
6	3	3	11.1	10.7	117
6	4	3	6.6	6.1	10
6	5	3	7.7	8.2	111
6	6	3	4.1	3.4	313
6	7	3	4.8	4.8	97
6	8	3	7.5	7.8	104
6	9	3	9.9	10.4	191
6	11	3	9.9	10.2	247
6	13	3	14.2	13.7	338
6	14	3	10.0	9.8	162
6	15	3	5.7	7.0	14
6	0	4	10.7	8.7	0
6	1	4	9.3	8.9	324
6	2	4	10.7	9.1	58
6	3	4	11.4	10.7	0
6	5	4	5.2	5.9	112
6	6	4	3.8	2.6	265
6	7	4	8.2	9.0	105
6	8	4	7.4	8.0	214
6	9	4	5.9	5.4	18
6	10	4	11.3	10.4	152
6	11	4	12.7	12.4	270
6	12	4	7.2	5.5	103
6	13	4	11.1	10.3	240
6	14	4	9.3	9.5	299
7	1	0	6.3	7.3	90
7	2	0	13.9	14.8	90
7	5	0	7.3	8.7	270
7	7	0	4.7	4.4	270
7	9	0	4.6	4.4	270
7	13	0	15.1	13.1	90
7	2	1	6.8	7.7	141
7	3	1	6.7	7.5	270
7	4	1	5.1	6.6	86
7	5	1	7.1	8.7	241
7	6	1	3.5	5.6	276
7	8	1	7.7	9.2	270
7	9	1	4.3	5.6	329
7	10	1	5.7	4.4	293
7	12	1	7.0	6.6	276
7	13	1	3.9	4.0	126
7	0	2	9.9	10.2	0
7	1	2	8.3	8.2	75
7	4	2	5.3	6.3	170
7	5	2	4.6	4.6	342
7	6	2	7.1	8.2	228
7	7	2	6.1	6.5	259
7	9	2	7.3	6.2	242
7	10	2	7.0	7.8	111
7	11	2	5.9	5.3	26
7	13	2	4.9	4.6	122
7	0	3	4.5	3.0	270
7	1	3	6.3	6.0	38
7	2	3	6.8	6.7	270
7	3	3	13.4	12.4	124
7	4	3	6.2	5.4	199
7	5	3	13.2	13.4	67
7	6	3	9.0	8.3	79
7	7	3	8.9	8.9	68
7	8	3	4.1	3.7	68
7	9	3	12.0	10.3	198
7	11	3	16.2	16.2	254
7	12	3	4.4	5.5	65
7	0	4	4.9	4.3	0
7	2	4	9.9	7.3	116
7	4	4	7.8	6.2	216
7	5	4	13.9	13.2	180
7	6	4	5.6	4.2	258
7	7	4	3.9	3.4	238
7	8	4	9.6	9.2	72
7	9	4	10.7	9.3	6
7	10	4	10.1	9.7	13
8	0	0	8.4	9.1	180
8	2	0	8.3	7.5	180
8	4	0	4.7	5.7	0
8	5	0	10.7	8.8	180
8	6	0	4.8	4.7	0
8	7	0	12.6	12.0	180
8	8	0	5.3	6.8	180
8	9	0	3.3	2.9	0
8	0	1	6.3	6.6	270
8	1	1	7.3	6.0	227
8	3	1	7.2	6.6	230
8	4	1	4.8	4.5	111
8	5	1	6.0	6.0	318
8	6	1	10.1	10.2	193
8	7	1	3.6	3.8	342
8	8	1	3.8	3.5	202
8	9	1	8.9	9.8	111
8	0	2	2.9	3.1	180
8	1	2	18.4	15.2	64
8	2	2	9.1	7.0	333
8	3	2	10.3	9.7	301
8	4	2	7.2	6.4	24
8	5	2	18.5	15.4	256
8	6	2	10.0	7.6	147
8	7	2	6.9	5.9	57
8	8	2	4.3	5.0	180
8	0	3	7.3	4.3	90
8	1	3	3.5	3.2	95
8	2	3	9.8	8.5	22
8	3	3	15.4	11.9	325
8	4	3	7.3	7.8	5
8	5	3	11.4	9.2	278
8	6	3	5.1	4.6	223
8	7	3	11.8	10.7	152
8	1	4	22.5	17.0	102
8	2	4	5.7	4.4	161
8	3	4	9.6	7.9	212
8	4	4	8.6	8.4	211

APPENDIX V

STATISTICAL ANALYSIS OF RESULTS

STANDARD DEVIATIONS IN BOND LENGTH (37)

The expression for the calculation of the estimated standard deviation of a bond length is

$$\sigma_{1-2} = \sqrt{\sigma_1^2 + \sigma_2^2}\ , \qquad (107)$$

where σ_1 and σ_2 refer to the isotropic standard deviations of the positions of Atoms 1 and 2. Equation (107) requires that the positional parameters of the atoms involved in a bond be uncorrelated. In general, any two atoms in a structure are not completely independent; however, the correlation is usually small.

Equation (107) also ignores errors in unit cell parameters, which contribute to the errors in bond lengths. In the present work, the estimated standard deviation was 0.002 A. for a 6.95 A. axis, or about 0.03%. An error of this size in the length of a unit cell edge would result in an error of 0.00045 A. in a bond length of 1.50 A. This value is an order of magnitude smaller than the average error in the positional parameters, and the unit cell errors were therefore ignored in all calculations.

STANDARD DEVIATIONS IN BOND ANGLES

If the errors are isotropic and positions of Atoms A, B, and C (Fig. 32) are uncorrelated, the standard deviation in a bond angle is given by the equation

$$\sigma_\theta = \sqrt{\sigma_A^2/(AB)^2 + \sigma_B^2(1/A^2B^2 - 2\cos\theta/[(AB)(BC) + 1/B^2C^2] + \sigma_C^2/B^2C^2}. \qquad (108)$$

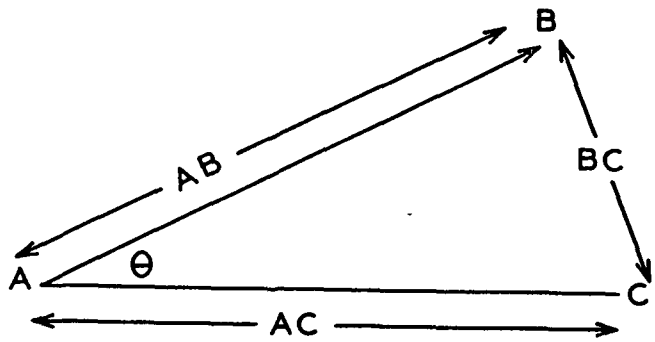

Figure 32. Bond Angle Relationship

LEAST SQUARES PLANES

The planarity of a set of atoms is discussed in terms of the least squares plane through the set of atoms, i.e., the plane which minimizes $\sum_{\underline{m}} \underline{d}_{\underline{m}}^2$, where $\underline{d}_{\underline{m}}$ is the perpendicular distance of the atom from the plane. The computer program used for the calculations adopted the method of Schomaker, et al. (65).

Once a plane has been calculated, one must test whether the distribution of atoms about it justifies the assumption of planarity.

If the σ's of the atoms in the set do not differ greatly, the ratio

$$\chi^2 = \frac{\sum_m d_m^2}{\sigma^2_{position}} \qquad (109)$$

follows the χ^2 distribution closely. From the tabulated values of χ^2 for ($\underline{m}$-3) degrees of freedom, we determine the probability that a planar set of atoms would have a ratio exceeding that found. The calculations for the ethylene grouping in trans-MIC are shown in Table XXXVII.

TABLE XXXVII

TEST FOR PLANARITY OF ETHYLENE GROUP

Atom	$\bar{\sigma}_{position}$, A.	Dev. from Least Squares Plane, A.
C1	0.0043	0.0032
C2	0.0043	0.0108
C3	0.0043	0.0034
C10	0.0053	0.0042

$$\sum_m d_m^2 = 153.3 \times 10^{-6} \text{ A.}^2 \tag{110}$$

$$\bar{\sigma}^2_{position} = 18.5 \times 10^{-6} \text{ A.}^2 \tag{111}$$

$$\chi^2 = 7.6. \tag{112}$$

The probability that a truly planar set of atoms would have a χ^2 as great as 7.6 was less than 0.01 and, therefore, the ethylene atoms were not considered planar within experimental error.

A least squares plane was calculated through ring Atoms C1, C3, C4, and C5. The four atoms were not planar, with $\underline{d}_m$'s of approximately 0.02 A.

COMPARISON OF sp^3-sp^3 C-C BOND LENGTHS WITH sp^2-sp^3 C-C BOND LENGTHS

Table XXXVIII shows the bonds under consideration. The following quantities were defined:

$$\text{Mean estimated standard deviation, } sp^3\text{-}sp^3, = 0.003 \text{ A.} \tag{113}$$

$$\text{Mean estimated standard deviation, } sp^3\text{-}sp^2, = 0.004 \text{ A.} \tag{114}$$

$$\text{Estimated standard deviation of difference} = 0.005 \text{ A.} \tag{115}$$

t is defined for a normal distribution such that the probability that a quantity x differs from its mean value in either direction by more than $t\sigma$ is equal to p. For the present case, t equals 2.60, which corresponds to p equal to 0.01. Therefore, there is only a 1% chance that if the two sets of bond lengths were equal that a difference of 0.013 A. would be found in their means, and the sp^3-sp^2 bonds are significantly shorter at the 99% confidence level.

TABLE XXXVIII

CYCLOHEXANE RING BOND LENGTHS

sp^3-sp^3	sp^2-sp^3	Length, A.	σ, A.
	C1-C2	1.530	0.006
	C2-C3	1.510	0.006
C3-C4		1.525	0.006
C4-C5		1.540	0.006
C5-C6		1.536	0.006
		1.532	0.006

Mean sp^3-sp^3 = 1.533 A.
Mean sp^2-sp^3 = 1.520 A.
Difference = 0.013 A.

In the above calculation several assumptions were made. First, no allowance for systematic errors of any kind was made. Second, the standard deviations were assumed to be isotropic. Third, and most important, the assumption was made that all of the bonds were independent, and the standard deviations were calculated by the following equation,

$$\text{Standard deviation of the mean} = \frac{\text{Standard deviation of individual bonds}}{(\text{Number of bonds})^2} \qquad (116)$$

The bonds are not independent, however, because they have atoms in common. Taking the interactions into account decreases the standard deviations involved in the calculations. Consequently, the same conclusion would be arrived at with regard to the significance of the difference between the two sets of bond lengths.

APPENDIX VI

ATTEMPTED SOLUTION OF CRYSTAL STRUCTURE OF cis-PINOCARVYL-p-NITROBENZOATE

PRELIMINARY PHOTOGRAPHS

Preliminary photographs indicated that the space group of cis-pinocarvyl-p-nitrobenzoate was either $P2_1$ or $P2_1/m$. These two space groups are indistinguishable by x-ray photograph symmetry or systematic extinctions. The reported $[\alpha]_D^{20}$ = +136° (66) ruled out the centrosymmetric $P2_1/m$ however, and the space group $P2_1$ was chosen.

UNIT CELL CONSTANTS

Unit cell data were obtained from zero layer, back-reflection Weissenberg exposures around the a and b axes. d_{001}[13], d_{010}, d_{100}, and $d_{\bar{1}01}$ were obtained by the procedures discussed in Appendix II. The value of the monoclinic angle, β, was found by the method of triangulation. See Fig. 33.

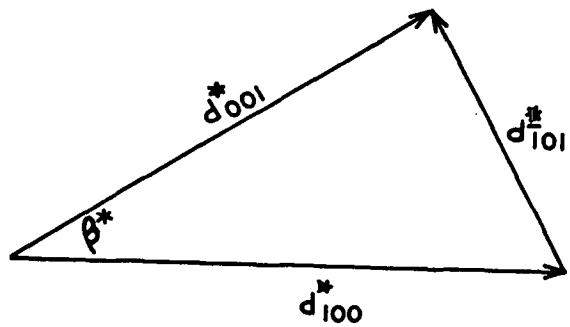

Figure 33. Reciprocal Space Relationship Between d^*_{001}, $d^*_{\bar{1}01}$, d^*_{100}, and β* in a Monoclinic Crystal

[13] "$d_{hk\ell}$" refers to the interplanar spacing for the hkℓ family of planes.

$d^*_{hk\ell}$ is defined as the reciprocal of $d_{hk\ell}$.

$$q^* = (d^*_{100} + d^*_{001} + d^*_{\bar{1}01})/2 \tag{117}$$

$$\beta^* = 2 \tan^{-1} ZZ \tag{118}$$

$$ZZ = ((q^* - d^*_{100})(q^* - d^*_{001})/(q^*(q^* - d^*_{\bar{1}01})))^{1/2} \tag{119}$$

The monoclinic angle, β, is the supplement of β^*.

$$\beta = 180 - \beta^* \tag{120}$$

The unit cell dimensions are functions of the interplanar spacing of the principal planes and the monoclinic angle.

$$a = d_{100}/\sin \beta \tag{121}$$

$$b = d_{010} \tag{122}$$

$$c = d_{001}/\sin \beta \tag{123}$$

$$V = abc \sin \beta \tag{124}$$

The unit cell constants for cis-pinocarvyl-p-nitrobenzoate are shown in Table XXXIX.

TABLE XXXIX

UNIT CELL CONSTANTS, cis-PINOCARVYL-p-NITROBENZOATE

	a axis[a]	b axis[a]	c axis[a]	beta[b]	Unit Cell Volume[b]
Low temperature	10.583(2)	6.740(1)	10.443(3)	90.46(5)	805.7(.5)
Room temperature	10.904(4)	6.778(2)	10.906(3)	91.77(9)	744.9(.3)

[a] Dimensions given in A. Estimated standard deviation x 10^3 in parentheses.

[b] Beta given in degrees. Volume given in A.^{3}. Estimated standard deviation in parentheses.

INTENSITY DATA COLLECTION

Low temperature intensity photographs were taken around the a axis (7 layers) and b axis (4 layers) by the equi-inclination Weissenberg technique. The intensities of individual reflections were measured by visual comparison with a standard scale.

The task of assigning indices to the reflections was made more difficult because the monoclinic angle was very nearly equal to ninety degrees. If β is very different from ninety degrees, it is possible to assign the positive and negative directions of the a and c axes from inspection of a zero-layer, b axis Weissenberg photograph. Figure 34 shows an example of such a case.

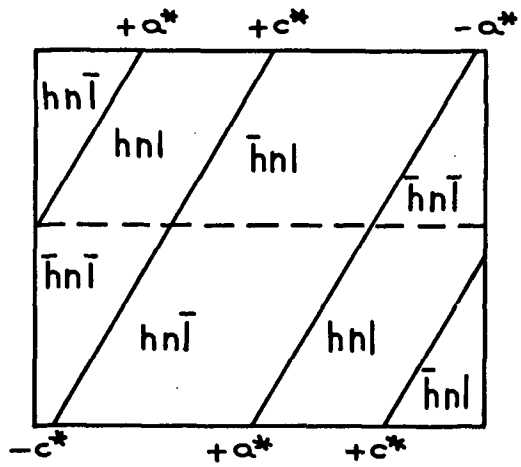

Figure 34. Appearance of Axial Lines on a b Axis, Zero-Level Weissenberg Photograph and the Associated Indices

β^*, by definition, must be less than 90°. Therefore, $+\underline{a}^*$ and $+\underline{c}^*$ must be closer together than $+\underline{c}^*$ and $-\underline{a}^*$ on a photograph. The middle axis is designated the $\underline{c}^*$ axis because $+\underline{a}^*$ lies to the left of $+\underline{c}^*$ according to the right-hand convention followed by crystallographers.

As β^* approaches ninety degrees, the distances between $+\underline{a}^*$ and $+\underline{c}^*$, and $+\underline{c}^*$ and $-\underline{a}^*$ both approach 45 mm., and it becomes very difficult to determine the positive

and negative axes. The procedure followed in the case of cis-pinocarvyl-p-nitrobenzoate was based on Fig. 35. The diagram illustrates the fact that the distance from the origin to a reflection $\underline{h}_1\underline{k}_1\underline{\ell}_1$ is greater than the distance from the origin to reflection $\bar{\underline{h}}_1\underline{k}_1\underline{\ell}_1$. Figure 36 illustrates the effect of this arrangement on an $\underline{n}$ layer Weissenberg. The difference between $\underline{D}_{\bar{h}k\ell}$ and $\underline{D}_{hk\ell}$ was extremely small and it was necessary to measure the distances with a microcomparator.

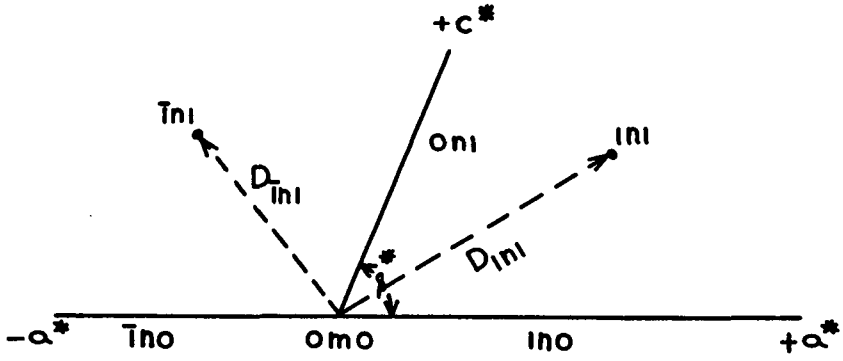

Figure 35. Diagram of Reciprocal Space Relationships on an $\underline{hn\ell}$ Photograph

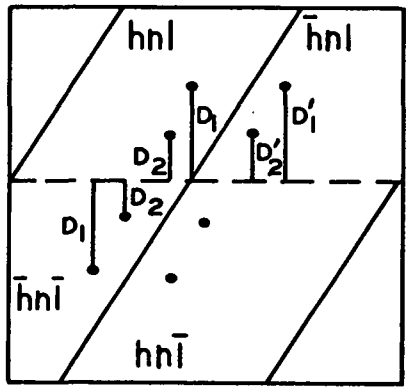

Figure 36. Effect of Sign on the Distance from a Reflection to the Origin

Once the $\underline{b}$ axis indices were assigned, the $\underline{a}$ axis reflections were indexed by matching the relative intensities of reflections common to both axes of rotation.

The $\underline{a}$ axis photographs were also indexed independently. The festoons of reflections which crossed the $\underline{c}^*$ axis on upper-level $\underline{a}$ axis exposures were shifted

in the direction of $+\underline{c}^*$ (see Fig. 37). The positive direction of the $\underline{c}^*$ axis was determined by comparing the distances from several $\underline{n}0\underline{l}$ reflections on either side of the center line to the origin. The shift becomes small when beta is close to ninety degrees and it was necessary to measure the distances with the microcomparator.

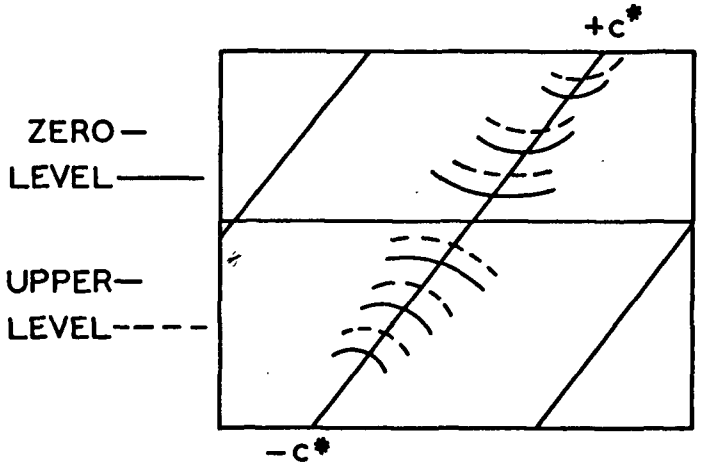

Figure 37. Zero-Level Festoons with $\underline{n}$th-Level Festoons Superimposed Showing the Shift on Upper-Level Weissenberg Films when Rotation is About the $\underline{a}$ Axis

Both methods of indexing gave the same results and, therefore, it was believed that the photographs had been indexed correctly.

A total of 1232 reflections were collected around the $\underline{a}$ axis. 129 were too light to be estimated and 5 were too intense, yielding 1098 observed reflections. The $\underline{b}$ axis produced 1054 observed reflections and 193 unobserved.

DATA REDUCTION

The data were reduced by the procedures discussed previously (pages 58-63). A discrepancy in the data was encountered during the interlayer scaling. A comparison of the relative structure factor amplitudes common to both axes of rotation revealed that the $\underline{b}$ axis $|\underline{F_h}|$'s were larger at low theta, whereas the $\underline{a}$ axis $|\underline{F_h}|$'s were the larger of the two at middle and high theta. Inspection of the $\underline{b}$ axis films indicated that the expanded $\underline{hn\ell}$ ($\underline{n}$=constant) reflections were more intense than their corresponding

contracted symmetry mates. This situation appeared to arise from a side-to-side variation of spot shape on the films which produced a contracting effect on the supposedly expanded $hn\ell$ reflections. Removal of all "expanded" $hn\ell$ data (n=1,2,3,4) alleviated most of the problem, although some of the discrepancies persisted at low theta in layers $4k\ell$, $\pm5k\ell$, and $\pm6k\ell$. A total of 1372 unique observed reflections were recovered from the interlayer scaling process.

The relative observed structure factor amplitudes were converted to normalized structure factors by Equation (125) (see pages 62-65).

$$|E_{hk\ell}|^2 = |F_{o,hk\ell}|^2 \exp(4.09 + 0.57((\sin^2\theta)/\lambda)^{1.5} \qquad (125)$$

The E statistics for cis-pinocarvyl-p-nitrobenzoate are shown in Table XL. Table XLI contains further information concerning the normalized structure factors.

TABLE XL

COMPARISON OF E STATISTICS AND THEORETICAL DISTRIBUTIONS

	$\lvert\bar{E}\rvert$	$\lvert\bar{E}\rvert^2$	$\lvert\lvert\bar{E}\rvert^2 - 1\rvert$
Centered (theor.)	0.798	1.000	0.968
Acentric (theor.)	0.886	1.000	0.736
Total data (1372 observed + 209 unobserved)	0.809	0.994	0.891

TABLE XLI

CHARACTERISTICS OF THE SET OF NORMALIZED STRUCTURE FACTORS FOR cis-PINOCARVYL-p-NITROBENZOATE

$\lvert E_n \rvert \geq 4$	$\lvert E_n \rvert \geq 3$	$\lvert E_n \rvert \geq 2$	$\lvert E_n \rvert \geq 1.5$
1	4	53	184

Number $|E_{n0\ell}| \geq 1.5$ = 28

Number $|E_{n0\ell}|$ = 165

ATTEMPTED STRUCTURE SOLUTION

No effort will be made to present a step-by-step account of the attempted analyses. Such an account would be confusing to the reader because many false leads were followed, and several unnecessary electron-density syntheses were computed. Even though the structure was not solved, the attempt has been educational and, for that reason, of value to this worker. It is believed that the analyses carried out thus far will contribute greatly to the eventual solution of the structure.

The symbolic addition method was chosen for solution of the phase problem. Sigma-2 listings were computed with 220 $|\underline{E}_{\underline{h}}| \geq 1.7$, and 420 $|\underline{E}_{\underline{h}}|$ 1.3. The following reflections (Table XLII) were chosen to fix the origin, according to the rules of Hauptman and Karle (31).

TABLE XLII

ORIGIN-DETERMINING REFLECTIONS, $P2_1$, (ORIGIN ONE)

$\underline{h}$	$\lvert\underline{E}_{\underline{h}}\rvert$	ϕ	Parity
7 0 8	2.92	0	UOG
10,0,3	2.12	π	GOU
-3 1 1	2.84	0	UUU

The matter of specifying the enantiomorph in space group $P2_1$ is not as straightforward as in $P2_12_12_1$. In general, the enantiomorph is determined by specifying the sign of an invariant or semi-invariant whose value differs from 0 or π. However, all invariants in $P2_1$ have the form GOG, which is centrosymmetric and, consequently, must be 0 or π. The matter is resolved during phase determination because one usually must assign one or more unknown symbols in order to continue. One of the letters will have a value close to $\pm$ 90°. Making a choice will determine the enantiomorph.

The connection between making this choice and specifying the sign of an invariant or semi-invariant is subtle, but is contained in the process (43). In the present case, reflection 256 ($|E_{256}|=2.84$) was assigned the unknown symbol e during phase determination. This symbol was then used to set the enantiomorph.

The phase determination produced 110 phases in terms of 0, π, and a. The value of a was taken to be 90° and the set of phases so obtained was cycled with the tangent formula. Expansion down to $|E_h|=1.3$ gave 330 phases for use in computing electron-density maps.

An eight atom fragment, believed to be a benzene ring, was located in the initial maps. A very large peak situated in the center of the ring was ignored because such spurious peaks have been reported to appear in benzene rings taken from E-maps. [See p. 377, Ref. (24).] Fourier cycling based on the initial eight atom fragment, and various portions of it, proved unsuccessful. Many peaks appeared in the Fourier maps, but none of them contributed to a sensible chemical structure. During this time many structure factor calculations were made with different combinations of atoms from the maps in the hope that the R-value would indicate a correct combination. The results were very unsatisfactory and substantiated the idea that the R-index has little meaning when only a partial structure is known, and should not be considered seriously until refinement of a complete structure is begun.

At this point in the work an electron-density projection was computed onto the 010 plane using 65 $|E_{h0\ell}| \geq 1.3$ whose phases were defined by symbolic addition. It was hoped that these phases were correct.

A number of projection peaks matched X and Z coordinates with peaks on the electron-density maps. These peaks bore no resemblance to a chemical structure, however. In fact, many of them were scattered about the cell, bearing no apparent relationship to other atoms.

Next, a three-dimensional, sharpened Patterson map was computed. Patterson maps contain information about the interatomic vectors in the structure. Since no phases were necessary, it was believed that the Patterson would provide an independent means for testing the validity of structural fragments found in electron-density maps.

The Patterson map also contains information about the absolute values of the $\underline{X}$ and $\underline{Z}$ coordinates of atoms in the structure. This situation exists because the vectors between corresponding atoms of molecules related by symmetry elements other than centers have one or two constant coordinates. Space group $P2_1$ contains pairs of atoms of the form $\underline{x},\underline{y},\underline{z}$, and $\bar{\underline{x}}$, $\underline{y}+1/2,\bar{\underline{z}}$. The corresponding vectors are $2\underline{x},1/2,2\underline{z}$, and appear in the plane $\underline{y}=1/2$[1]. Therefore, the Patterson map provides two criteria of correctness for a structure or structural fragment.

1. All interatomic vectors in a fragment must be present in the Patterson map.
2. Peaks at $2\underline{x}_i,1/2,2\underline{z}_i$ must be present in the Patterson map for all the atoms $(\underline{x}_i,\underline{y}_i,\underline{z}_i)$ in the fragment.

Application of these two Patterson criteria to the peaks found in the initial electron-density maps revealed that seven of them satisfied the first requirement, whereas only two of the seven met both requirements. These results suggested that the seven atom fragment was real, but was incorrectly oriented in the unit cell.

The symbolic addition method can lead to such results in some instances (67). If one or two important reflections are incorrectly phased early in the determination

[1]The concentrations of vector points which arise due to the symmetry elements of the space group are called Harker lines and planes.

their errors will propagate rapidly during the development of the set of phases. [See Ref. (68) for an example.] A set of phases may be obtained which produces no recognizable chemical entity, or, if only a certain subset of the phases are incorrect, a sensible structure may appear incorrectly oriented in the unit cell.

One test for correct orientation is to plot the fragment along with its symmetry mates. An incorrectly oriented fragment will often assume an impossible relationship with respect to a symmetry mate. Such was the case with the "benzene ring" fragment discussed previously. In that instance, two rings were situated only 1.7 A. apart.

The usual procedure for correcting the above situation is to modify the starting set of phases so that the phase generation process will avoid the phases accepted incorrectly originally. Unfortunately, one does not know which phases were incorrect, and, therefore, has no guide for modifying the origin and/or enantiomorph phases. In the present case two approaches were taken.

First a completely new set of starting phases was chosen (Table XLIII). Unknown symbols $\underline{b}$ and $\underline{c}$ were assigned to reflections 7 0 8 and 10,0,3, respectively, during phase generation. The set of phases obtained with $\underline{b}=0$ and $\underline{c}=\pi$ was practically identical to the set on which the first electron-density maps were based.

TABLE XLIII

SECOND SET OF STARTING PHASES

$\bar{h}$	$\lvert E_{\bar{h}} \rvert$	ϕ
8 0 7[a]	1.93	0
9 0 9[a]	2.29	0
5 1 8[a]	2.47	0
4 5 7[b]	2.36	$\underline{a}$

[a] Origin-determining.
[b] Enantiomorph-specifying.

Two hundred forty new phases were obtained by setting $\underline{b}=\pi$, and $\underline{c}=0$. Electron-density maps based on these phases produced four peaks which satisfied the Patterson criteria. Three of the peaks were bonded together and the fourth was isolated (see Fig. 38). Peaks 23 and 25 had occurred on the first maps with different $\underline{y}$ and $\underline{z}$ coordinates. The bond length of 1.26 A. was the same, however. In fact, this two-atom grouping appeared in all four electron-density maps that were eventually computed.

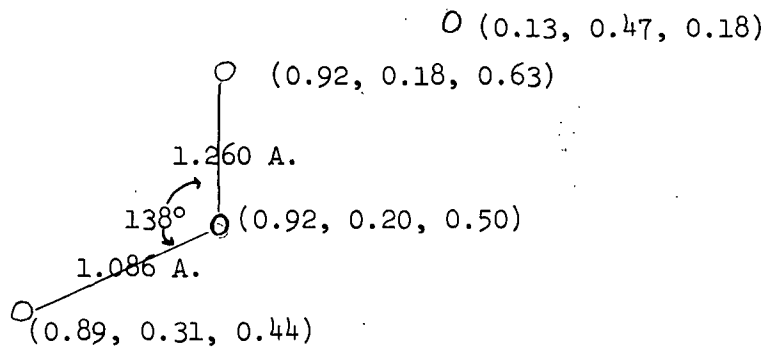

Figure 38. Four Atom Fragment from the Second Set of Electron-Density Maps

Table XLIV shows the third set of starting phases which were tried.

TABLE XLIV

THIRD SET OF STARTING PHASES

$\overline{h}$	$\lvert E_{\overline{h}} \rvert$	ϕ
7 0 8[a]	2.92	0
10,0,3[a]	2.12	0
3 1 1[a]	2.84	0
5 5 2[b]	2.38	$\underline{a}$ (=90°)

[a] Origin-determining.
[b] Enantiomorph-specifying.

The E-maps based on the set of phases derived from this starting set contained five peaks which satisfied the Patterson criteria. Two of the peaks were situated 1.26 A. apart. The remaining three peaks were located at distances greater than 2.0 A. apart.

The five atoms represented, at most, 16% of the total electron density in the compound. This was too small a percentage to expect success with a Fourier cycling approach.

An alternative approach was to use the tangent formula recycle technique of Karle and Karle (68). The method involves the following steps: 1. calculate a set of structure factors based on a structural fragment; 2. select all calculated structure factors, which correspond to $|E_{\underline{h}}| \geq 1.5$, where $|F_{c,\underline{h}}| \geq 0.4|F_{o,\underline{h}}|$; 3. calculate the $\phi_{\underline{h}}$'s associated with the selected $|F_{c,\underline{h}}|$'s; 4. recycle the tangent formula using these $\phi_{\underline{h}}$'s as a fixed starting set in order to develop a completely new set of phases. This new set of phases is then used to compute a new set of E-maps. The Karles have applied this procedure successfully in a number of problems, sometimes beginning with small structural fragments.

A set of structure factors was calculated based on the five-atom fragment. Seventy-two $|F_{o,\underline{h}}| \geq 0.4|F_{o,\underline{h}}|$ were selected and the tangent formula reiterated, starting with the seventy-two phases. During the cycling the starting phases were held constant. Two hundred forty-two phases were defined. E-maps based on these phases failed to reveal any new peaks.

The results of the three E-maps led to the conclusion that either the symbolic addition method had failed, or there was something wrong with the data. There was some basis for believing that the symbolic addition method had failed. The sigma-2 formula, used for the hand generation of pahses, is an approximate relationship

which should be used only in conjunction with probability tests. The fact that phases are accepted on a probability basis implies that the possibility always exists that an incorrect phase will be accepted. The sigma-2 relationship is restrictive in that it is applicable only to large $|\underline{E}_{\underline{h}}|$. The tangent formula, on the other hand, is valid for all $|\underline{E}_{\underline{h}}|$ values, and when applied iteratively it minimizes the errors in the known phases. A variation on the symbolic addition method has been reported by Oh and Maslen (30) for space group $P2_12_12_1$.

Their procedure involves defining about 20 phases by the sigma-2 formula. These 20 or so phases are then applied directly with the tangent formula to define all the rest of the phases. The authors reported good results with their work and expressed the belief that the method should be generally applicable. The procedure was tried in the present problem.

The starting set of phases is listed in Table XLV. These phases were obtained by the use of the sigma-2 formula. The starting phase set was extended in steps and the new phases were refined with the tangent formula. The strategy was to introduce a limited number of new phases at a time by gradually lowering $|\underline{E}|_{min}$, which in this work was lowered progressively from 1.8 to 1.7, then to 1.6, 1.5, 1.4, and finally to 1.3. At each step the tangent formula was reiterated until the maximum phase change in the last cycle was 8°. Reflections with phases which oscillated violently from cycle to cycle were omitted, as were phases whose $|\underline{E}_{\underline{c}},\underline{h}|$ were less than 0.3. Table XLVI shows the progression of phase generation.

An E-map based on the 198 phases revealed a four-atom cluster which satisfied the Patterson maps and had reasonable bond lengths and angles. A fifth, isolated peak also was found (see Fig. 39). A large number of other peaks were present which made no chemical sense and could not be found in the Patterson maps.

TABLE XLV

STARTING PHASES FOR TANGENT FORMULA REITERATION

$\bar{h}$	$\lvert E_{\bar{h}} \rvert$	$\phi_{\bar{h}}$
7 0 8	2.92	0
10,0,3	2.12	180
$\bar{3}$ 1 1	2.84	0
2 5 6	2.84	90
1 2 8	1.93	0
4,0,12	2.38	180
5 1 1	2.52	-90
5 5 1	2.94	-90
5 5 2	2.38	-90
5 6 6	1.86	-90
$\bar{4}$ 3 7	2.01	90
8 2 1	2.11	90
9 3 5	3.05	90
11,3,1	3.50	-90
3 1 0	2.52	180
7 2 1	1.90	0
3 7 1	2.85	0
8 2 0	2.03	90
0 6 0	2.05	0
3 5 0	2.51	0
8 0 7	1.93	0

TABLE XLVI

PROGRESSION OF PHASE GENERATION BY TANGENT FORMULA REITERATION

$\lvert\underline{E}\rvert_{min}$	$\phi_{\underline{h}}$ Defined	Number Cycles	$\underline{R}$
1.8	72	10	0.23
1.7	92	4	0.22
1.6	103	6	0.25
1.5	155	5	0.31
1.4	184	4	0.35
1.3	198	4	0.36

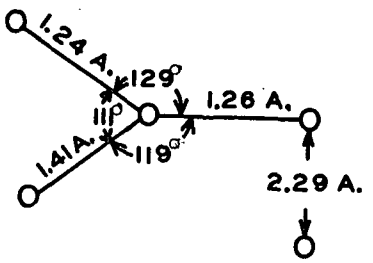

Figure 39. Five Atoms Located in the Fourth E-Map

In light of the repeated failure, it was decided that the data should be checked for errors. The possible errors were divided into two groups; those inherent in the intensity data, and those introduced in data handling.

Errors in the first group were considered to be less likely due to the care taken during data collection. Two complete sets of data had been taken around the a axis because the cryostat had been positioned too close to the crystal during the first set of exposures and several reflections were influenced by absorption due to the ice present on the cryostat nozzle.

The effects of x-ray absorption in the crystal were ignored because small crystals were used for the data collection.

In the second group of possible errors, incorrect indexing appeared most likely. Such an error would completely invalidate all symbolic addition procedures. A thorough check confirmed the initial assignments, however.

The data reduction results appeared to be in order, also.

CONCLUSIONS

The determination of the structure of cis-pinocarvyl-p-nitrobenzoate was abandoned for the present. No reason could be found for the failure to solve the structure. It is possible that the symbolic addition approach was unsuccessful in this instance. Any failure in this area was probably due to lack of insight and/or experience on the part of this worker. The Karles have enjoyed excellent success with the method.

In the course of this study, it became apparent that an efficient approach to the evaluation of electron-density maps would involve the following steps.

1. Assign coordinates to all possible atoms in the map.
2. Carry out bond length and bond angle calculations with these atoms.
3. Select all atoms which are related by chemically sensible bond angles and distances.
4. Construct a three-dimensional model of these atoms and their symmetry mates. The quickest way to accomplish this is to plot the atoms on transparent plastic sheets which will fit in a rack.
5. Choose a recognizable structure or structure fragment from the model.

If a structure fragment is located:

6. Check the orientation of the fragment and its symmetry mates in the unit cell. It is possible for a fragment to be oriented incorrectly, so that chemically impossible relationships occur between the atoms.

7. Calculate all of the interatomic vectors and Harker vectors for the fragment. Check a three-dimensional Patterson map for the presence of all these vectors.

8. Compute new electron-density maps based on the fragment. The phases for these new maps may be obtained from a structure factor calculation, or from recycling the tangent formula.

9. Repeat Steps 1 to 8.

Refinement can be started whenever a complete structure is found.